AD-A181 428 FUNDAMENTAL ASPECTS OF PRESSUREMETER TESTING(U) PURDUE 1/2
UNIV LAFAYETTE IN SCHOOL OF CIVIL ENGINEERING
J L CHAMEAU ET AL 30 APR 87 AFOSR-TR-87-0777
UNCLASSIFIED AFOSR-84-0330 F/G 8/10 NL

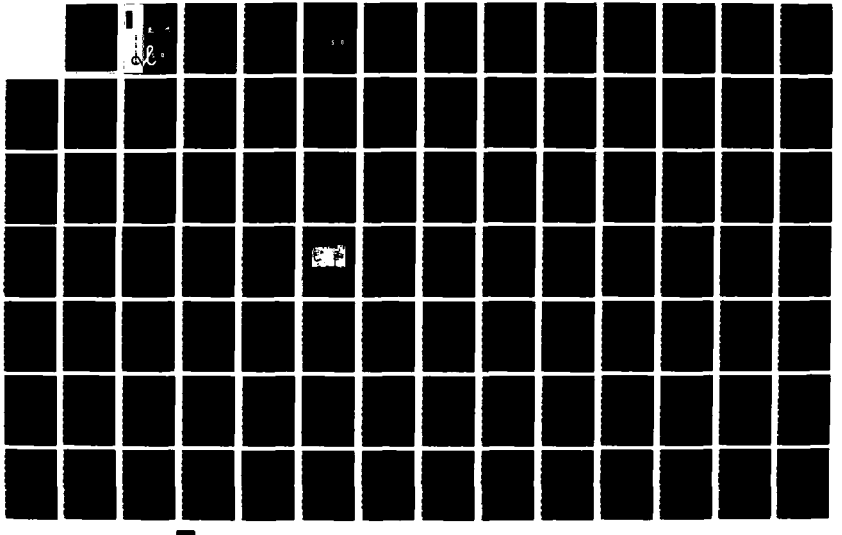

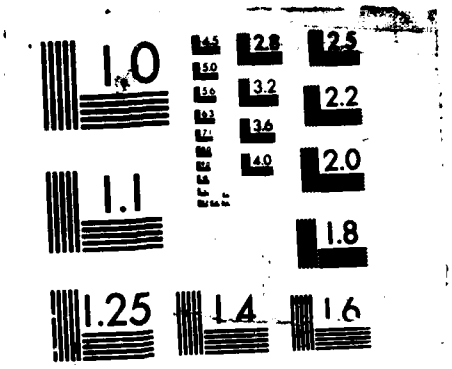

SCHOOL OF CIVIL ENGINEERING

AFOSR-TR- 87-0777

FUNDAMENTAL ASPECTS OF PRESSUREMETER TESTING

FINAL REPORT

Prepared by:

J. L. Chameau
R. D. Holtz
N. Sivakugan
S. Prapaharan

With contributions from:

A. B. Huang
A. G. Altschaeffl

PURDUE UNIVERSITY

UNCLASSIFIED

SECURITY CLASSIFICATION OF THIS PAGE

A181428

REPORT DOCUMENTATION PAGE

1a. REPORT SECURITY CLASSIFICATION: UNCLASSIFIED	1b. RESTRICTIVE MARKINGS
2a. SECURITY CLASSIFICATION AUTHORITY	3. DISTRIBUTION/AVAILABILITY OF REPORT: Approved for Public Release; Distribution Unlimited.
2b. DECLASSIFICATION/DOWNGRADING SCHEDULE	
4. PERFORMING ORGANIZATION REPORT NUMBER(S)	5. MONITORING ORGANIZATION REPORT NUMBER(S): AFOSR-TR- 87-0777
6a. NAME OF PERFORMING ORGANIZATION: SCHOOL OF CIVIL ENGINEERING, PURDUE UNIVERSITY; 6b. OFFICE SYMBOL (If applicable)	7a. NAME OF MONITORING ORGANIZATION: AIR FORCE OFFICE OF SCIENTIFIC RESEARCH
6c. ADDRESS (City, State, and ZIP Code): WEST LAFAYETTE, IN 47907	7b. ADDRESS (City, State, and ZIP Code): AFOSR/NA, Bld 410, BOLLING AFB, D.C. 20332
8a. NAME OF FUNDING/SPONSORING ORGANIZATION: AIR FORCE OFFICE OF SCIENTIFIC RESEARCH; 8b. OFFICE SYMBOL (If applicable): AFOSR/NA	9. PROCUREMENT INSTRUMENT IDENTIFICATION NUMBER: AFOSR-84-0330
8c. ADDRESS (City, State, and ZIP Code): Bld 410, BOLLING AFB, D.C. 20332	10. SOURCE OF FUNDING NUMBERS: PROGRAM ELEMENT NO 61102; PROJECT NO 2302; TASK NO C1; WORK UNIT ACCESSION N

11. TITLE (Include Security Classification)

FUNDAMENTAL ASPECTS OF PRESSUREMETER TESTING

12. PERSONAL AUTHOR(S)

CHAMEAU, J.L., HOLTZ, R.D., SIVAKUGAN, N., AND PRAPAHARAN, S. with contributions from Huang, A.B. & Altschaeffl, A.G

13a. TYPE OF REPORT	13b. TIME COVERED	14. DATE OF REPORT (Year, Month, Day)	15. PAGE COUNT
Final	FROM 9/1/84 TO 2/28/87	1987 April 30	186

16. SUPPLEMENTARY NOTATION

17. COSATI CODES			18. SUBJECT TERMS (Continue on reverse if necessary and identify by block number)
FIELD	GROUP	SUB-GROUP	FUNDAMENTAL ASPECTS OF PRESSUREMETER TESTING

19. ABSTRACT (Continue on reverse if necessary and identify by block number)

Of all in-situ soils tests, the pressuremeter offers the greatest possibility for significantly improving our understanding of in-situ soil behavior and our ability to determine analysis and design parameters. Because the test directly provides the load-deformation response of the soil, with proper interpretation it is possible to obtain the constitutive relationship of the in-situ soil. At present, this interpretation is largely empirical, and the effects of a number of test procedures and soil characteristics are not well known. This research was undertaken to increase our understanding of the influence of test procedures and certain soil conditions on the interpretation of pressuremeter test, as it affects the determination of soil stress-strain and strength characteristics.

(continued)

20. DISTRIBUTION/AVAILABILITY OF ABSTRACT	21. ABSTRACT SECURITY CLASSIFICATION
☒ UNCLASSIFIED/UNLIMITED ☐ SAME AS RPT ☐ DTIC USERS	UNCLASSIFIED

22a. NAME OF RESPONSIBLE INDIVIDUAL	22b. TELEPHONE (Include Area Code)	22c. OFFICE SYMBOL
Dr. Spencer T. Wu	202/767-4935	AFOSR/NA

DD FORM 1473, 84 MAR — 83 APR edition may be used until exhausted. All other editions are obsolete.

SECURITY CLASSIFICATION OF THIS PAGE

UNCLASSIFIED

Both analytical and experimental studies were carried out, and the report is a detailed summary of these investigations. Analytical work included studies of the influence on the derived pressuremeter and interpreted stress-strain curves of strain rate, pore pressure generation and dissipation, and borehole disturbance. It was found that these factors can significantly affect the stress-strain response and the shear strength of the soil, and their relative importance was quantified. The presence of a remolded annulus was found to be significant; however initial unloading can even be more significant, especially for highly anisotropic and strain softening soils. Parametric studies indicate that pressuremeter expansion curves, and thus interpreted stress-strain response, obtained from commercially available probes with a standard strain rate (1%/min) should not be significantly affected by partial drainage. The initial shear modulus was particularly sensitive to the above factors as well as interpretation methods, and it was tentatively concluded that the pressuremeter test is an inappropriate tool for determination of this soil property.

Additional analytical work included the extension of the Cam Clay and Modified Cam Clay soil models to consider an initial K_o consolidated state (rather than only isotropic), development of the Skempton pore pressure parameter for K_o consolidated specimens, and the influence of the intermediate principal effective stress on the strength response.

Experimental work concentrated on model pressuremeter tests performed in a calibration chamber on two cohesive soils. Variables included strain rate, disturbance, and pore pressure response. Most of the test apparatus was developed for this or closely related research. Reference K_o triaxial, one-dimensional consolidation, and cuboidal shear tests were also performed on the same two soils to obtain reference soil properties for pressuremeter tests. The experimental results corroborated the analytical results with respect to the effect of strain rate and borehole disturbance on derived initial shear moduli and strength. On the other hand, shear moduli derived from unload-reload loops were not sensitive to stress disturbance occurring prior to the test. The substantial anisotropy of ϕ' measured in cuboidal shear tests may contribute significantly to the observed overestimation of undrained shear strength in pressuremeter tests.

(2)

FUNDAMENTAL ASPECTS OF PRESSUREMETER TESTING

FINAL REPORT

Prepared by:

J. L. Chameau
R. D. Holtz
N. Sivakugan
S. Prapaharan

With contributions from:

A. B. Huang
A. G. Altschaeffl

PURDUE UNIVERSITY
School of Civil Engineering
West Lafayette, IN 47907

April 30, 1987

TABLE OF CONTENTS

CHAPTER 1

INTRODUCTION

Conventional practice in geotechnical engineering usually requires sampling of soil materials and subsequent laboratory testing to determine the soil properties necessary for design. This procedure suffers from the impossibility of ever testing the soil in the state at which it exists in the ground. Besides sampling and testing disturbances, removal of the sample from the ground causes changes in the stress system acting on the sample. The severity of the effect of this change depends on the nature of the soil fabric and its sensitivity to microstrains. It is not possible to make a determination of the fabric sensitivity a priori. The particulate nature of soils, their fabric, and the associated influence of environmental conditions all serve to reduce our confidence in the conventional determination of in situ soil behavior parameters.

One way to improve the situation is to forego sampling and use in situ testing devices to determine soil properties directly. In situ testing promises increasing effectiveness and efficiency for foundation engineering design. However, the results of most in situ tests must be empirically correlated to soil properties. Of all the in situ methods now in use, the pressuremeter offers the greatest possibility for markedly improving our ability to determine design parameters and in situ behavior. This is because load-deformation information is directly obtained from the test, and this information may with proper interpretation yield the constitutive relationship for the soil.

The research study undertaken at Purdue attempts to increase our understanding of the influence of certain soil conditions and testing

procedures on the stress-strain and strength properties of soil materials. The research program was organized around issues which directly affect the determination of in situ soil properties by the pressuremeter or self-boring pressuremeter. However a number of the theoretical and experimental avenues of research which were investigated are expected to prove useful in other areas.

The work performed to date has involved both experimental and analytical developments. Experiments were performed in a calibration chamber using model pressuremeters, as well as in K_o triaxial/plane strain and cuboidal shear devices. Analytical work dealt with both the interpretation of experimental data and theoretical developments related to pressuremeter testing. These research accomplishments are summarized in the following six chapters. Each chapter provides a description of the experimental and/or analytical techniques developed during the investigation and presents the most important results and conclusions. Whenever necessary, references are made to dissertations and technical papers written during the course of the study. The main conclusions of the research are re-evaluated globally in the final chapter. Appendix I contains a listing of the technical papers and discussions already published or in preparation on the results of this research.

CHAPTER 2

CALIBRATION CHAMBER RESEARCH

2.1 Introduction and Objectives

Calibration chambers (CC) have been used by a number of researchers to investigate the behavior of in situ tests in granular soils under controlled conditions. In a CC, uniform and reproducible samples can be created, which can then be subjected to known stress history and boundary conditions. CC studies have helped considerably in understanding the behavior of, for example, the pressuremeter test (PMT) in granular soils.

CC testing with cohesive soils is, however, unprecedented. Consequently, previous experimental studies on the PMT have been limited to field tests and comparisons with conventional laboratory tests on samples from the same site. Sample disturbance and the natural variation in soil properties such as water content, plasticity, and stress-strain behavior, even for soils from the same deposit, make comparisons with field test results problematic. Thus the CC approach is a more desirable alternative for cohesive soils.

In this research, a calibration chamber system and pressuremeter testing procedures were developed for cohesive soils with the following objectives:

1. Investigate the effects of strain rate and partial drainage on pressuremeter test results.
2. Study the stress paths and conditions for the existence of radial cracking in the soil during a PMT in cohesive soils.
3. Consider the effects of the variation of initial stress conditions on the test results.
4. Evaluate the PMT holding test.

To achieve these objectives, a series of model pressuremeter tests in a calibration chamber were performed under different boundary and initial conditions. Other variables were strain rate, plasticity and overconsolidation ratio of the clays. Following the pressuremeter expansion, a stress or strain controlled holding test was performed, and the pore pressures developed during the tests were monitored. The research also involved reference CK_oU axial compression and axial extension triaxial tests and vertical and horizontal oedometer tests on undisturbed samples of the clays tested in the calibration chamber. The background and research approach, laboratory equipment and testing procedures, and the interpretation and analysis of the data are detailed in the dissertation by Huang (1986). Huang, Holtz, and Chameau (1985 and 1987) also describe various aspects of the CC testing system and procedures.

2.2 Description of Equipment Developed

Specialized laboratory equipment developed for this research included a double wall calibration chamber system, model pressuremeters, a slurry consolidometer to prepare undisturbed triaxial samples, a triaxial device capable of consolidating a sample under K_o conditions, and related instrumentation. The design concepts and mechanical details of these devices are given in detail by Huang (1986) and summarized by Huang, Holtz and Chameau (1985 and 1987). Only a brief description follows.

The time required to consolidate clay samples and handling difficulties led us to build a small scale, flexible wall chamber system and to use model pressuremeters to perform calibration chamber tests. The basic concept is to first consolidate a clay sample from a high water content slurry (about 2.5 times the LL) in the slurry consolidometer (Fig. 2.1). First stage consolidation

occurs with the model pressuremeter and miniature piezometers already in place. Since there is no need for a boring in which to insert the pressuremeter, the primary source of soil disturbance is eliminated. In addition, the sample is consolidated in a rubber membrane which in the second stage consolidation becomes the CC inner membrane. Thus, there is no sample extrusion, and disturbance of the sample is further reduced.

The double wall CC is shown in Fig. 2.2, and Fig. 2.3 is a schematic diagram of the CC control system. Instrumentation specially developed for this research includes the model pressuremeter and miniature piezometers (Fig. 2.4). The reference K_o testing was carried out in the K_o triaxial shown in Fig. 2.5. A similar procedure as for the CC tests was used to consolidate triaxial samples directly in a membrane using the apparatus shown in Fig. 2.6.

All of this equipment was instrumented with pressure transducers (gage and differential) and LVDT's. The chamber and triaxial cell were placed in a temperature controlled room where the temperature was maintained within a range of 23.0 to 24.0° C. All instrument outputs are in DC voltage. A MACSYM 2 (Analog Devices, Inc.) data logging system was used to perform analog/digital conversion and to take readings. This device was interfaced with an IBM personal computer for data display, storage, and reduction.

2.3 Reference Soil Tests

In addition to basic classification tests, K_o triaxial and oedometer tests were performed to provide reference properties for the soils utilized in the chamber pressuremeter tests. Georgia kaolinite and an Indiana silt were utilized in the experiments. Fig. 2.7 shows the grain size distribution of the kao-

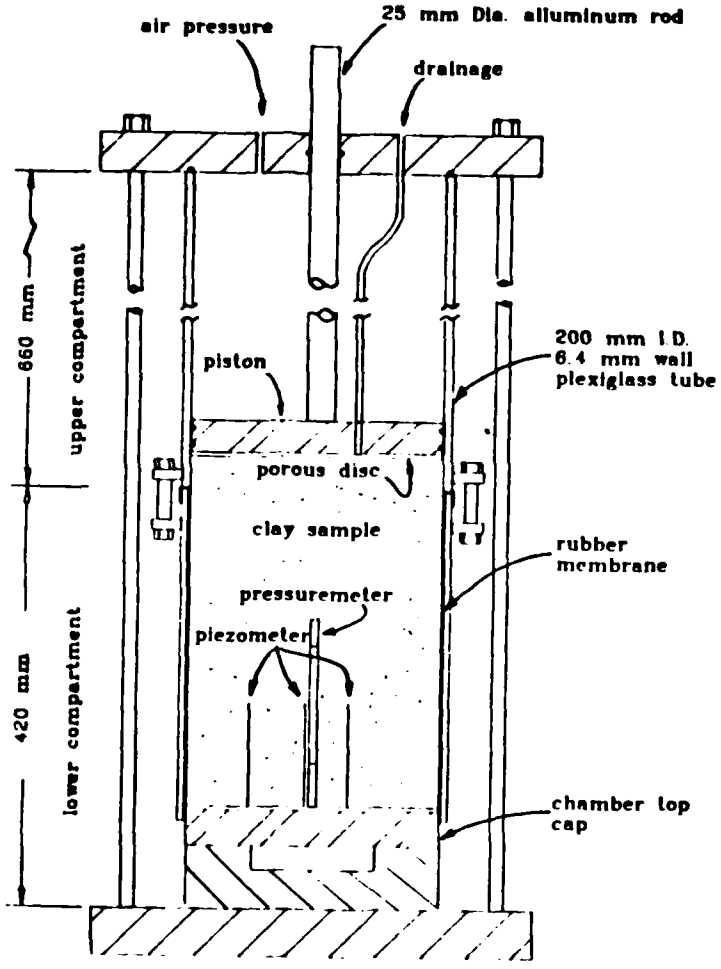

Figure 2.1 The chamber slurry consolidometer

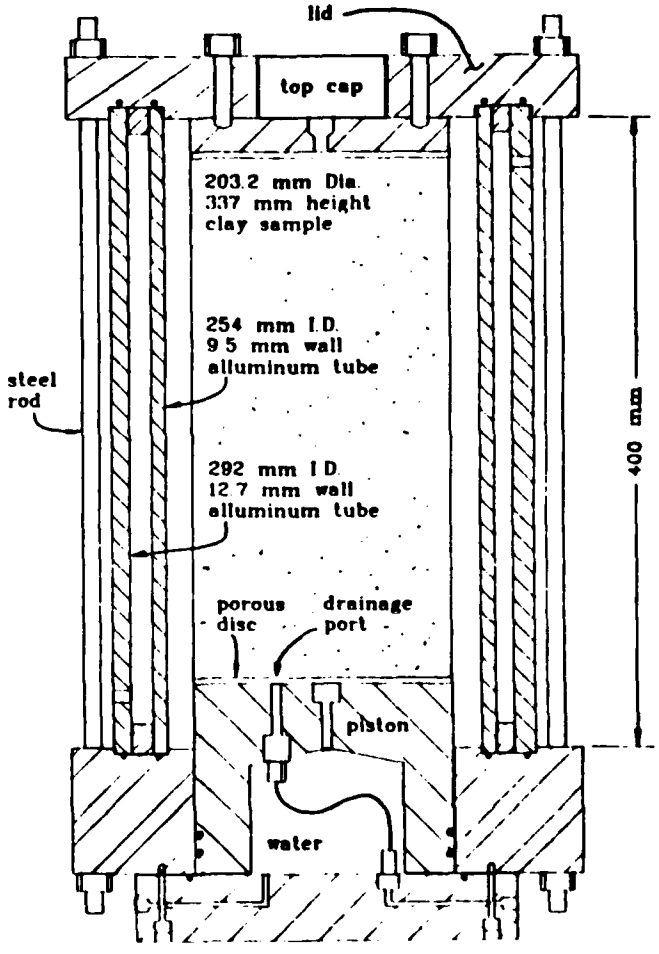

Figure 2.2 The double wall calibration chamber

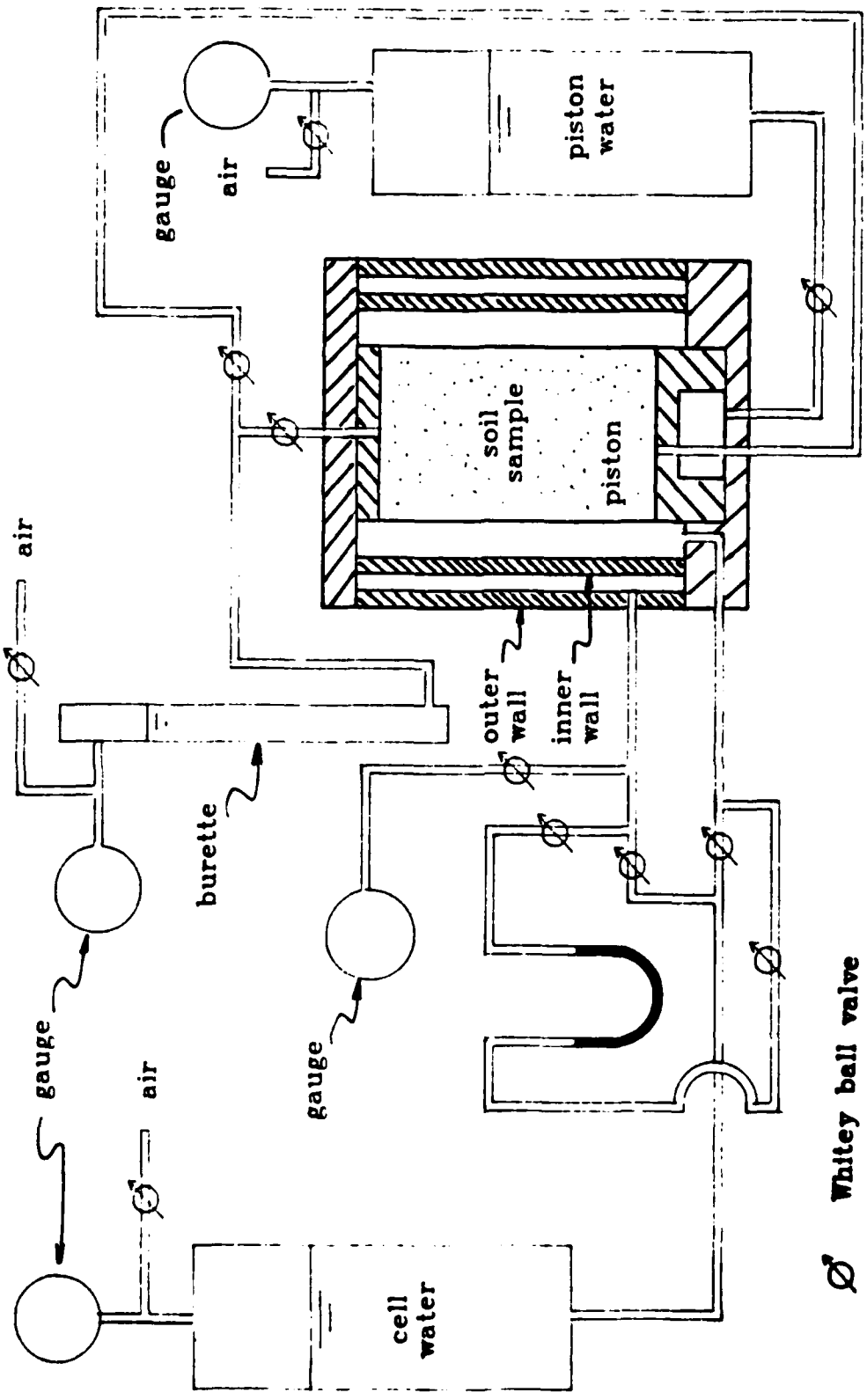

Figure 2.3 The calibration chamber control system

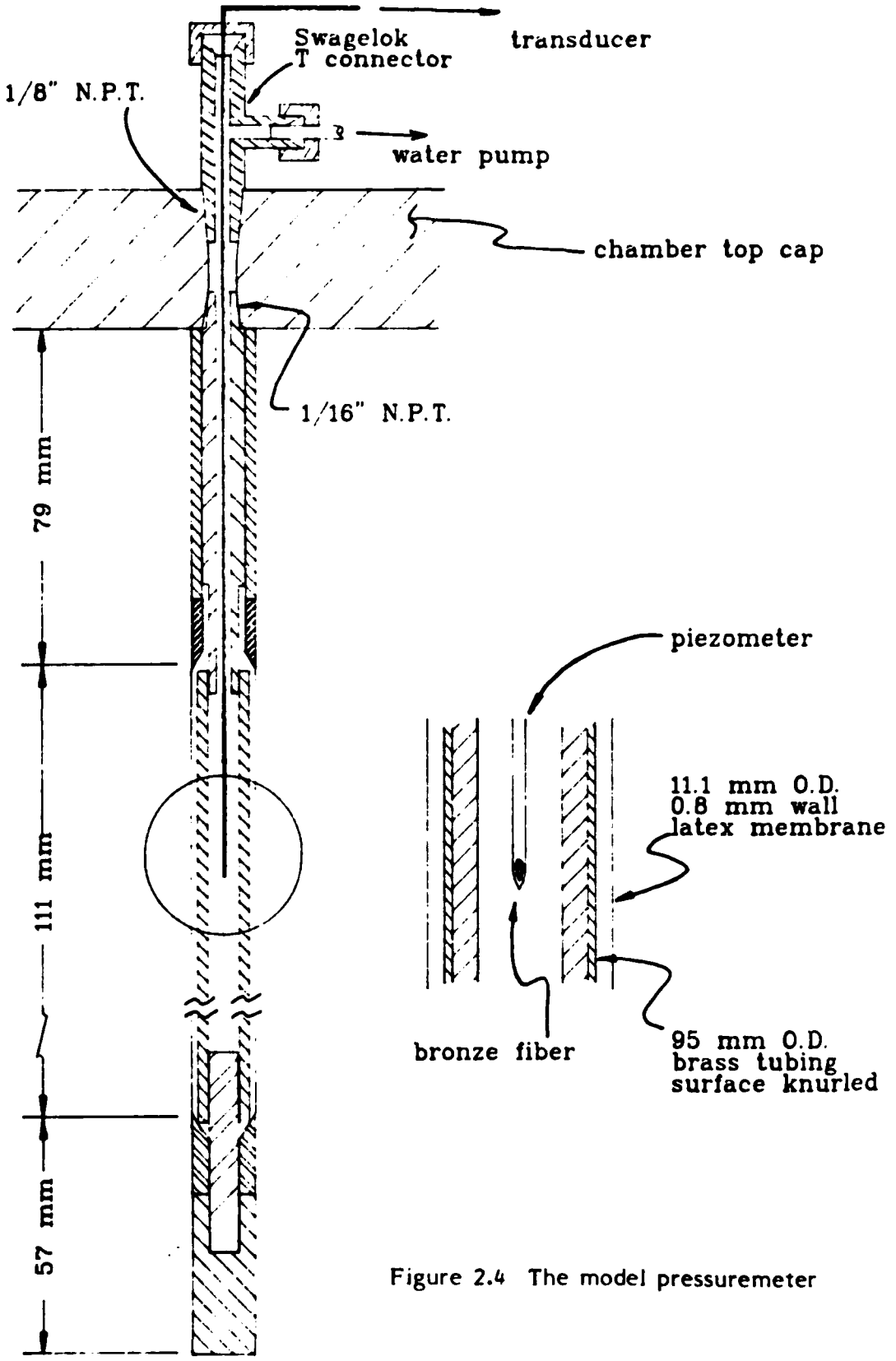

Figure 2.4 The model pressuremeter

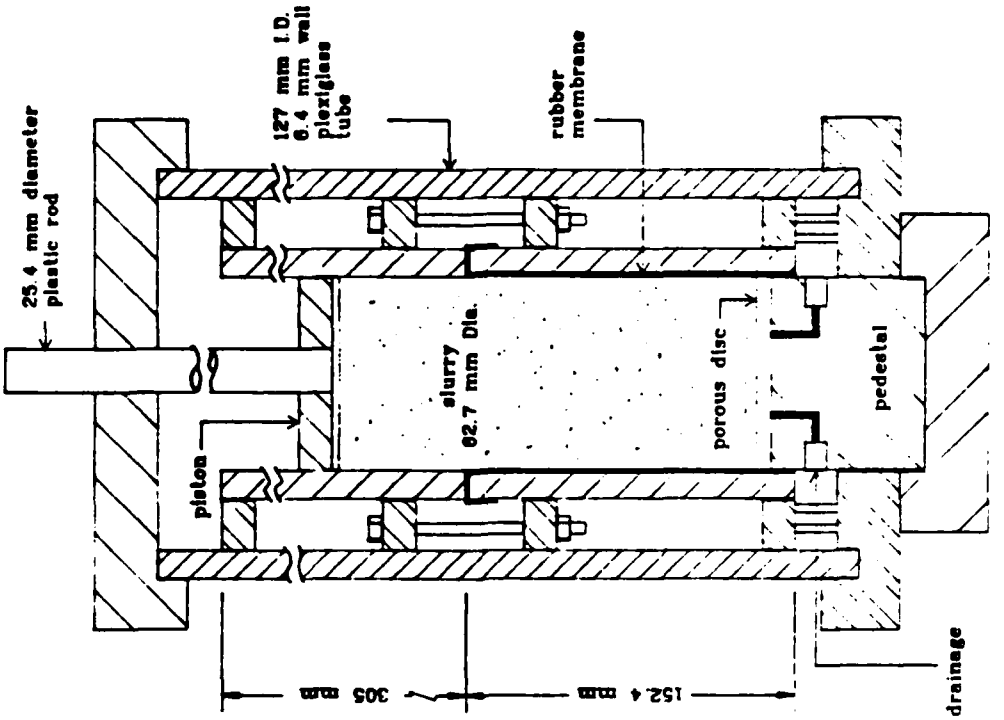

Figure 2.6 The triaxial slurry consolidometer

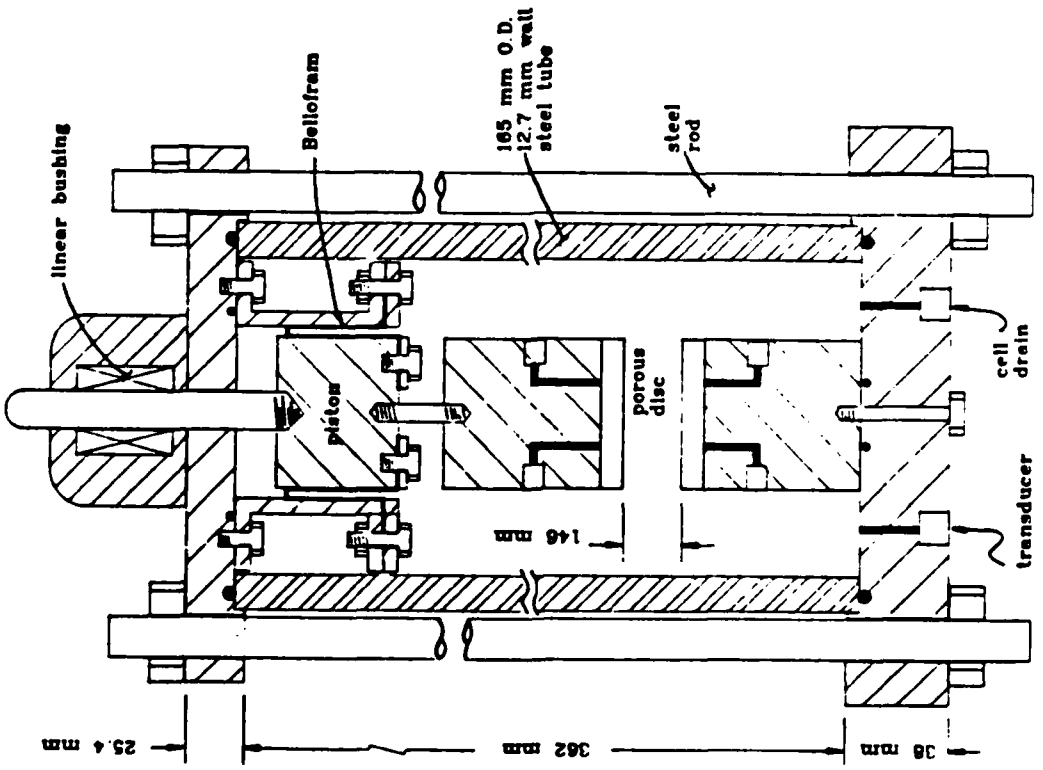

Figure 2.5 The K_o triaxial cell

linite and silt. The specific gravity and Atterberg limits are given in Table 2.1. Two types of soil mixtures were utilized in the experiments: 100% kaolinite, and a mixture of 50% kaolinite and 50% silt (by dry weight). The 100% kaolinite will hereinafter be referred to as the K100 soil and the 50/50 blend will be called K50.

The K_o triaxial tests provided stress-strain relationships and strength data for the K50 and K100 soils in axial compression and axial extension. The same consolidation pressures and OCR values as in the CC tests were used. Table 2.2 presents the test plan, and consolidation data, while Table 2.3 is a summary of all the triaxial test results. Graphs of all tests performed are given by Huang (1986), as are details of soil and slurry preparation, tests procedures, and an analysis of test errors.

Stress controlled oedometer tests were performed in both the vertical and horizontal direction to determine the consolidation characteristics of K100 and K50 for the chamber holding tests. These results are summarized in Table 2.4.

2.4. Chamber Pressuremeter Tests -- Presentation and Analysis of Results

Table 2.5 gives the soil, OCR, test condition, and strain rate for the 19 tests considered acceptable for this research. Details of sample preparation and set up, CC testing procedures, pore pressure monitoring, data reduction, and interpretation of the chamber pressuremeter tests results are given by Huang (1986).

Because such tests had not been previously performed, a study of the quality of the samples and tests was made. Huang, et al. (1985), and Huang (1986) summarized the results of these investigations. Basically, the data

Table 2.1 Properties of Experimental Clays

Soil	Liquid Limit	Plastic Limit	Specific Gravity
Kaolinite	63	36	2.65
K50	37	23	2.69

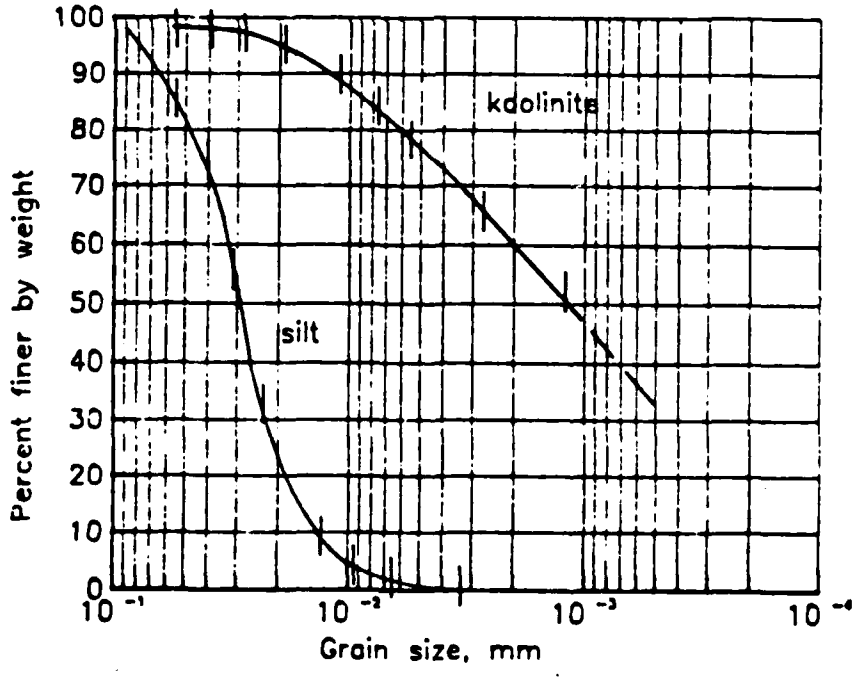

Figure 2.7 Grain size distribution curves

Table 2.2 Test plan and consolidation data

Test No.	Soil	O.C.R.	Shearing Mode	σ'_{vc} (final) kPa	B Value	K_o^{NC}	K_o^{OC}
KT-7	K100	1	CKU-AC	276.7	0.99	0.56	-
KT-19	K100	1	CKU-AC	275.3	0.99	0.56	-
KT-28	K100	1	CKU-AE	274.8	1.00	0.55	-
KT-20	K100	10	CKU-AC	27.58	1.00	0.55	1.49
KT-22	K100	10	CKU-AE	27.51	0.99	0.56	1.55
KT-21	K50	1	CKU-AC	276.3	1.00	0.52	-
KT-23	K50	1	CKU-AE	275.8	1.00	0.49	-
KT-25	K50	10	CKU-AC	28.46	0.99	0.49	1.47
KT-29	K50	10	CKU-AE	27.82	1.00	0.50	1.49

Table 2.3 Summary of Triaxial Test Results

Test No.	s_u kPa	ε_f %	A_f	E_{50}/s_u	ϕ'^* Degree	c'^* kPa	ϕ'^X Degree	c'^X kPa	M^+	s_u/σ'_{vc}
KT-7	76.30	0.18	0.52	1520	20.7	0.39	21.4	-2.25	0.78	0.276
KT-19	76.05	0.22	0.55	1690	21.0	-0.56	22.7	-6.98	0.81	0.276
KT-28	26.23	-3.41	1.01	-	12.4	-0.59	12.4	-0.59	0.40	0.095
KT-20	35.90	3.51	0.01	289	-	-	-	-	-	1.300
KT-22	18.56	-2.73	-0.58	-	-	-	-	-	-	0.675
KT-21	84.77	0.12	0.42	1690	23.5	-0.12	25.2	-6.41	0.92	0.310
KT-23	25.81	-2.91	1.09	-	15.3	1.54	15.3	1.54	0.49	0.094
KT-25	45.56	2.44	0.06	275	-	-	-	-	-	1.600
KT-29	19.73	-2.53	-0.31	-	-	-	-	-	-	0.709

See Table 2.2 for the triaxial test plan.

* Based on peak principal stress difference

X Based on peak stress ratio (σ'_1/σ'_3)

+ $M = \frac{q}{p'}$ where $q = \sigma_1 - \sigma_3$, $p' = \frac{\sigma_1+\sigma_2+\sigma_3}{3} - u$

Table 2.4 Consolidation characteristics of K100 and K50 samples

Test No.	Soil	C_c	loading			unloading		
			m_v $10^{-4}kPa^{-1}$	C_v m^2/yr	C_h m^2/yr	m_v $10^{-5}kPa^{-1}$	C_v m^2/yr	C_h m^2/yr
C01	K100	0.41	1.6	6.1	–	5.0	15.6	–
C02	K100	0.38	1.5	–	7.4	2.9	–	15.9
C03	K50	0.21	0.8	10.3	–	1.5	21.4	–
C04	K50	0.22	1.0	–	10.7	2.9	–	22.6

C_c = compression index

m_v = coefficient of volume change

C_v = coefficient of consolidation in vertical direction

C_h = coefficient of consolidation in lateral direction

Table 2.5 Summary of chamber pressuremeter tests

Test No.	Soil	O.C.R.	Test Condition	Strain Rate %/minute
CP4	K50	1	Perfect	0.10
CP6	K100	1	Perfect	0.73
CP8	K50	1	Perfect	0.73
CP10	K50	1	Perfect	0.73
CP12	K100	1	Perfect	0.73
CP15	K100	1	Overstressed	0.73
CP16	K100	10	Perfect	0.73
CP17	K50	1	Overstressed	0.73
CP18	K100	1	Perfect	4.40
CP19	K50	1	Perfect	4.40
CP20	K100	10	Perfect	4.40
CP21	K10C	1	Understressed	0.73
CP23	K50	10	Perfect	0.73
CP25	K50	10	Perfect	4.40
CP26	K50	1	Understressed	0.73
CP27	K100	10	Overstressed	0.73
CP28	K100	10	Understressed	0.73
CP29	K50	10	Overstressed	0.73
CP30	K50	10	Understressed	0.73

suggested that the samples were very uniform and reproducible, as shown in a comparison of duplicate tests CP6 and CP12 (K100 soil) and CP8 and CP10 (K50 soil) in Figs. 2.8 and 2.9. Another concern was possible shear stress between the probe and adjacent soil induced during chamber consolidation, but analysis indicated that the probe boundary shear stress can be considered insignificant.

Wood and Wroth (1977) noted negative circumferential stresses in their analyses of self-boring pressuremeter (Camkometer) tests. It was of concern that this might cause radial cracking in the soil and thus violate the assumption of plane strain. First an attempt was made to investigate experimentally the possibility of radial cracking using acoustic emission (AE) techniques, but unfortunately it was impossible to detect any significant difference in emission "counts" during several tests. A summary of our AE work is presented in Appendix II.

Next, a detailed analysis of the effective stress paths of N.C. and O.C. clays was made. No negative values of the circumferential stress were observed in any case. Therefore, the possibility of radial cracking was not considered further in the analyses of the chamber pressuremeter results.

Analyses of Chamber Pressuremeter Data -- The pressuremeter tests conducted included different strain rates and different levels of stress disturbance. A total of 11 CC tests were performed in two types of N.C. and O.C. clays under so-called "perfect" conditions (Table 2.5) in which no mechanical disturbance of the soil occurred before pressuremeter expansion. The results are shown in Figs. 2.8 to 2.13. The results have been interpreted using the Simplex curve fitting technique described in Chapter 4 of this report, and for simplicity, only the interpretation which has the least

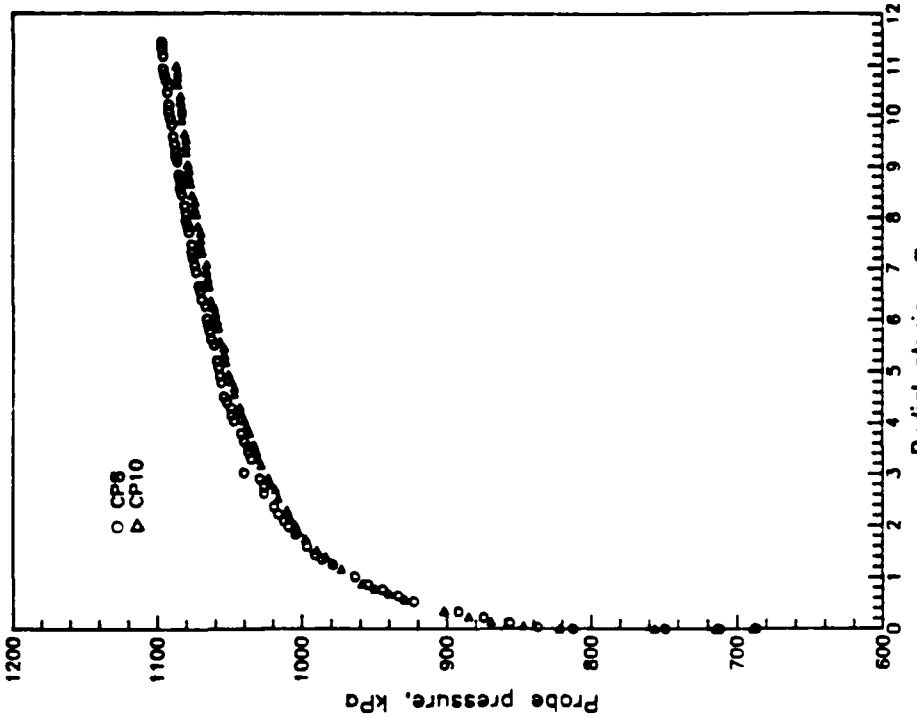

Figure 2.9 Comparison of CP8 and CP10

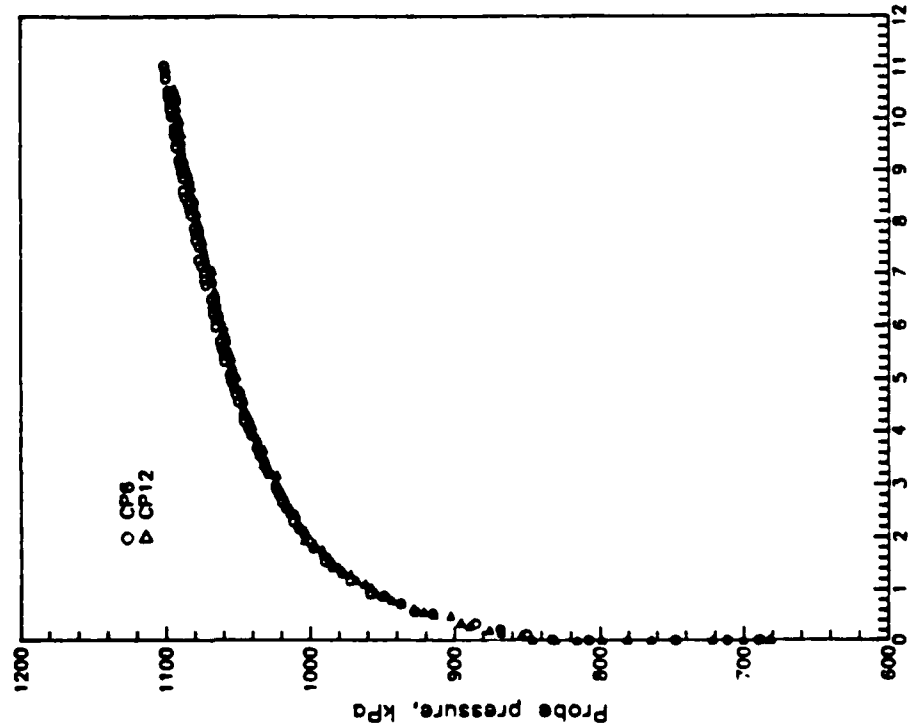

Figure 2.8 Comparison of CP6 and CP12

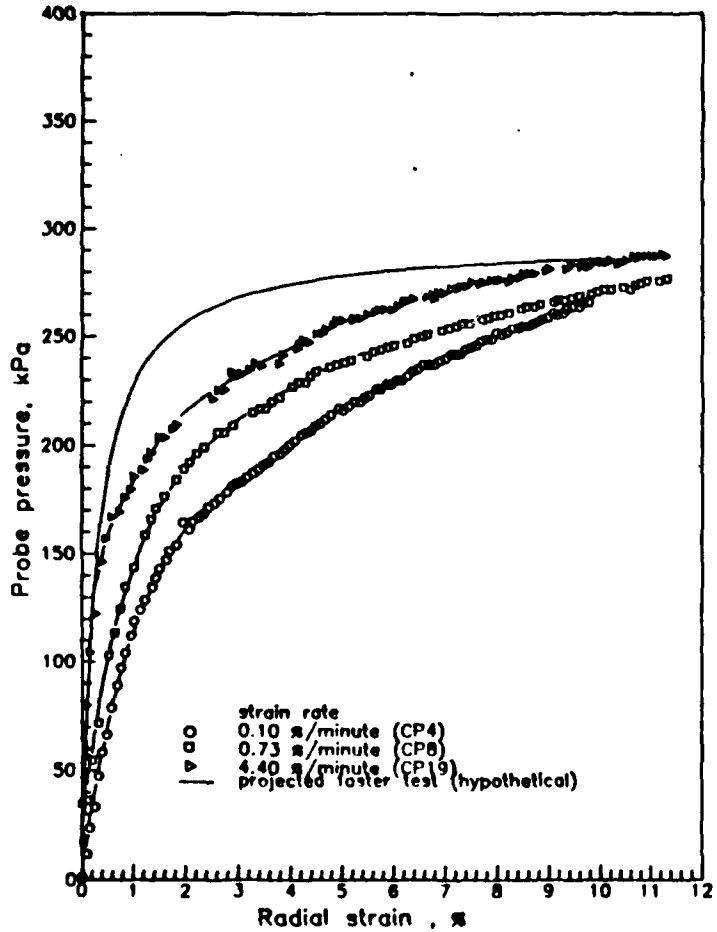

Figure 2.10 Perfect pressuremeter tests in N.C., K50 soil

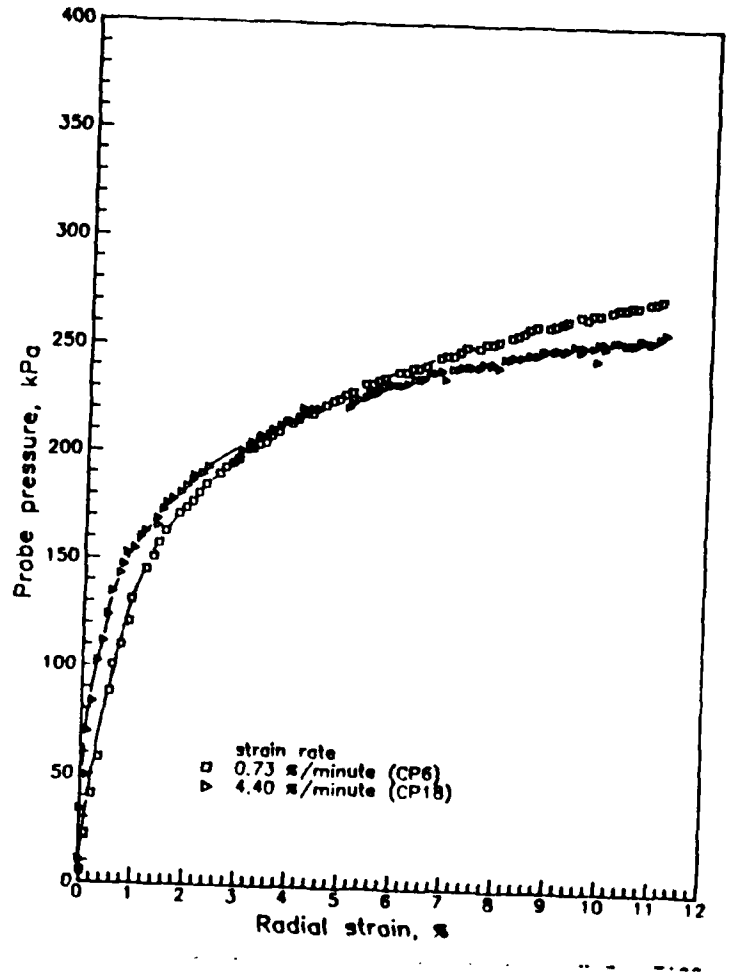

Figure 2.11 Perfect pressuremeter tests in N.C., K100 soil

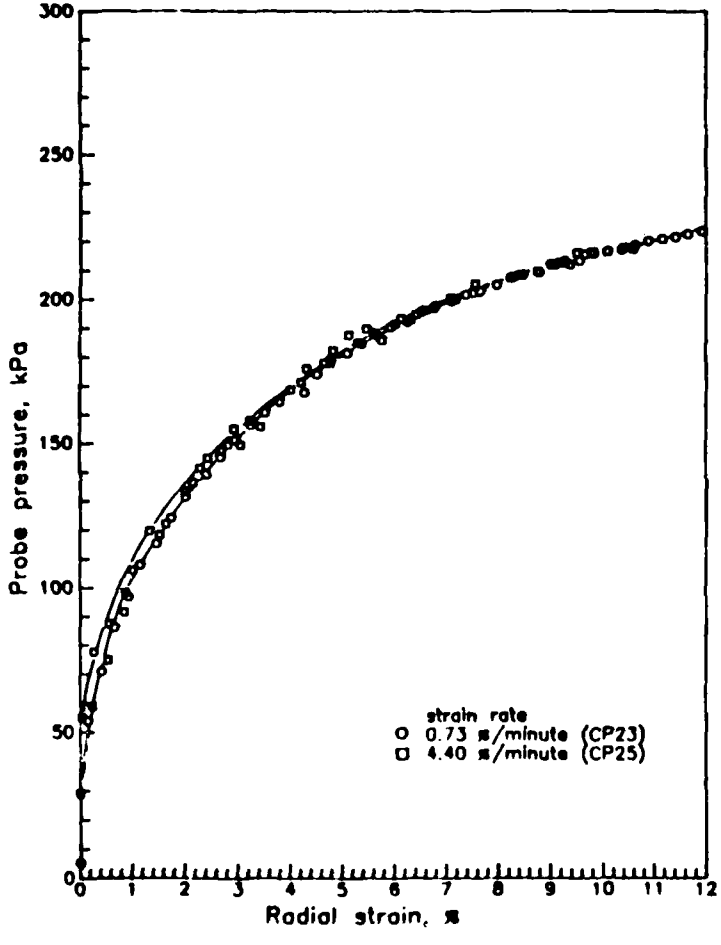

Figure 2.12 Perfect pressuremeter tests in O.C., K50 soil

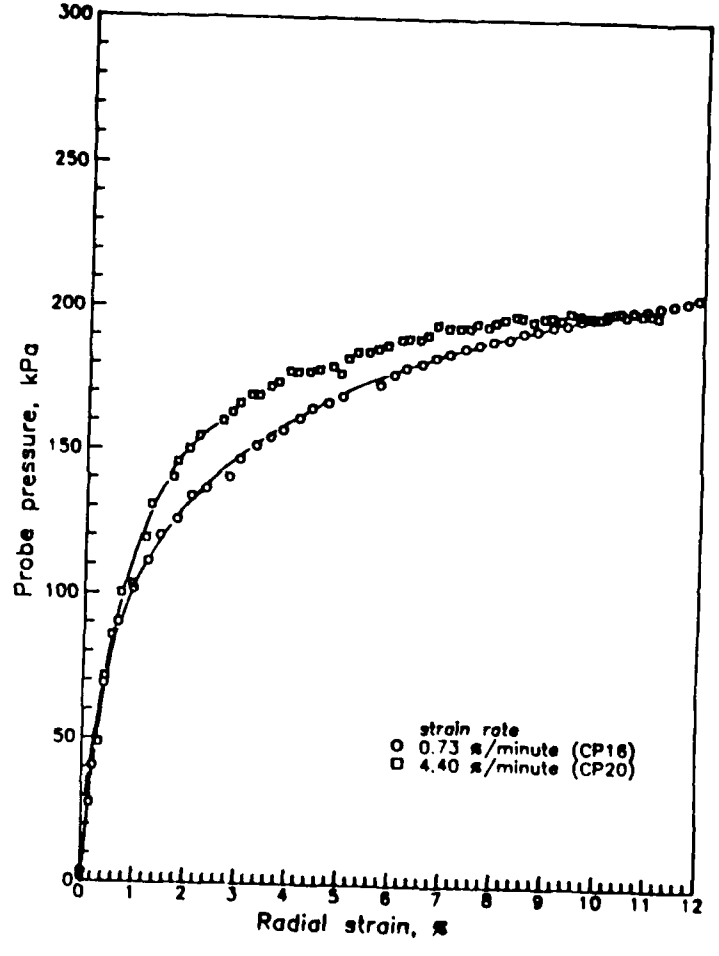

Figure 2.13 Perfect pressuremeter tests in O.C., K100 soil

standard deviation is shown (called "Simplex interpretation"). Table 2.6 summarizes the results of Simplex interpretation of these tests. Figures 2.14 to 2.17 show the stress-strain curves interpreted according to the Simplex procedure.

Strain Rate Effects -- The test results indicate that the initial shear modulus increases with the strain rate. On the other hand, the peak stress difference decreases with the strain rate (The only exceptions are tests CP16 and CP20). The data further indicate that the limit pressure, P_l (asymptotic probe pressure as the radial strain approaches infinity), is relatively insensitive to strain rate.

As the strain rate increases, the probe pressure curve becomes steeper initially and then levels off to reach almost the same limit pressure (Figs. 2.10-2.13). The soil stress strain relationship involved in all the curve fitting interpretation methods is directly related to the derivatives of the pressuremeter curve. Thus, this relatively rapid initial increase of probe pressure at the higher strain rates results in higher principal stress differences and higher initial shear moduli. When the curves level off, strain softening results because of the smaller derivatives, and this causes the stress-strain curve to have a peak at small strains (Compare, e.g., Figs. 2.10 and 2.14.). The combination of the initial shear modulus and the radial strain where strain softening occurs determines the peak stress difference in the interpretation.

From the model pressuremeter tests, it appears that the effect of higher initial shear modulus (higher stress difference at the same strain) for the higher strain rate tests is more than compensated for by the strain softening effect. This provides an explanation as to why the peak stress difference tends to decrease as strain rate increases in these tests. If the relatively

Table 2.6 Simplex interpretation of perfect pressuremeter tests

Test No.	Soil Type	O.C.R.	Strain Rate %/minute	S_u kPa	G_i kPa	ε_{rf} kPa
CP4	K50	1	0.10	65	7500	0.53
CP8	K50	1	0.73	63	20100	0.54
CP19	K50	1	4.40	45	112000	0.54
CP6	K100	1	0.73	62	13200	0.82
CP18	K100	1	4.40	43	55000	0.25
CP23	K50	10	0.73	46	14000	–
CP25	K50	10	4.40	42	17700	–
CP16	K100	10	0.73	41	11000	0.22
CP20	K100	10	4.40	54	25000	0.87

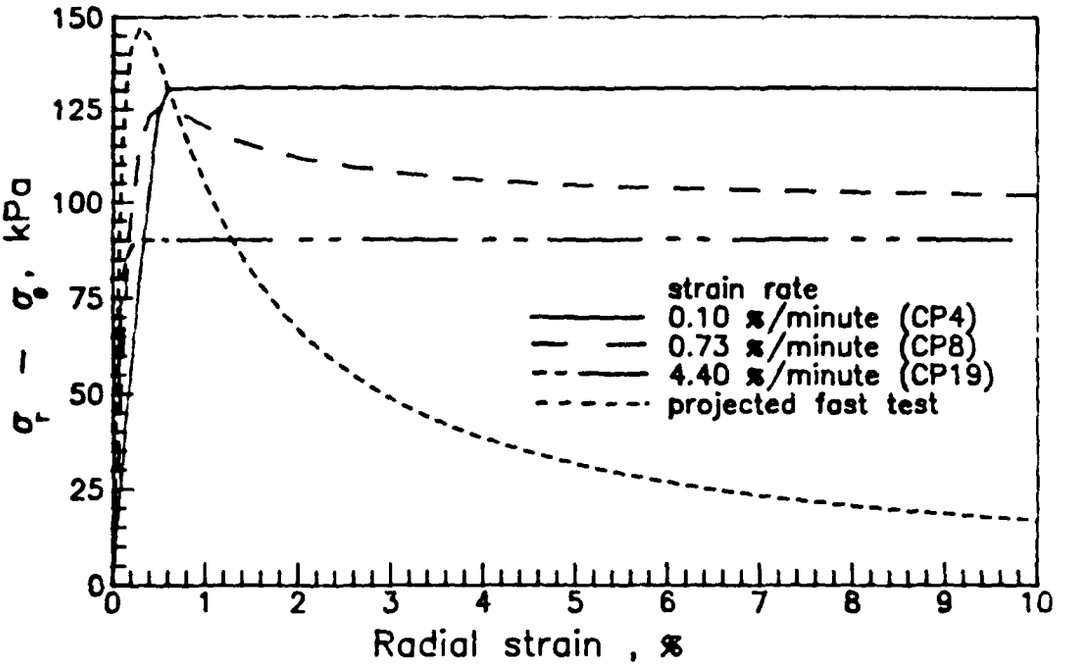

Figure 2.14 Interpretation of tests in N.C., K50 soil

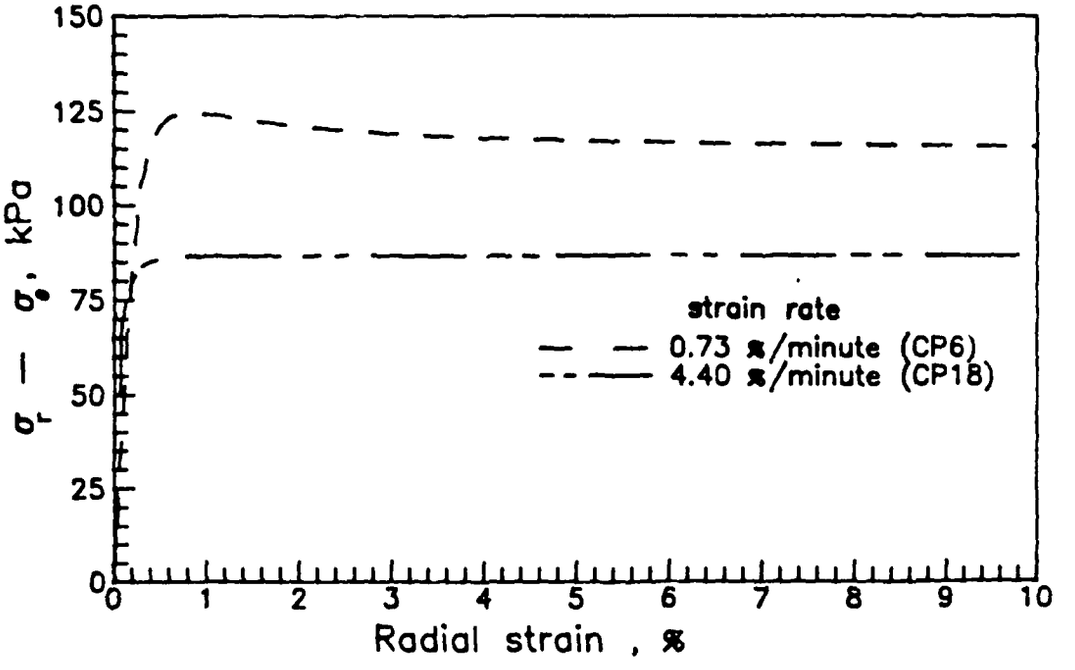

Figure 2.15 Interpretation of tests in N.C., K100 soil

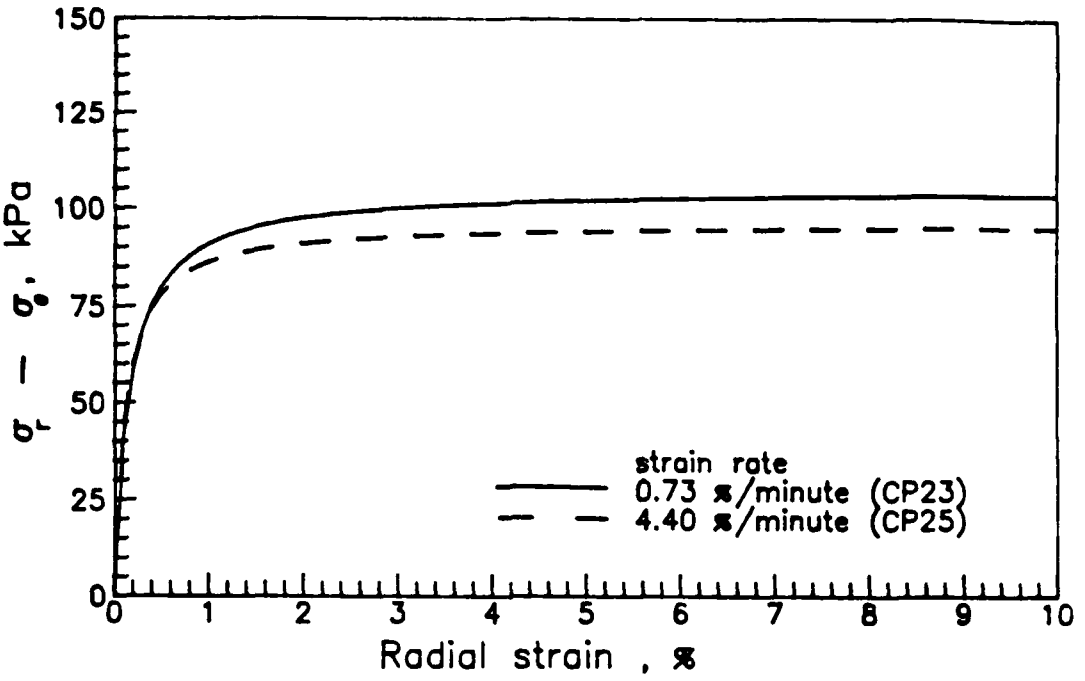

Figure 2.16 Interpretation of tests in O.C., K50 soil

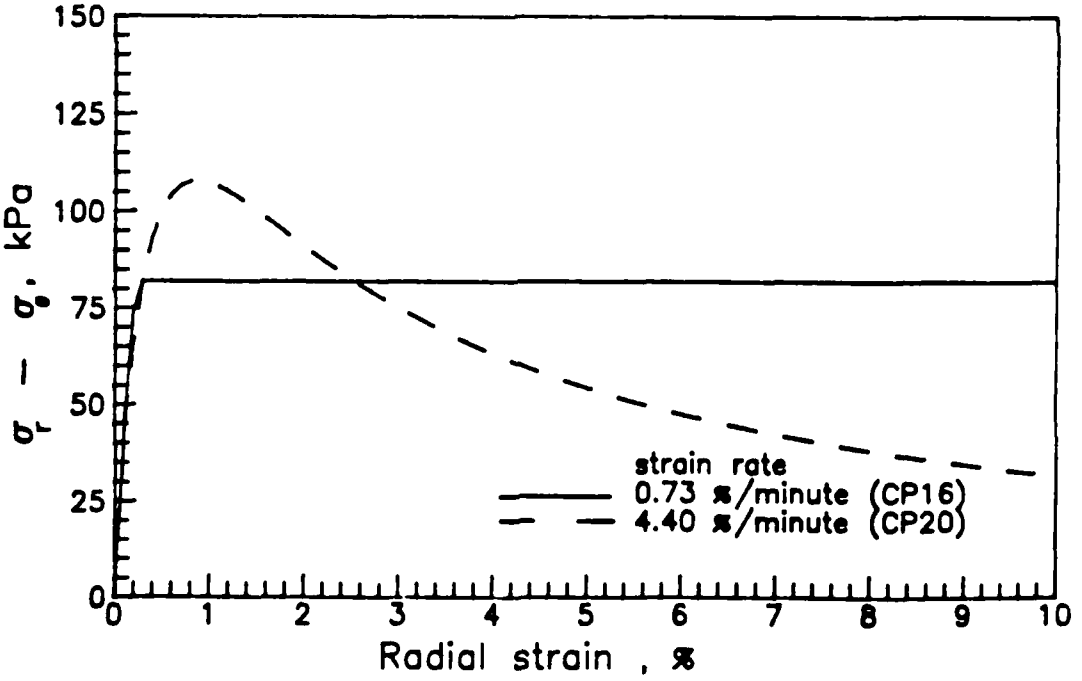

Figure 2.17 Interpretation of tests in O.C., K100 soil

constant limit pressure would prevail at even higher strain rates, the effect of high modulus would eventually overcome that of the strain softening, and the peak stress difference would again increase with strain rate. The interpretation would then yield a stress strain curve which has a very high peak stress difference and significant strain softening (See test CP20, Fig. 2.17). To further illustrate this phenomenon, a hypothetical pressuremeter curve representing an extremely rapid test has been added to Fig. 2.10 ("projected fast test"). The interpretation of this pressuremeter curve shows a much higher peak stress difference and very strong strain softening (Fig. 2.14). It is interesting that curves exhibiting a similar high peak stress difference and strain softening are commonly obtained from full size self boring pressuremeter tests (e.g. Ladd, et al., 1980).

Unfortunately, the maximum strain rate that the present apparatus could provide was 4.4 %/min.. Additional research at even higher strain rates or alternatively, gradually increasing probe diameters are needed to further validate these findings.

Disturbance Effects -- In addition to the "perfect" tests (Table 2.5), both "overstressed" and "understressed" tests were performed to investigate the effects of borehole disturbance. All tests were conducted at a strain rate of 0.73 %/min. Typical probe pressure vs. time records are shown in Fig. 2.18. Figs. 2.19 and 2.20 give the complete pressuremeter curves for the tests on NC and OC K100 soil (the results on the K50 soil are very similar).

In the interpretation, only the final expansion curve, starting from points A and B for overstressed and understressed, respectively, as shown in Figs. 2.19 and 2.20, was considered, as if there was no knowledge of the previous stress disturbance. The results of these interpretations are given in Table

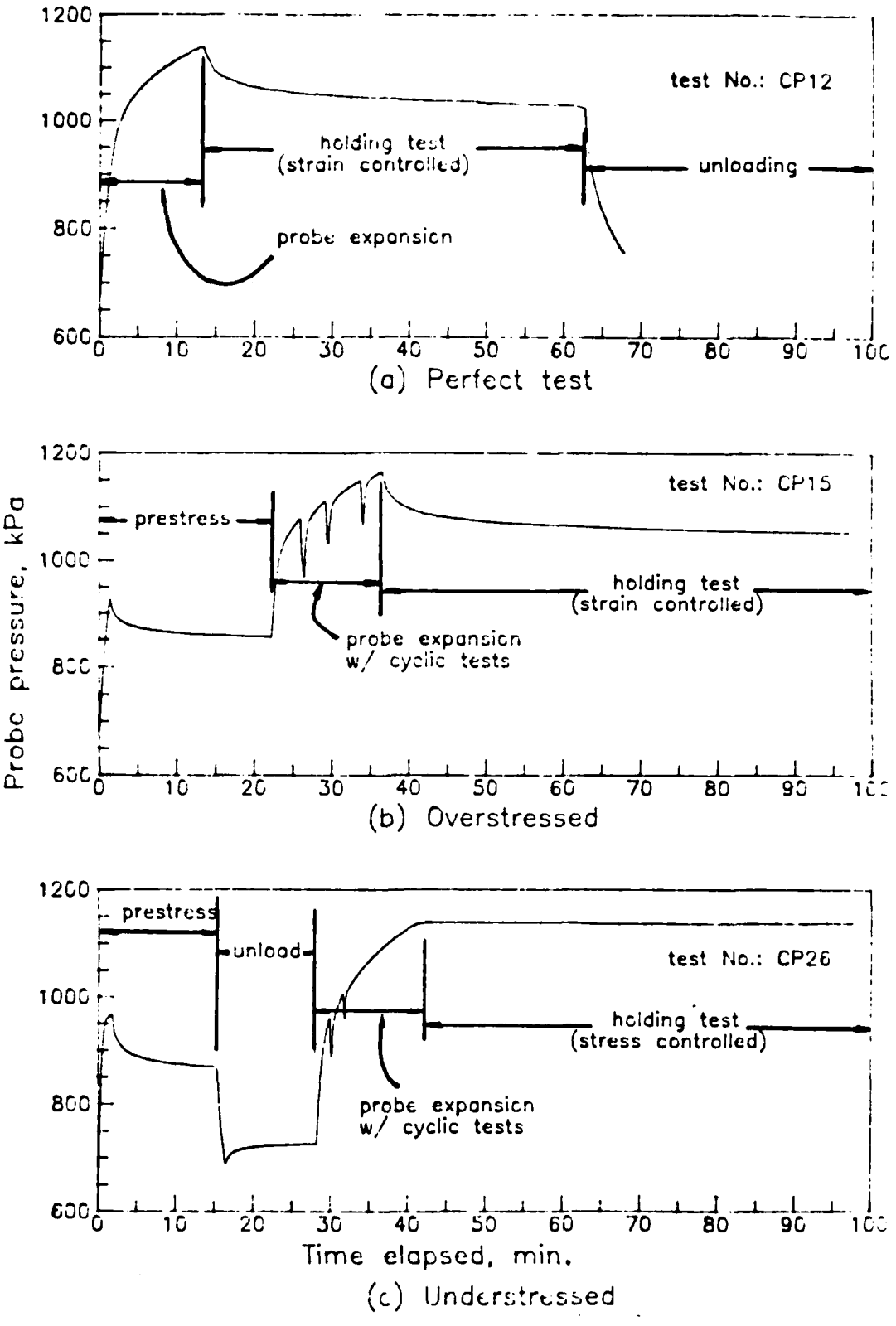

Figure 2.18 Probe pressure records for the perfect, overstressed, and understressed tests

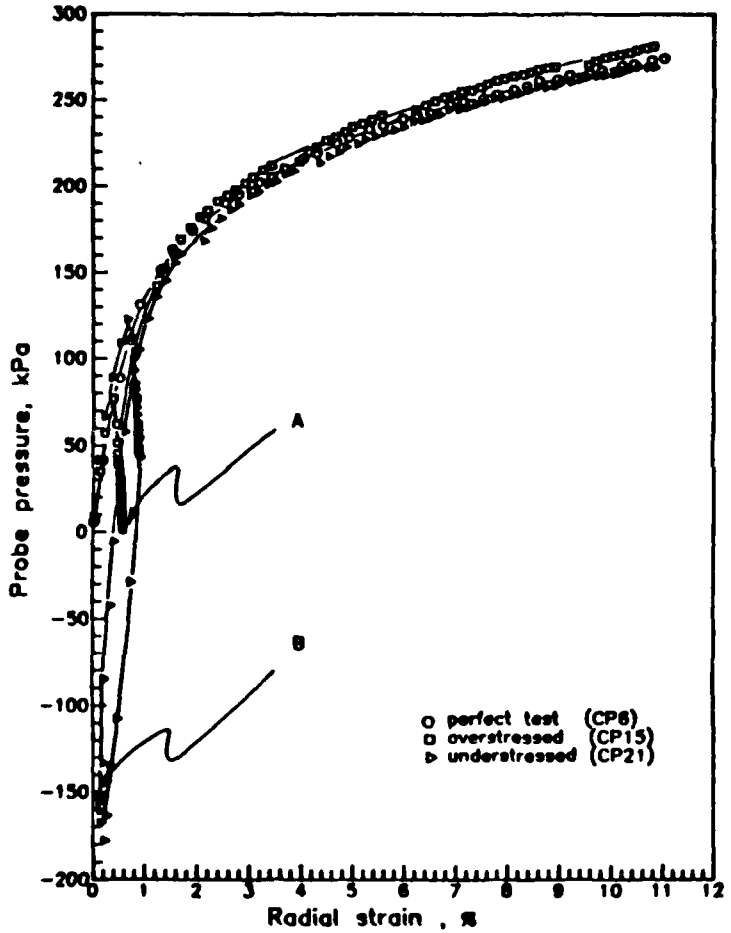

Figure 2.19 Pressuremeter tests in N.C., KI00 soil with stress disturbance

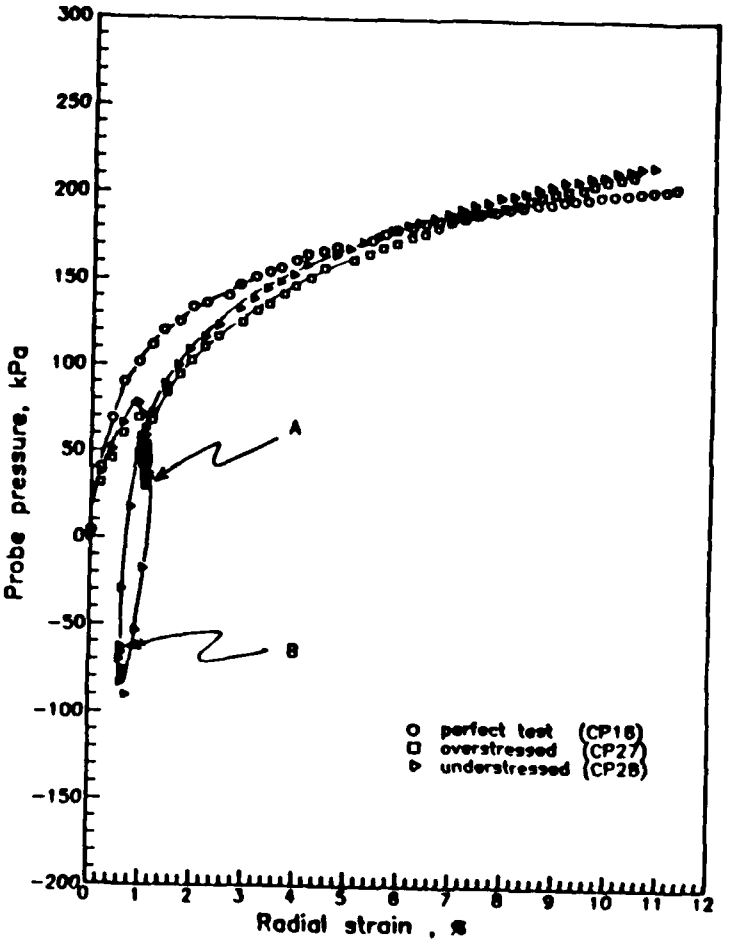

Figure 2.20 Pressuremeter tests in O.C., KI00 soil with stress disturbance

2.7 for both soils, and Figs. 2.21 and 2.22 (for K100 only -- results for K50 were quite similar).

Overstressing and the consolidation that followed made the soil stronger, since all overstressed tests showed slightly higher limit pressures as compared to the "perfect" results. For the overstressed tests in N.C. clays, the interpreted peak stress differences are lower than those of perfect tests. The overstressed tests in O.C. clays show higher peak stress differences than those of the "perfect" tests. This is again mainly due to the very similar limit pressures and the nature of the interpretation as described previously.

The understressed condition was caused by initially overstressing the probe; after the pore pressure dissipated, the probe pressure was reduced to the same level as the applied back pressure and held again until the excess pore pressure stabilized prior to the final probe expansion (Fig. 2.18). This testing procedure conceptually considered the overstressed condition as the original condition. The lowering of the probe pressure to the back pressure simulated the conditions in either a pre-bored pressuremeter test or a self-boring pressuremeter with an oversized cutter, where the lateral support of the bore hole is provided solely by drilling fluid. In both cases, disturbance can be considered as "severe". Although the probe pressure increased during the last holding period, the measured horizontal normal stress σ_h for all understressed tests (Table 2.7) is significantly lower than the original lateral earth pressure. For all tests, the interpretation results show relatively high initial shear moduli and peak stress differences. This is mainly due to the low σ_h which results from understressing. The findings suggest that if a relationship between the undrained shear strength and (P_1 - σ_h) can be established, then the results will most likely not be affected by disturbance, provided σ_h is

Table 2.7 Simplex interpretation of pressuremeter tests with stress disturbance

Test No.	Soil Type	O.C.R.	stress disturbance	σ_h kPa meas'd/orig.	s_u kPa	G_i kPa	ε_{sf} %
CP8	K50	1	no	820/820	63	20100	0.78
CP17	K50	1	overstressed	916/814	46	7100	–
CP26	K50	1	understressed	806/816	73	15400	1.40
CP6	K100	1	no	827/827	62	13200	0.82
CP15	K100	1	overstressed	837/837	48	30000	–
CP21	K100	1	understressed	720/830	93	42000	0.38
CP23	K50	10	no	755/755	46	14000	–
CP29	K50	10	overstressed	797/734	49	5000	–
CP30	K50	10	understressed	691/754	57	39000	10.40
CP16	K100	10	no	748/748	41	11000	–
CP27	K100	10	overstressed	810/755	54	3200	–
CP28	K100	10	understressed	697/759	51	54000	9.44

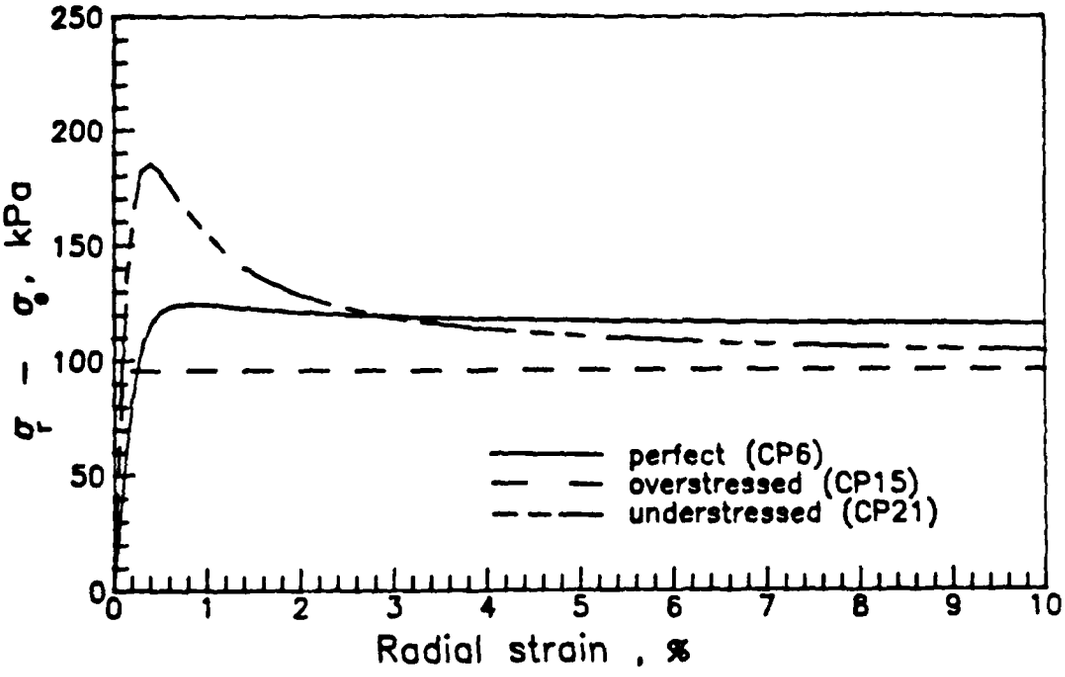

Figure 2.21 Simplex interpretation of perfect and disturbed pressuremeter tests in N.C., K100 soil

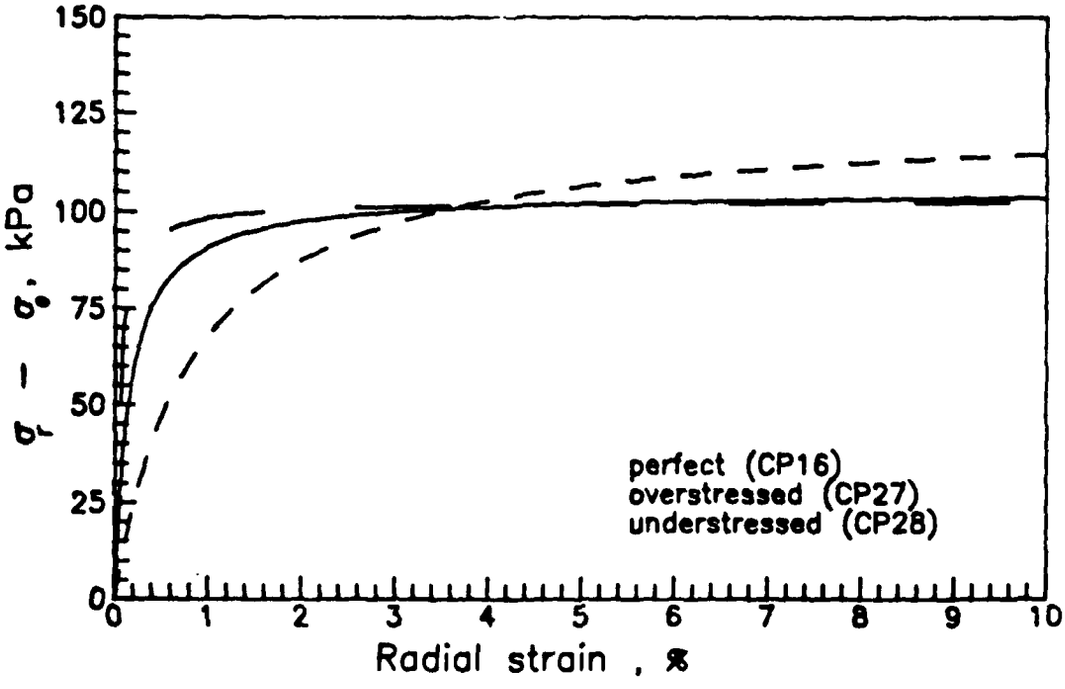

Figure 2.22 Simplex interpretation of perfect and disturbed pressuremeter tests in O.C., K100 soil

obtained by other dependable means. The results also indicate that the modulus measurements in "disturbed" pressuremeter tests are not valid. If some disturbance is inevitable, it may be advisable to overstress the soil somewhat, as this usually provides a lower modulus and a lower undrained shear strength; thus the values would be conservative for use in practice.

Soil Modulus -- So far, all the interpretations of the tests results have included the initial shear modulus. As shown by Huang (1986), this value can be easily computed after the stress-strain function is determined from the curve fitting process. The test results confirm previous experience with the determination of initial shear modulus: the results are extremely sensitive to soil disturbance, and in comparison with laboratory tests values range from about the same to much higher (Huang, 1986).

Considering all the uncertainties involved in the determination of initial shear modulus, it seems advisable not to use the pressuremeter to determine this soil parameter.

Wroth (1984) suggested that the shear modulus G can be measured by conducting unload-reload cycles or "loops" during probe expansion. If the clay behaves linear elastically during this cycle, then the loop will be a straight line. The G values from all unload-reload loops conducted during model pressuremeter tests are shown in Table 2.8. In all tests, the loops were fairly linear; however, the determination of the loop gradient was very sensitive to "noise" in the data, especially when the hysteresis was large. Based on experience in this research, the determination of G values from unload-reload loops is subject to considerable judgment, and therefore the G values shown in Table 2.8 are only approximate. As these values are from tests with different strain rates and different degrees of disturbance, neither of these factors has a

Table 2.8 Moduli from unload-reload loops

Test No.	Soil Type	O.C.R.	Strain Rate %/minute	Stress Disturbance	G kPa
CP17	K50	1	0.73	overstressed	13500
CP19	K50	1	4.40	no	11000
CP26	K50	1	0.73	understressed	14300
CP18	K100	1	4.40	no	10000
CP21	K100	1	0.73	understressed	12000
CP23	K50	10	0.73	no	10000
CP29	K50	10	0.73	overstressed	7000
CP30	K50	10	0.73	understressed	7000
CP16	K100	10	0.73	no	10000
CP20	K100	10	4.40	no	8500
CP27	K100	10	0.73	overstressed	8000
CP28	K100	10	0.73	understressed	7600

significant effect on the measurement of G.

Holding Test Results -- The installation of piezometers in the calibration chamber enabled the monitoring of the pore pressure distribution during pressuremeter expansion and during subsequent holding tests. Figs. 2.23 and 2.24 show the pore pressure distribution at the end of pressuremeter expansion in NC and OC clays, respectively. The data points in these figures are compiled from all the tests at the 0.73%/minute strain rate, including those with stress disturbance. It can be seen that the pore pressure distributions are very similar for both K50 and K100 soils, probably due to their similar consolidation properties (see c_h measurements in Table 2.4 and similar G/s_u values in Tables 2.9 and 2.10). The data also indicate that stress disturbance has little effect on the pore pressure distribution. However, the pore pressure measurements at the end of pressuremeter expansion (beginning of the holding test) for both the NC and OC clays are much lower than those predicted by Randolph and Wroth (1979) using the measured G/s_u values (Figs. 2.23 and 2.24). This difference is probably due to the significant drainage which occurs during the probe expansion because of the relatively small size of the model pressuremeter. It is difficult to conduct realistic undrained tests in the present apparatus.

Holding tests, both strain and stress controlled, were performed following pressuremeter expansion in most tests. Fig. 2.25 shows an example of each on NC K50 soil. Typically, the pore pressure dissipation in a stress controlled holding test is slower than in a strain controlled test, because the probe pressure decreases during a strain controlled test. The c_h values derived using the procedures by Clarke, et al. (1979) based on the test data are shown in Tables 2.9 and 2.10. As suggested by Wroth (1984), the shear moduli required

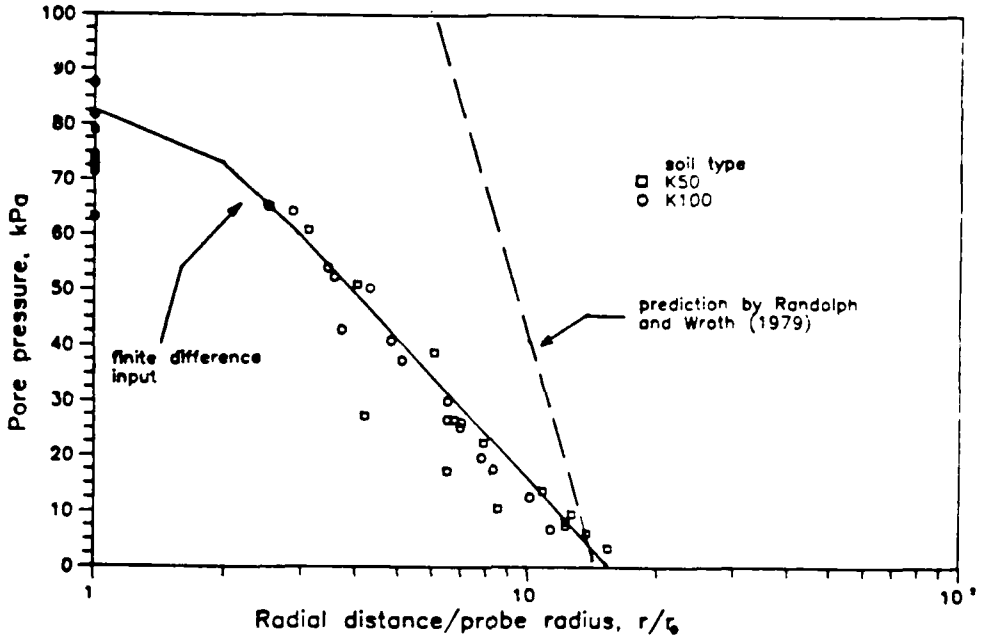

Figure 2.23 Pore pressure distribution at the end of pressuremeter tests in N.C. clay

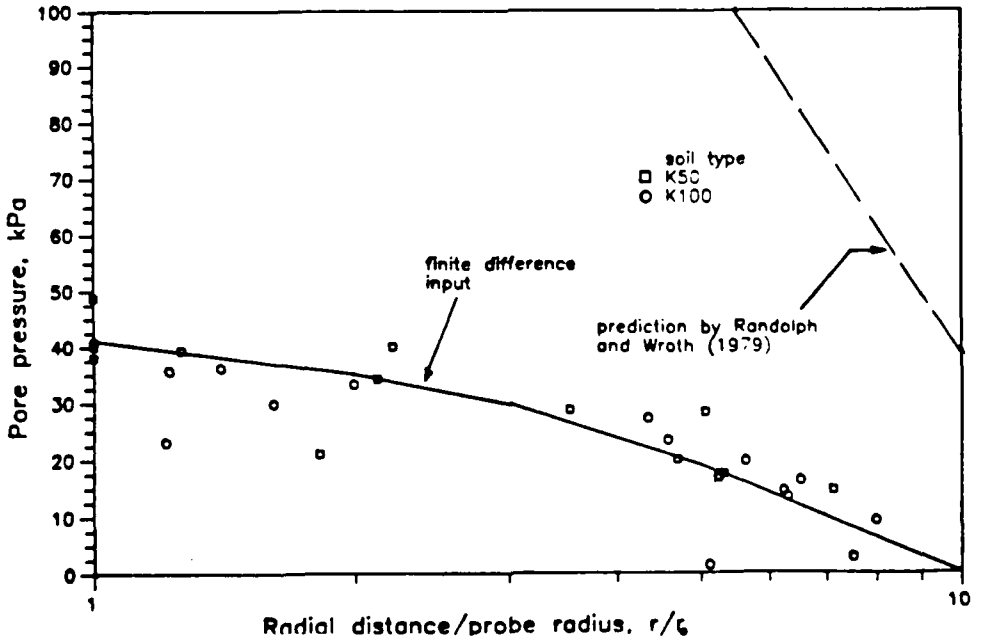

Figure 2.24 Pore pressure distribution at the end of pressuremeter tests in O.C. clay

Table 2.9 Results of strain controlled holding tests

Test No.	u_i kPa	u_f kPa	t_{50} minute	G/s_u	c_h, m^2/yr Clarke, et al. (1979)	c_h, m^2/yr Finite Difference
CP21	87.4	11.0	4.8	161 - 194	15.9 - 17.1	21.3
CP15	71.3	8.8	4.2	161 - 194	18.2 - 19.5	24.3
CP18	84.2	9.5	4.6	161 - 194	16.6 - 17.8	-
CP16	29.6	0.0	4.7	186 - 244	17.1 - 19.0	23.2
CP20	43.2	0.0	5.2	186 - 244	15.5 - 17.2	-
CP17	63.0	11.0	5.1	175 - 227	15.5 - 17.1	20.1

Table 2.10 Results of stress controlled holding tests

Test No.	u_i kPa	u_f kPa	t_{50} minute	G/s_u	c_h, m^2/yr Clarke, et al. (1979)	c_h, m^2/yr Finite Difference
CP26	74.1	16.0	14.1	175 - 227	5.6 - 6.2	7.3
CP30	39.3	6.0	17.2	152 - 217	4.3 - 5.0	6.4
CP27	36.0	7.5	18.6	186 - 244	4.3 - 4.7	5.8
CP28	35.6	9.0	17.0	186 - 244	4.7 - 5.3	6.4

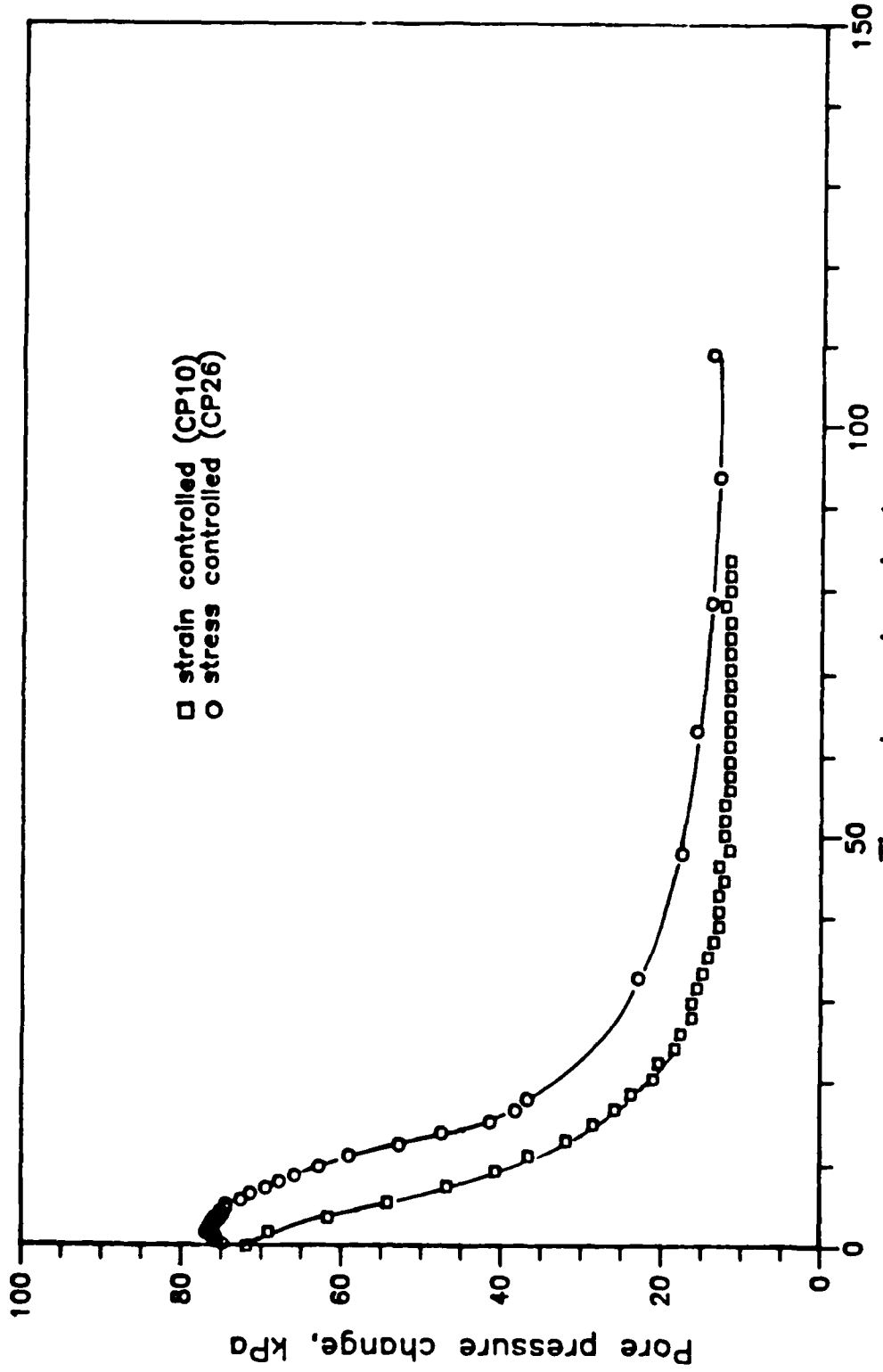

Figure 2.25 Holding tests of N.C., K50 soil

for the interpretation of the holding tests were taken from the unload-reload loops (Table 2.8) because its stress path is similar to that of a holding test. The s_u values needed were based on a Simplex interpretation of the perfect tests (Table 2.6). The t_{50} was taken as the time when the pore pressure in the holding test reached an average value. The results show that for the same type of soil and stress history (Tables 2.8) the c_h values from strain controlled tests are approximately three to four times those of stress controlled tests. On the other hand, the c_h values from stress controlled tests are very close to those of virgin loading as determined in horizontal oedometer tests (Table 2.4).

2.5 Conclusions

1. Uniform and reproducible samples of cohesive soil can be prepared using the calibration chamber system. The results of model pressuremeter tests performed in the chamber were quite repeatable.

2. Because of the small size of the model pressuremeter probe, significant drainage occurred during the pressuremeter tests, which resulted in conditions closer to drained than undrained.

3. The undrained shear strengths derived from model pressuremeter tests with strain rates between 0.1 and 0.73%/minute agree very well with the plane strain shear strengths predicted using the Prevost (1979) procedures and the corresponding triaxial test results. A higher pressuremeter expansion rate results in a greater initial pressure increase; however, the limit pressures were found to be relatively insensitive to strain rate. Thus, the derived initial shear moduli increase with strain rate.

4. The maximum principal stress difference initially decreases with strain rate, but after reaching a minimum value, it increases with strain rate. The soil stress strain relationship becomes increasingly strain softening at higher strain rates. This is probably why even high quality self boring pressuremeter tests yield very high peak shear strengths with subsequent large strain softening.

5. Stress disturbance, either by overstressing or understressing the soil around the probe, appears to affect only the early part of the pressuremeter curve. This does, however, result in a significant variation of the lateral earth pressure and initial shear modulus. These variations in turn affect the interpretation of the undrained shear strength.

6. The initial shear moduli are very sensitive to strain rate, stress disturbance, and the method of interpretation. Therefore, it is suggested that for practical applications, the pressuremeter not be used to determine this soil property.

7. Both the pore pressure distribution at the end of probe expansion and the shear modulus as determined from unload-reload loops are not sensitive to stress disturbance occurring prior to the test.

8. The coefficient of horizontal consolidation c_h determined from stress controlled holding tests with probe pressure exceeding the lateral preconsolidation pressure agrees well with those obtained from virgin loading in oedometer tests. However, strain controlled holding tests tends to overestimate c_h by three to four times.

CHAPTER 3

CUBOIDAL SHEAR TESTING

Conventional triaxial testing is always associated with two equal principal stresses while the third one, being different from the other two, provides the principal stress difference. Such an axisymmetric loading situation is not so common in practice. To model the behavior of a soil element under more realistic loading conditions, it is desirable to have means of applying three independently controlled principal stresses. For this purpose, a cuboidal shear device, also called a true triaxial device, was developed.

This device was used to study the effects of anisotropy and stress path on undrained shear strength and pore pressure development. A slurry consolidometer was used to prepare 102 mm cubical specimens. An overall view of the entire testing arrangement is shown in Fig. 3.1. The design concepts and the relevant details of the cuboidal shear device, slurry consolidometer, and the appurtenant components are described first. Then the test program is presented, followed by a discussion of the results.

3.1 Description of the Cuboidal Shear Device and Appurtenant Components

3.1.1 Cuboidal Shear Device

The first cuboidal shear device was developed by Kjellman (1936). Its use, especially as a research tool, has increased markedly since the 1960s. The devices differ from each other mainly in the specimen dimensions and boundary conditions. The device developed in this research is a flexible boundary

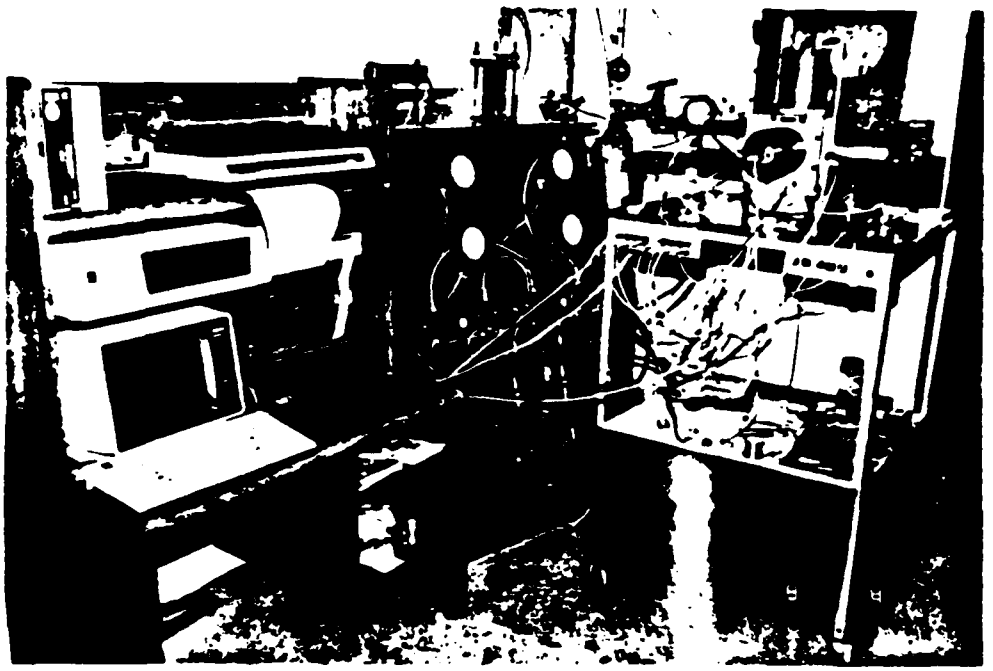

Figure 3.1 Cuboidal Shear Device, Control Board, and Data Acquisition System

type, in which the specimen "floats" between six silicone rubber membranes. The specimen is loaded by compressed air applied to these membranes. Friction between the membranes and the specimen is minimized by the application of a thin coating of silicone oil on the surface of the membranes. Assuming the absence of friction between the membrane and the soil specimen, the three pairs of orthogonal stresses can be assumed to be the principal stresses. An isometric view of the device is shown in Fig. 3.2.

Linear variable differential transformers (LVDTs) with sensitivities of 1.6 volt/mm were used to measure the deformation of each side of the specimen. One side has three LVDTs while the other five sides have one each. The LVDTs are contained in a cylindrical casing, their leads are taken out through the end cap to an A/D convertor, the DASH-8 board.

The cylindrical casings on opposite sides of the cube are connected to each other and to the air pressure source. Thus, equal pressure is assured on the opposite sides of the specimen. One of the two casings of all three directions has a pressure transducer at the end cap to measure the applied pressure. A diagonal port was drilled through the corner of the space frame towards the center of the cube to provide for pore pressure measurements using locally made "needle" piezometers (Fig. 3.3).

The silicone rubber membranes were made of RTV 664 silicone rubber compound (General Electric Company) by a procedure developed in this research. Drainage ports were provided at two diagonally opposite corners of the space frame to allow for back pressure and drainage.

3.1.2 Slurry Consolidometer

A slurry consolidometer made of plexiglass was constructed for the preparation of undisturbed specimens sedimented and consolidated under K_o

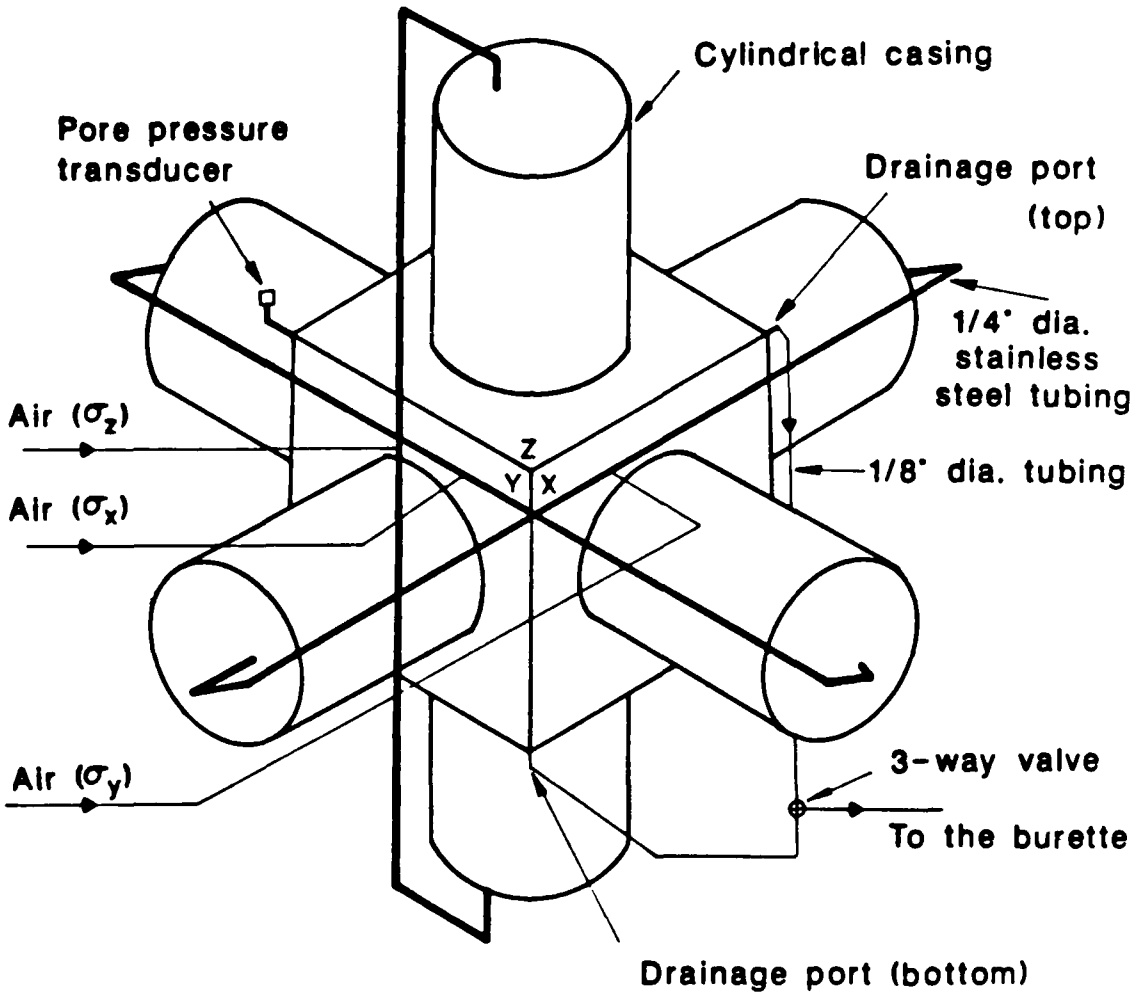

Figure 3.2 Isometric View of Cuboidal Shear Device

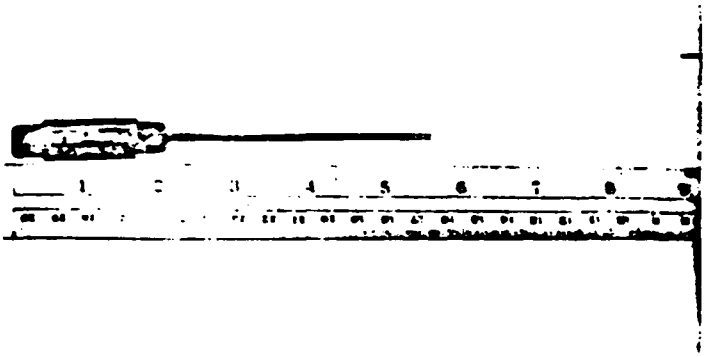

Figure 3.3 Needle Piezometer

conditions. An isometric view of the slurry consolidometer is given in Fig. 3.4. To reduce the consolidation time, drainage is provided at the top and bottom of the specimen. A detailed mechanical description of the consolidometer is given in Sivakugan (1987).

3.1.3 Control Board

The control board comprises the servo control system and the controls for flushing, back pressuring, and saturation of the specimen. Air pressure regulators, pressure gages, solenoid valves, saturation tank, drainage burette, and necessary valves and assorted fittings make up the control board.

The servo control system was used in K_o consolidation and strain controlled loading. Its salient features are described in Sivakugan (1987). In the servo control system developed in this research, both normally opened and normally closed, AC-operated two way solenoid valves were used. The schematic diagram of the servo control system is shown in Fig. 3.5. The valves were activated or deactivated through a double-pole-double-throw relay output accessory board (Model ERB-24, Metrabyte Corporation). The relay output board in turn was operated by a 24 bit parallel digital I/O interface board (Model PIO12, Metrabyte Corporation), which occupies one of the five expansion slots of an IBM PC. The 24 bit parallel digital I/O interface was driven by programs written in BASIC.

One of the four diagonal ports in the space frame is allocated for flushing operations. Two other diagonal ports provide for drainage through spaghetti tubing. The last one is for pore pressure measurement using a needle piezometer. A lexan burette, capable of withstanding 1500 kPa, collects the drained water during consolidation and provides the air-water interface for back pressure application.

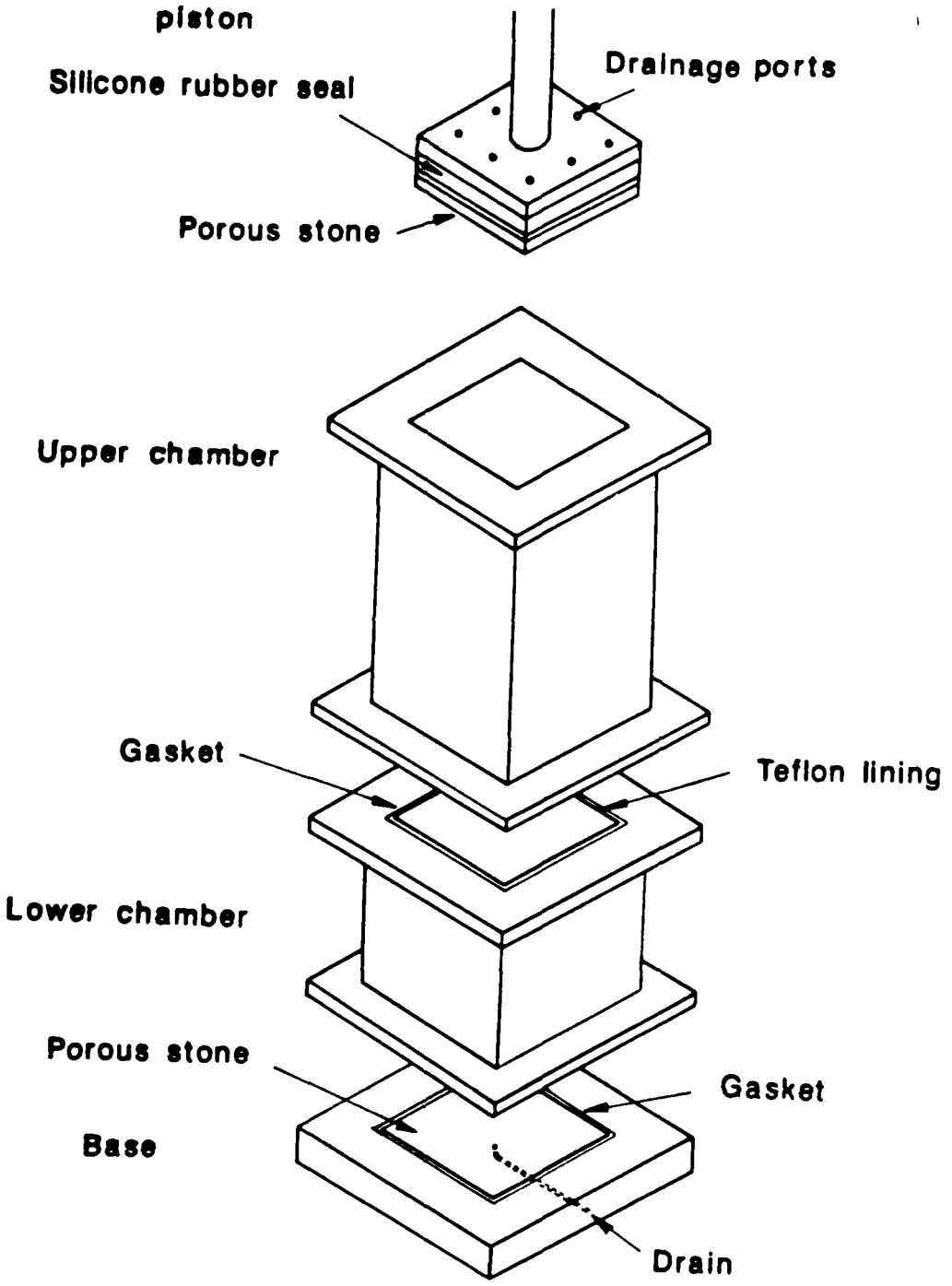

Figure 3.4 Isometric View of Slurry Consolidometer

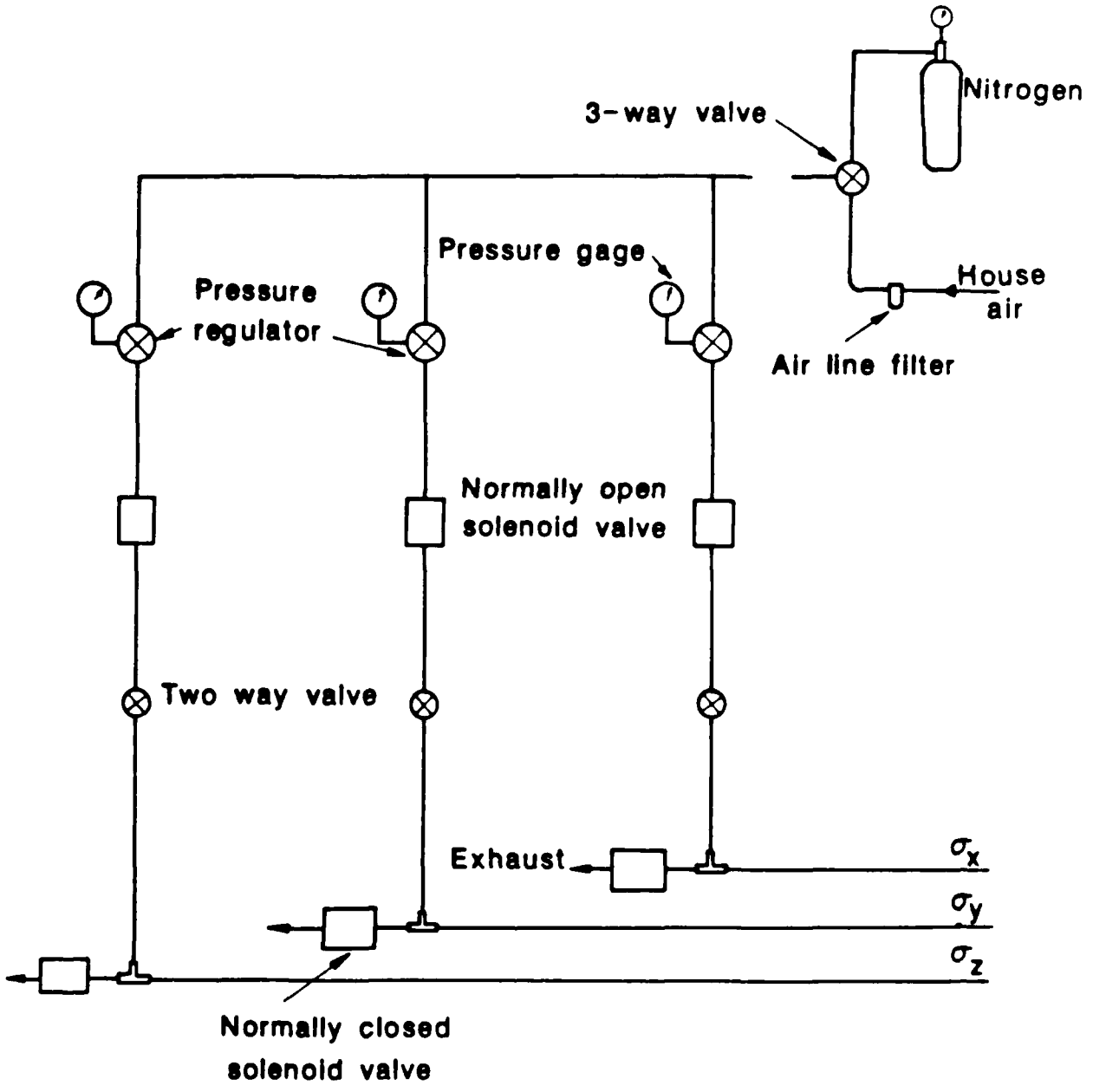

Figure 3.5 Schematic Diagram of the Servo Control System

3.1.4 Data Acquisition System

An eight channel high speed A/D convertor and timer-counter interface (Model DASH-8, Metrabyte Corporation) was used for automatic data acquisition. Since there were more than eight channels of measurements, analog input expansion sub-multiplexers (Model EXP-16, Metrabyte Corporation) were required. An 8253 programmable counter-timer in the DASH-8 board provides periodic interrupts for the A/D convertor. A schematic diagram of the hardware interfacing is given in Fig. 3.6. The software for data acquisition was written in BASIC. All necessary routines for data acquisition and control are included in an interactive and user friendly program DATACQ.

3.2 Experimental Program and Test Results

Cuboidal shear specimens were sedimented and consolidated from a slurry in the consolidometer. Then they were extruded and reconsolidated hydrostatically or non-hydrostatically to a higher stress level in the cuboidal shear device. At the end of consolidation, stress paths simulating axial compression and lateral compression were applied under undrained conditions. All the tests reported herein are stress controlled. Therefore possible strain softening could not be observed. Nevertheless, the soils studied were of very low sensitivity, and thus significant strain softening effects were not expected. A brief description of each stage of the testing program, the experiments performed, test results, and the analysis are presented below. Full details are available in Sivakugan (1987).

3.2.1 Slurry Preparation

The slurry was mixed using deionized and deaired water to a water content of 2 to 2.5 times the liquid limit in a large batch, sufficient for 10 to 15

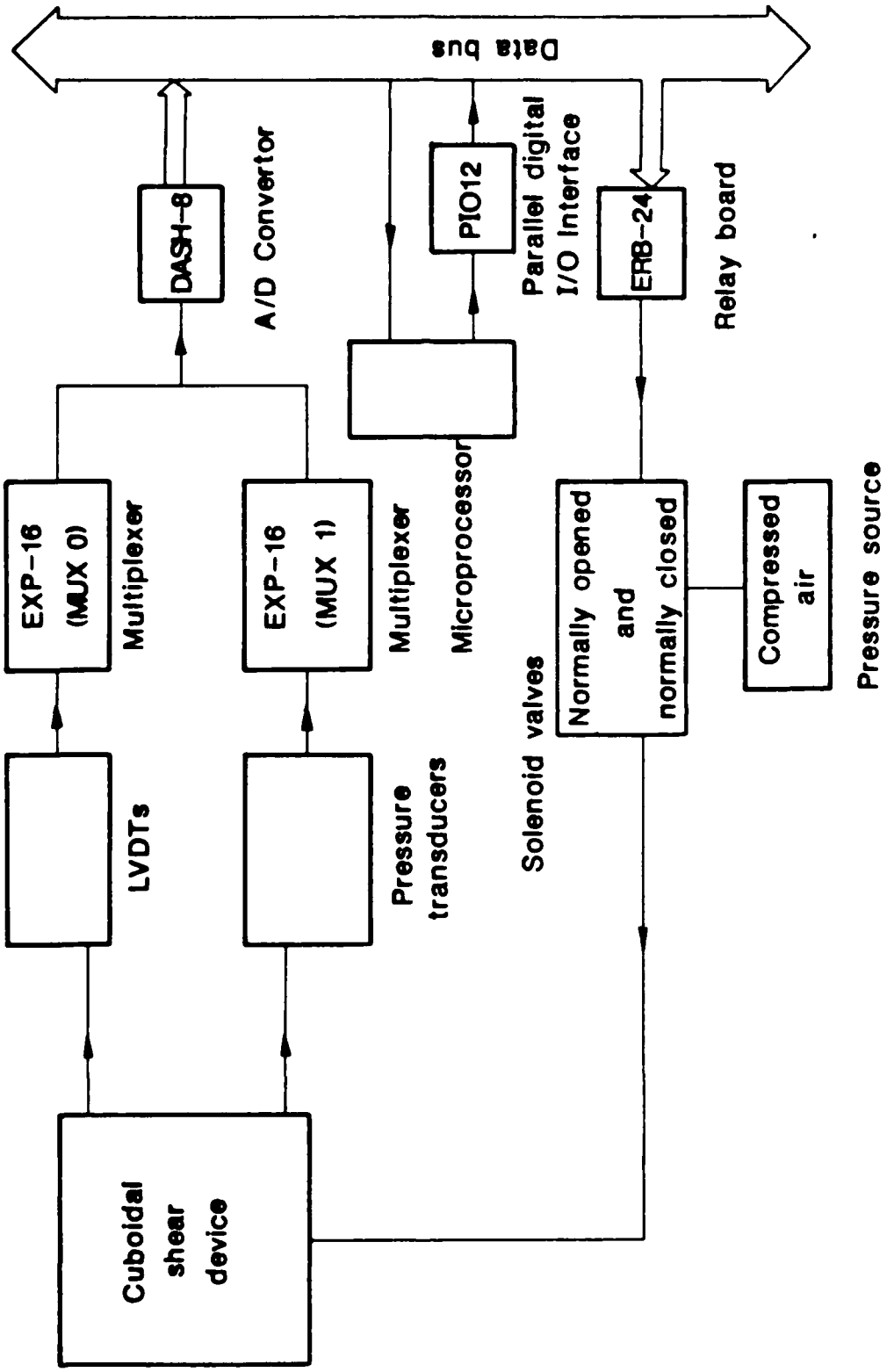

Figure 3.6 Schematic Diagram of the Data Acquisition System

specimens, in a Patterson-Kelley dual barrel mixer. During the last few minutes of mixing, samples for water content were taken at three different times. They were found to vary $\pm$ 0.5%. To reduce friction, silicone oil was applied to the inner walls of the consolidometer and the lower chamber was lined with teflon. The porous stones were boiled in deionized water to remove any entrapped air. Filter papers (102 mm square, Whatman No. 1) were used on both porous stones. The slurry was deaired under a vacuum of 500 mm mercury for about 6 hours, and was poured into the consolidometer.

3.2.2 Slurry Consolidation

To avoid slurry being squeezed out between the walls and piston seal, the first increment applied was always very low, for example 10 to 20 kPa. All specimens were consolidated to about 170 kPa, applied in two equal increments, in the slurry consolidometer. The lower chamber of the consolidometer was dimensioned such that the extruded specimen was exactly 102 mm on each side. Thus no trimming was required prior to insertion into the cuboidal shear device. A hydraulic jack with a 102 mm square teflon piston was used to extrude the specimen. The teflon lined lower chamber, application of silicone oil, and the teflon piston served to reduce the friction. The consolidated cake from the upper chamber was used in oedometer tests to study the directional variation of compressibility and consolidation characteristics.

3.2.3 Seating the Specimen in the Space Frame

Silicone oil was applied to the space frame and the membranes. The extruded specimen with filter paper on each side was placed at the center of the space frame. To prevent air bubbles entering the needle piezometer, the needle and the attached fittings were flushed with water and capped by the

transducer when fully saturated. Then the needle was inserted through a diagonal port into a bottom corner of the specimen.

3.2.4 Flushing and Back Pressure Saturation

All specimens were flushed with a low head of about 10 kPa at the air-water interface under an all around confining pressure of about 25 to 30 kPa. Back pressure was increased in increments until it reached about 415 kPa, and it was maintained for 24 hours before consolidation was started. The difference between the all around cell pressure and back pressure was maintained at 25 to 30 kPa throughout the saturation process. At the end of saturation, a B-parameter check gave values greater than 0.96 in all cases. The applied back pressure was maintained throughout consolidation and shearing.

3.2.5 Consolidation in the Cuboidal Shear Device

After ensuring full saturation, the specimen was consolidated isotropically or anisotropically to stresses higher than during slurry consolidation. This obscured any effects of friction and disturbance encountered previously. The one dimensional consolidation was carried out with servo control. The flow chart for this process is shown in Fig. 3.7.

The filter paper on all six sides of the specimen allows drainage in both the horizontal and vertical directions. This reduces the time required for consolidation. The deformation-time curves (e.g., Fig. 3.8) were very similar in shape to those from oedometer tests, except that c_v is larger due to additional drainage taking place horizontally. For normally consolidated kaolinite, the average value of c_v was 30×10^{-4} cm^2/s in oedometer tests and 60×10^{-4} cm^2/s in the cuboidal shear tests.

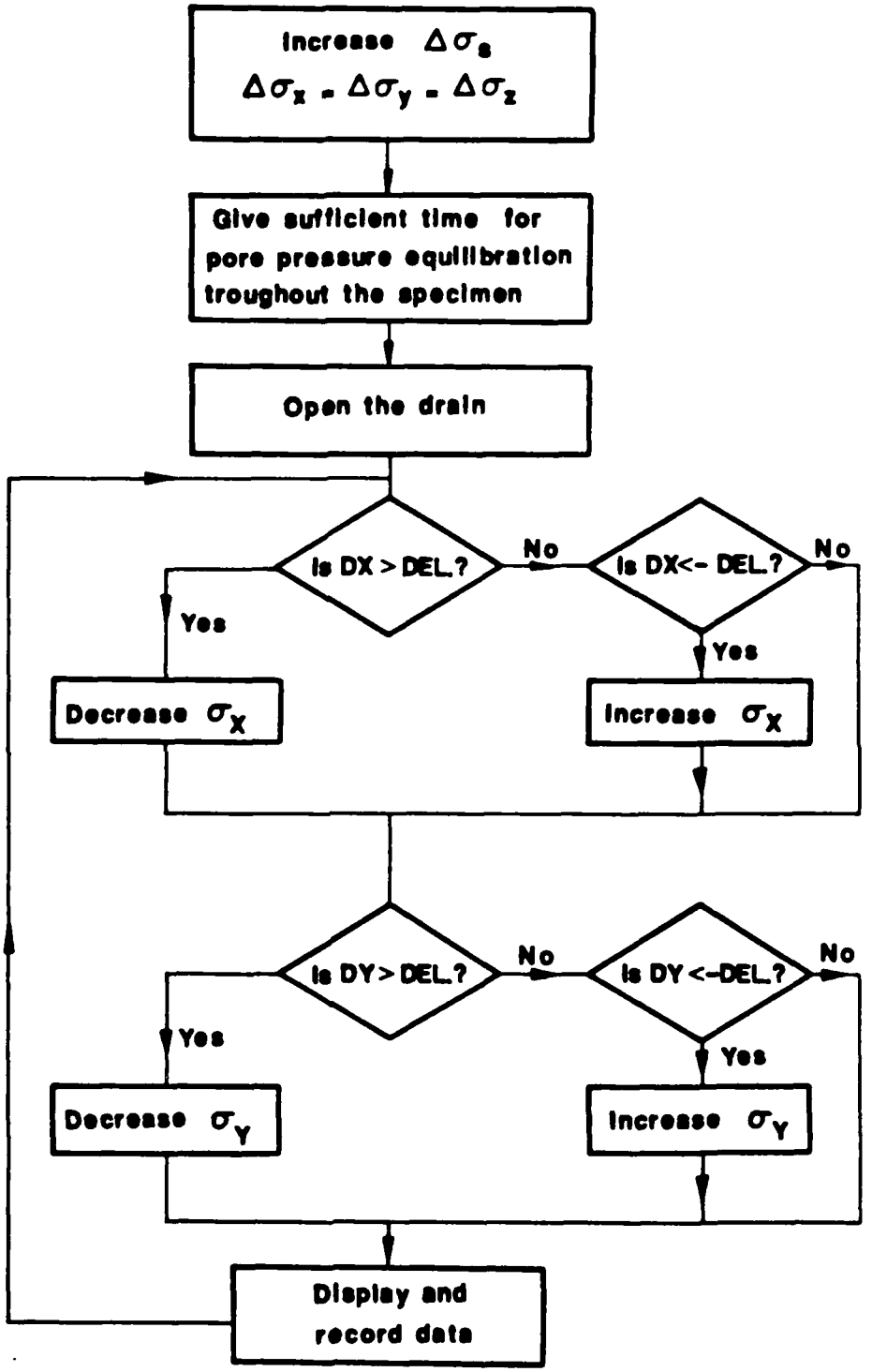

Figure 3.7 Flow Chart for Servo Controlled K_o Consolidation

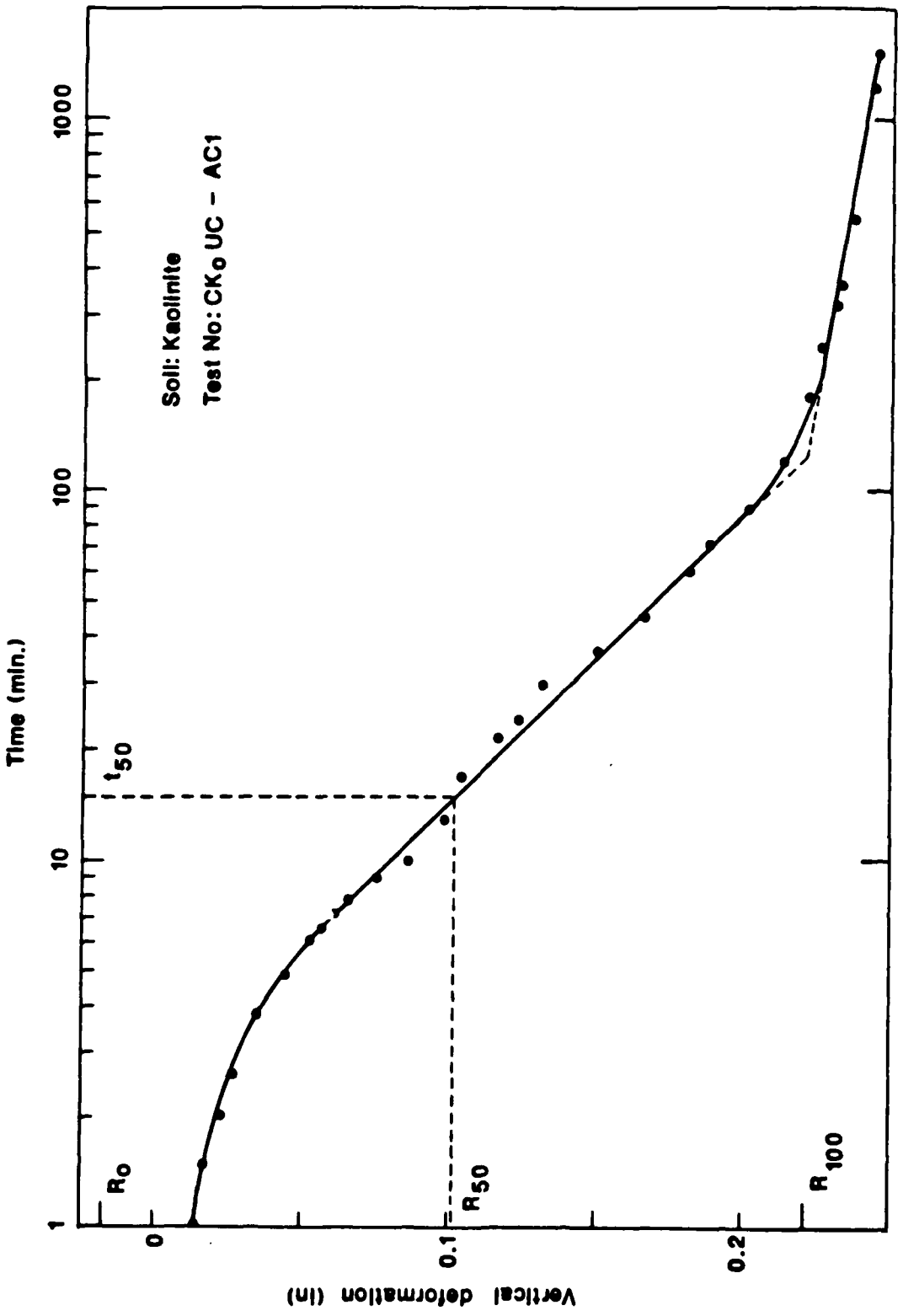

Figure 3.8 Deformation-Time Curve for One Dimensional Consolidation in Cuboidal Shear Device

3.2.6 Undrained Shear

All specimens were sheared under undrained conditions with stress controlled loading. The loading rate was about 15 to 20 kPa applied every 15 minutes. The strain rate was chosen such that failure occurs in about 3 hours.

3.2.7 Experimental Program

All tests were performed on normally consolidated specimens. Two different stress paths, axial compression and lateral compression, were applied to isotropically or anisotropically consolidated kaolinite and K50 specimens under undrained conditions. Five tests on K50 and four tests on kaolinite were performed. The experimental results are given in Table 3.1 and 3.2.

AC refers to axial compression tests where the major principal stress acts vertically throughout the entire test. The other two total principal stresses during loading remained the same as they were at the end of consolidation and they were maintained equal throughout the test. This series of tests is similar to conventional CIUC and CK_oUC tests.

LC refers to lateral compression tests where the applied load during shear was increased horizontally in one direction. The other two total principal stresses remained the same as they were at the end of consolidation. This is different from lateral compression tests performed in triaxial cells where two of the principal stresses are always equal.

The interpretation of the cuboidal shear test is quite simple and straightforward. The displacements, principal stresses, and pore pressures are stored on diskettes throughout the entire test. From the displacements and original dimensions of the specimen, the strains can be computed. By neglecting the friction on the faces, it can be assumed that the normal stresses and strains

Table 3.1 Cuboidal Shear Test Results for Kaolinite

Test	σ'_{vc} (kPa)	A_f	$\frac{\tau_f}{\sigma'_{vc}}$	ϕ' (deg)	M
CIUC-AC1	259.9	1.15	0.29	26.9	1.07
CIUC-LC1	275.8	1.04	0.29	25.1	0.99
CK_oUC-AC1	275.8	1.03	0.27	24.2	0.95
CK_oUC-LC1	275.8	0.82	0.29	43.9	1.79

Table 3.2 Cuboidal Shear Test Results for K50

Test	σ'_{vc} (kPa)	A_f	$\frac{\tau_f}{\sigma'_{vc}}$	ϕ' (deg)	M
CIUC-AC1	331.0	1.06	0.34	31.9	1.28
CIUC-AC2	282.7	1.07	0.34	32.2	1.30
CIUC-LC1	282.7	1.11	0.32	32.4	1.30
CK_oUC-AC	235.8	1.05	0.32	29.1	1.16
CK_oUC-LC	238.6	0.75	0.29	42.9	1.76

on the sides of the specimen are principal components of the stress and strain tensors.

Stress Path Followed in the Tests

Four different stress paths, CIUC-AC, CIUC-LC, CK_oUC-AC, and CK_oUC-LC, were applied to the kaolinite and K50 specimens. The isotropic or anisotropic consolidation and undrained shear were carried out as described before. The parameters obtained for kaolinite and K50 are given in Tables 3.1 and 3.2 respectively.

Undrained Strength Anisotropy

Undrained strength anisotropy consists of two major components. One is inherent anisotropy, which occurs due to preferred particle arrangement during sedimentation. Particles are oriented in such a way that their long axis is perpendicular to the major principal stress during deposition. Therefore the fabric is not identical in all directions. The other component is stress induced anisotropy which is caused by the anisotropic state of stress at the end of consolidation. Inherent anisotropy means that the fabric is anisotropic and the soil behaves anisotropically even if the initial stress state is isotropic. Stress induced anisotropy means that the soil behaves anisotropically depending on the direction of loading due to its initial anisotropic stress state even if the soil properties such as c' and ϕ' are isotropic.

To quantify undrained strength anisotropy, several techniques have been proposed by previous researchers (Aas, 1965; Duncan and Seed, 1966; Lo and Morin, 1972; Berre and Bjerrum, 1973; Krishnamurthy, et al., 1980; Nakase and Kamei, 1986). In the experimental program described herein, the specimen is never rotated. The axis remains vertical during consolidation and

shear. Anisotropy is measured by the ratio of the undrained shear strength of a horizontally loaded specimen to the undrained strength of a vertically loaded replicate specimen. The anisotropy with respect to compressibility and consolidation characteristics are also studied. The results are given in Tables 3.3 and 3.4.

3.3 Analysis

For axial compression of isotropically or K_o consolidated specimens, normalized undrained shear strength and ϕ' were considerably greater for K50 than kaolinite. Skempton's A_f was about the same for both soils.

For kaolinite and K50, the parameters obtained from CIUC-AC and CIUC-LC tests were essentially the same (Tables 3.1 and 3.2) and the stress paths followed during the tests were similar. Therefore, upon isotropic consolidation, the direction of loading did not have any impact on the subsequent behavior during shear. In other words, inherent anisotropy of the soil fabric was insignificant for both soils.

Nevertheless, even for soils which are isotropic with respect to the initial fabric, shear strength will depend to a large extent on the stress path followed during shear. Depending on where the effective stress path intersects the failure envelope, different values will be observed for shear strength. For example, in triaxial compression tests (CIUC-AC and CK_oUC-AC tests in cuboidal shear device), while both the total horizontal principal stresses are maintained constant, the total vertical principal stress is increased to failure. In a pressuremeter test, the total vertical stress remains constant while the two horizontal principal stresses vary, one increasing and the other decreasing by the same amount. Even if the soil is isotropic and consolidated to the same stress level, the effective stress paths in the pressuremeter test and triaxial

Table 3.3 Compressibility and Consolidation Characteristics

Soil	Vertical specimen			Horizontal specimen		
	C_c	C_r	$c_v \times 10^4$ cm^2/s	C_c	C_r	$c_v \times 10^4$ cm^2/s
Kaolinite	0.35	0.054	10-20	0.24	0.073	20-40
K50	0.22	0.022	15-40	0.19	0.022	15-40

Table 3.4 Measures of Anisotropy

Soil	$\frac{(C_c)_H}{(C_c)_V}$	$\frac{(C_r)_H}{(C_r)_V}$	$\frac{(c_v)_H}{(c_v)_V}$	$\frac{\left[\frac{\tau_f}{\sigma'_{vo}}\right]_H}{\left[\frac{\tau_f}{\sigma'_{vo}}\right]_V}$
Kaolinite	0.68	1.35	2.0	1.00 (CIUC)
				1.07 (CK_oUC)
K50	0.86	1.00	1.00	0.94 (CIUC)
				0.91 (CK_oUC)

compression test would be quite different.

For both soils, a significant increase in ϕ' was observed for lateral loading of one dimensionally consolidated specimens (Figs. 3.9 and 3.10). This indicates that the failure envelopes in the field would not be the same for horizontal and vertical loading. Saada and Bianchini (1975) tested three K_o consolidated clays under different stress paths in a hollow cylinder apparatus. They reported much higher values for ϕ' in extension than in compression for all three clays. The difference was as high as 23° for one of the clays, which is of the same order as in the case of kaolinite and K50 observed in the present study. In other words, the failure envelope is not unique, and it depends on the direction of loading. It is necessary to use the ϕ' appropriate to the loading situation.

At the end of one dimensional consolidation, $\sigma_x' = \sigma_y' = K_o \sigma_z'$. Here, subscripts x and y refer to the horizontal directions and z refers to the vertical direction. During vertical loading (i. e., CK_oUC-AC), σ_x and σ_y remain the same as they were at the end of consolidation; σ_z is increased until failure occurs. The major principal stress acts in the same direction, vertically, during consolidation and shear. At the end of consolidation itself the specimen is subjected to a shear stress. Therefore, when loaded in the same direction, very few increments are required to reach failure. During horizontal loading (i. e., CK_oUC-LC), σ_x and σ_z remain the same as they were at the end of consolidation, and σ_y is increased until failure occurs. During the initial stages of loading, σ_y is the intermediate principal stress. Upon further increase, σ_y exceeds σ_z, and thereafter becomes the major principal stress until failure occurs. In this case rotation of principal stresses takes place.

The normalized shear strength was about the same for CK_oUC–AC and

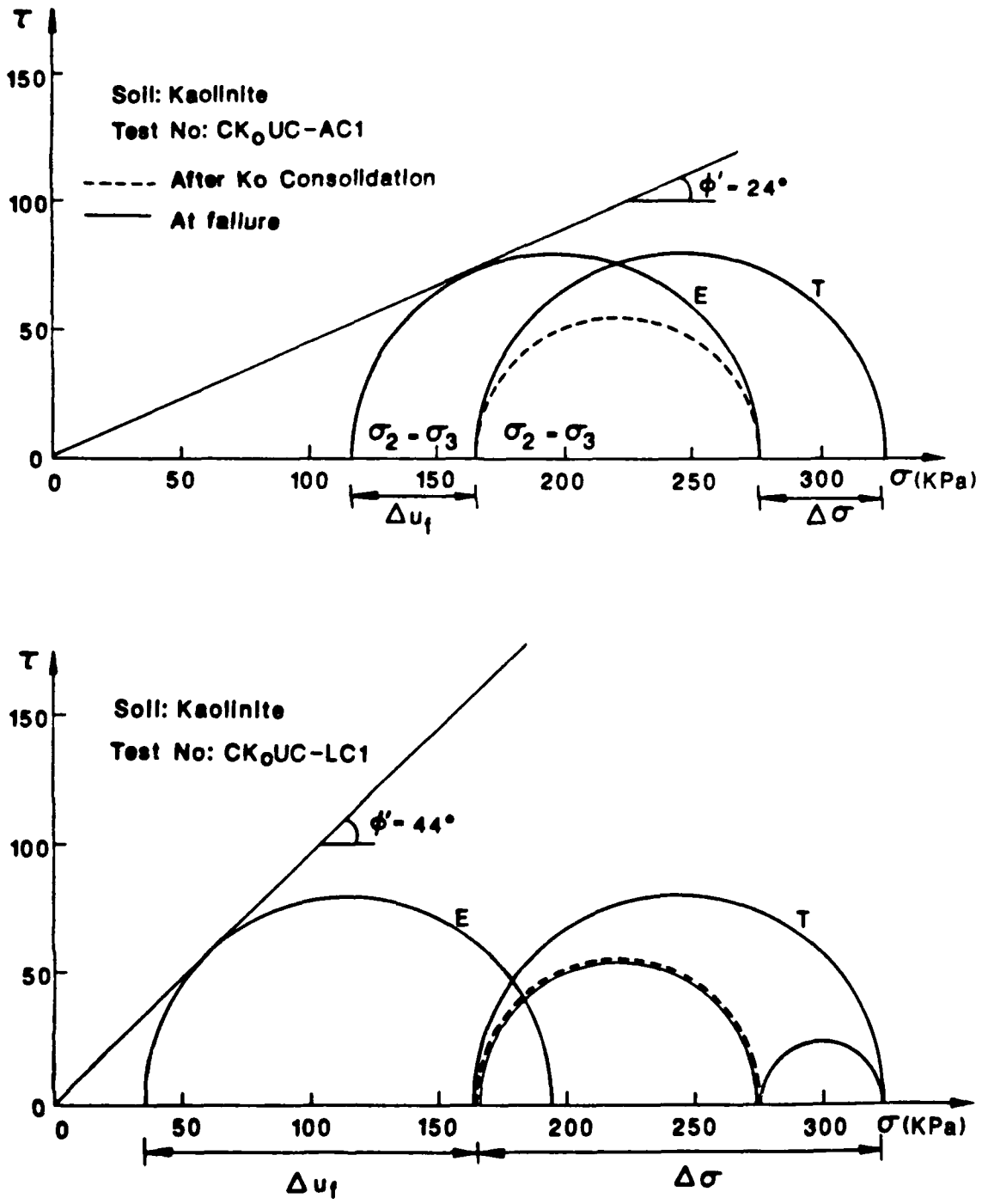

Figure 3.9 Mohr Circles for CK_oUC-AC and CK_oUC-LC for Kaolinite

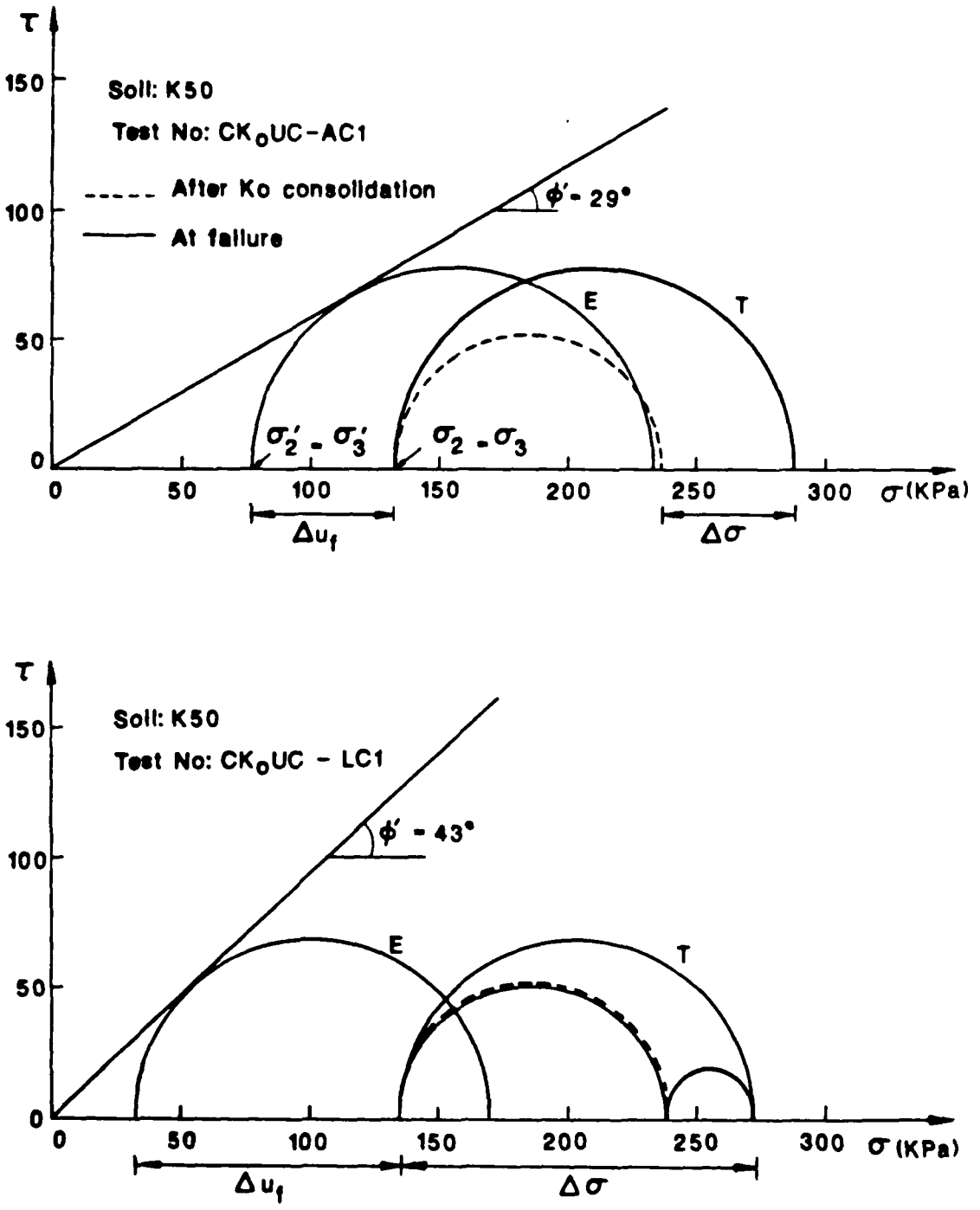

Figure 3.10 Mohr Circles for CK_oUC-AC and CK_oUC-LC for K50

CK_oUC–LC tests (Tables 3.1 and 3.2). Therefore, for replicate specimens consolidated to the same stress level, the Mohr circles at failure in terms of total stresses are about the same. The total stress increase ($\Delta\sigma$) required to cause failure is considerably greater for horizontal loading, mainly due to principal stress rotation. A_f was slightly less, but of the same order, for horizontal loading. Therefore, excess pore pressure at failure was considerably greater for horizontal loading. This shifts the Mohr circle in terms of effective stresses for CK_oUC–LC tests more to the left and the failure envelope becomes steeper. The marked increase in ϕ', or in other words a steeper failure envelope, for horizontal loading contributes greatly to the consistent overestimation of undrained shear strength in pressuremeter testing.

The compression index (C_c), recompression index (C_r), and coefficient of consolidation (c_v for normally consolidated specimens in the stress range of 200 to 700 kPa) of horizontally and vertically trimmed specimens of kaolinite and K50 given in Table 3.3 show that compressibility and consolidation parameters appear to be more anisotropic for kaolinite than for K50 (Table 3.4). In terms of undrained shear strength, the anisotropy was less prominent for both soils.

3.4 Summary

Isotropically or anisotropically consolidated specimens were loaded horizontally or vertically under undrained conditions in a cuboidal shear device. A significantly larger ϕ' was observed when the loading was horizontal in direction, which is the case in pressuremeter testing. The steeper failure envelope can contribute significantly to the observed overestimation of the undrained shear strength in the pressuremeter testing in clays when compared to laboratory test results.

CHAPTER 4

INTERPRETATION OF PRESSUREMETER TEST RESULTS

A new interpretation technique to evaluate stress-strain and strength relationships from pressuremeter test data has been developed in the research. It uses the Simplex curve fitting algorithm, and essentially all the existing interpretation methods can be included in the algorithm.

4.1 Interpretation by Curve Fitting:

The currently available pressuremeter interpretation procedures (a detailed review is given in the dissertation by Huang, 1986) can be categorized as either by derivatives (Group 1) or by curve fitting (Group 2). Taking derivatives from data points either numerically or manually, is subject to large scatter (Ladd, et al., 1980; Battaglio, et al., 1981). In order to minimize the "noise", some type of curve fitting procedure is often employed. Thus in this case, methods of Group 1 become essentially the same as the methods in Group 2. The curve fitting methods differ from each other by the assumed function(s) for the soil σ-ϵ relationship and the techniques used for curve fitting. In the methods by Prevost and Hoeg (1975) and Arnold (1980), a single continuous function is assumed for the σ-ϵ relationship, and curve fitting can be performed with a conventional least-squares algorithm. However, in the Gibson and Anderson (1961) and Denby (1978) procedures, two different σ-ϵ functions are used for the pre- and post-peak strain data points. The least-squares algorithm is not well suited for these procedures. This is probably one of the reasons these authors suggest that manual graphical curve

fitting techniques be used, even though such procedures are time consuming and rather operator dependent. The purpose of all the methods is to derive soil σ-ϵ and strength parameters from the predicted cavity expansion curve which best fits the data points. If a "universal" numerical algorithm could be used, then all the existing interpretation methods would differ only by the assumptions made for the soil σ-ϵ behavior, e.g. elasto-plastic, hyperbolic, etc. Errors and problems associated with the differences in curve fitting techniques would thus be eliminated. The Simplex algorithm is proposed herein as the curve fitting algorithm for this purpose.

4.2 Curve Fitting by The Simplex Algorithm:

The Simplex algorithm has been used extensively as an optimization tool in linear programming (Kreko, 1968). Caceci and Cacheris (1984) described the application of the Simplex algorithm to curve fitting. Consider a set of N data points (x_i, y_i) to be fitted by a series of functions $f_i(x)$ as shown in Fig. 4.1. The coefficients of the functions and the x values where the functions $f_i(x)$ and $f_{i+1}(x)$ intersect are the variables to be optimized. The purpose of the optimization is to determine a set of variables which correspond to the lowest sum of the squares of residuals, SSR, defined as:

$$SSR = \sum_{i=1}^{n_1} W_i(f_1(x_i)-y_i)^2 + \sum_{i=n_1+1}^{n_2} W_i(f_2(x_i)-y_i)^2 + \cdots$$

$$+ \cdots \sum_{i=n_{k-1}+1}^{N} W_i(f_k(x_i)-y_i)^2 \qquad (4.1)$$

where the W_is are weighting factors (optional), and N is the total number of data points.

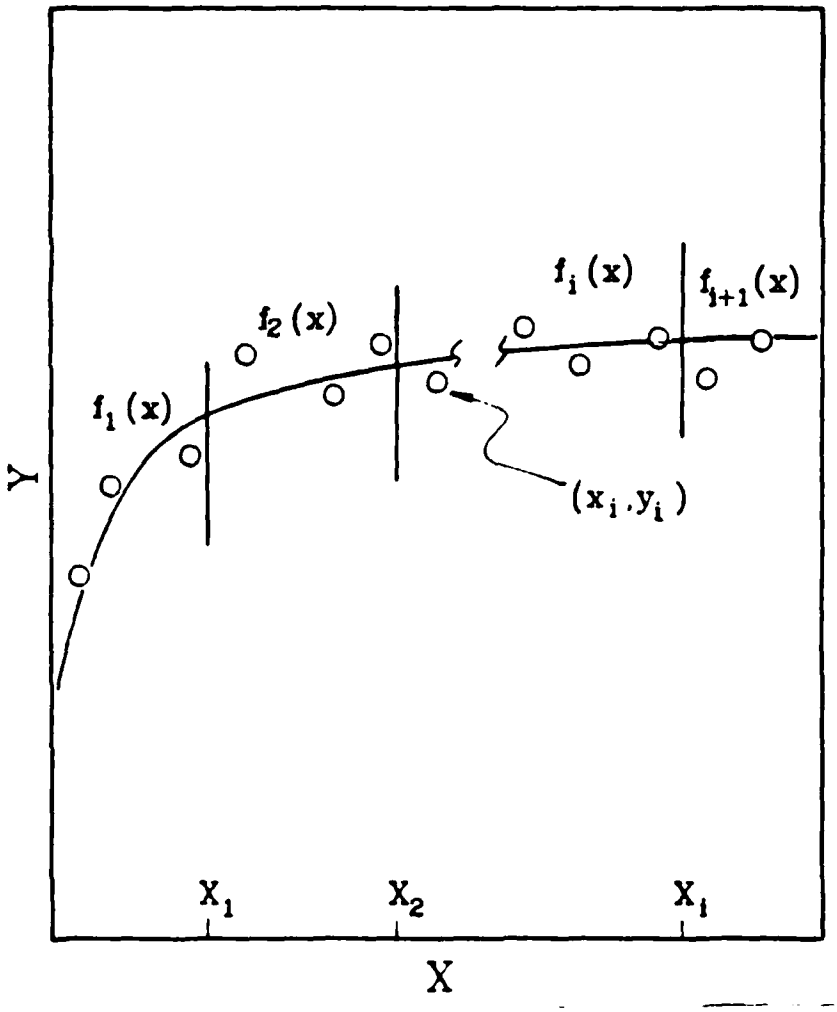

Figure 4.1 Data points fitted to a series of functions.

The basic concept is to consider each set of M variables as a vector in a space of dimension M (M is the total number of variables to be optimized, i.e. coefficients of the functions and the x values as stated above). The vector is called a vertex and a Simplex is a geometrical figure which consists of M + 1 vertexes. For example, if a set of data points is to be fitted to a hyperbolic function:

$$y = \frac{bx}{a + x} \tag{4.2}$$

The coefficients a and b must be optimized. The total number of variables to be optimized is 2 (M = 2) and the Simplex is a triangle (M + 1 = 3) in a two dimensional space (Fig. 4.2). The optimization starts by arbitrarily assigning values to the M + 1 vertexes. To reach the lowest SSR, the Simplex is moved according to the following rules: (1) Find the vertexes with the highest (worst) and lowest (best) SSR; and (2) Replace the worst vertex by another one determined according to one of four mechanisms: reflection, expansion, contraction, and shrinkage (Figure 4.2). Details on these rules are given elsewhere (Huang, Chameau and Holtz, 1986).

In the interpretation of PMT results when using curve fitting methods, the general procedure is to express the assumed σ-ϵ relationship as a function (or a set of functions):

$$(\sigma_r - \sigma_0) = f_1(\epsilon_r) \text{ for } 0 \leq \epsilon_r \leq \epsilon_1$$

$$\cdots\cdots\cdots\cdots \tag{4.3}$$

$$(\sigma_r - \sigma_0) = f_n(\epsilon_r) \text{ for } \epsilon_{n-1} \leq \epsilon_r \leq \epsilon_n$$

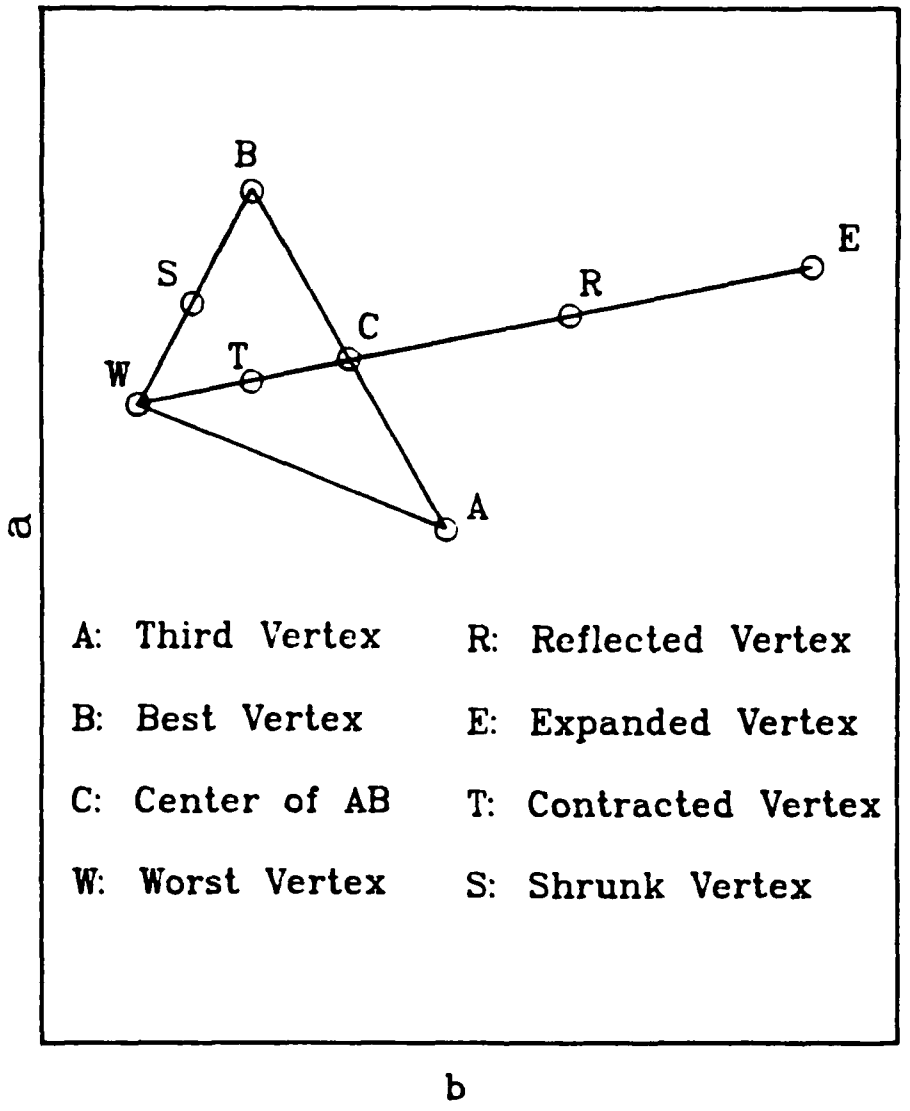

Figure 4.2 A two dimensional Simplex and its optimization mechanisms.

Then Eq. 4.3 is integrated to satisfy the boundary conditions and obtain a function (or a series of functions) of probe pressure P_r versus radial strain at the probe boundary, ϵ_{ro}:

$$P_r = f_1(\epsilon_{ro}) \text{ for } 0 \leq \epsilon_{ro} \leq \epsilon_1$$

$$\cdots\cdots\cdots\cdots \qquad (4.4)$$

$$P_r = f_n(\epsilon_{ro}) \text{ for } \epsilon_{n-1} \leq \epsilon_{ro} \leq \epsilon_n$$

The interpretation of PMT data can then be performed by curve fitting Eq. 4.4 to the data points. The best vertex at the end of the Simplex optimization yields the coefficients of Eqs. 4.3 and 4.4. The specific functions and parameters to be optimized depend only on the choice of the σ-ϵ relationship. These functions and parameters are listed in Table 4.1 for four common interpretation techniques.

A program called HSIMPLE was written on a personal computer to perform the Simplex optimization. The user can select any or all of the four methods in Table 4.1 to interpret pressuremeter data using the Simplex optimization. Other σ-ϵ functions, such as Ramberg-Osgood (Desai and Christian, 1977) can also be included in the program.

Fig. 4.3 shows the data points and the probe expansion curves plotted using the functions determined by HSIMPLE for test CP12 of our experimental program. Also shown in Fig. 4.3 are the plots of principal stress difference $(\sigma_r - \sigma_\theta)$ versus radial strain. Table 4.2 shows the various parameters obtained for test CP12. Except for Arnold's (1981) method, the derived undrained shear strengths agreed within 6%. The standard deviations shown in Table 4.2 indicate how close the curve fitting is. They range from 2.42 to

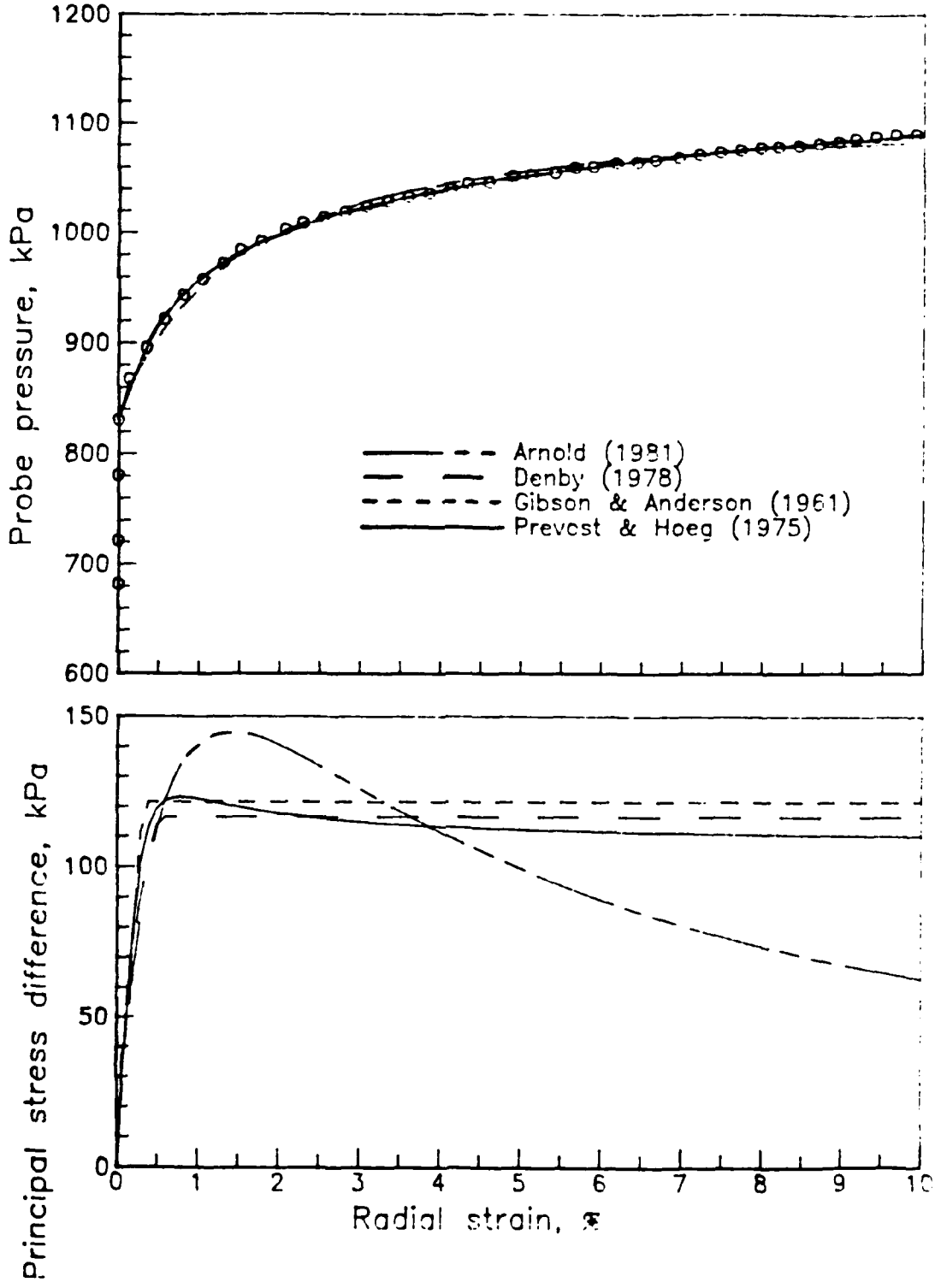

Figure 4.3 Pressuremeter data and results of interpretation (data from test CPI2).

Table 4.1 Functions and parameters to be optimized.

Method	Pressuremeter functions	Soil σ–ϵ functions	Parameters to be optimized
Arnold (1981)	$P_r = Q + \frac{b\epsilon_{r0}}{a + \epsilon_{r0}}$	$\sigma_r - \sigma_\theta = \frac{2ab\epsilon_r}{(a + \epsilon_r)^2}$	Q, a, b
Denby (1978)	$P_r = \frac{\tau_u}{R_f} \ln\left(1 + \frac{R_f}{\tau_u} 2G_i\epsilon_{r0}\right) + \sigma_h$ for $0 \leq \epsilon_{r0} \leq \frac{\tau_u}{2G_i(1 - R_f)}$	$\sigma_r - \sigma_\theta = \frac{2\epsilon_r}{1/2G_i + (R_f/\tau_u)\epsilon_r}$ for $0 \leq \epsilon_r \leq \frac{\tau_u}{2G_i(1 - R_f)}$	G_i, R_f, τ_u, σ_h
	$P_r = \tau_u \ln\left[\frac{2G_i(1 - R_f)\epsilon_{r0}}{\tau_u}\right] + \frac{\tau_u}{R_f} \ln\left(\frac{1}{1 - R_f}\right) + \sigma_h$ for $\epsilon_{r0} > \frac{\tau_u}{2G_i(1 - R_f)}$	$\sigma_r - \sigma_\theta = 2\tau_u$ for $\epsilon_r > \frac{\tau_u}{2G_i(1 - R_f)}$	
Prevost & Hoeg (1975) (strain softening)	$P_r = \sigma_h + \frac{a}{2(3c)^{1/2}}\left[\frac{b}{c^{1/2}} \ln(1 + c\bar{\epsilon}^2) + 2\tan^{-1}(c^{1/2}\bar{\epsilon})\right]$ $\bar{\epsilon} = \frac{2}{3^{1/2}}\epsilon_{r0}$	$\sigma_r - \sigma_\theta = \frac{2a}{3^{1/2}} \frac{b\bar{\epsilon}^2 + \bar{\epsilon}}{1 + c\bar{\epsilon}^2}$ $\bar{\epsilon} = \frac{2}{3^{1/2}}\epsilon_r$	a, b, c, σ_h
Prevost & Hoeg (1975) (strain hardening)	$P_r = \sigma_h + \frac{1}{3^{1/2}} q_{ult} \ln\left(\frac{d + \bar{\epsilon}}{d}\right)$	$\sigma_r - \sigma_\theta = \frac{2}{3^{1/2}} q_{ult} \frac{\bar{\epsilon}}{d + \bar{\epsilon}}$	d, q_{ult}, σ_h
Gibson & Anderson (1961)	$P_r = \sigma_h + 2G\epsilon_{r0}$ for $0 \leq \epsilon_{r0} \leq \tau_u/2G$	$\sigma_r - \sigma_\theta = 4\epsilon_r G$ for $0 \leq \epsilon_r \leq \tau_u/2G$	G, τ_u, σ_h
	$P_r = \sigma_h + \tau_u + \tau_u \ln\left[\frac{G}{\tau_u} \frac{2\epsilon_{r0} + \epsilon_{r0}^2}{(1 + \epsilon_{r0})^2}\right]$ for $\epsilon_{r0} > \tau_u/2G$	$\sigma_r - \sigma_\theta = 2\tau_u$ for $\epsilon_r > \tau_u/2G$	

Table 4.2 Parameters Derived from Test CPI2.

METHOD	S_u^{pmt} (kPa)	G_i (kPa)	ϵ_{rf} %	STANDARD DEVIATION (kPa)
ARNOLD	73	10340	1.40	5.0
DENBY	58	14250	0.53	2.4
GIBSON AND ANDERSON	61	9300	0.33	2.6
PREVOST[a] AND HOEG	62	13600	0.78	2.5

(a) strain softening function

4.98 kPa with the worst value corresponding to Arnold's method. With a total pressure range on the order of 300 kPa in this particular test, these standard deviations represent a possible error of 0.8% to 1.7% in the curve fitting. However, it should be kept in mind that the closeness of curve fitting for different methods may vary from test to test depending on how well the assumed σ-ϵ relationship agrees with the in situ soil behavior.

The Simplex algorithm can provide an objective means for identifying the most appropriate interpretation technique for a particular test. The fitted curve can be selected which gives the minimum standard deviation. For the example in Fig. 4.3, Denby's (1978) method appears to be the most appropriate one with a standard deviation of 2.42 kPa, but for this particular test the Gibson and Anderson (1961) and Prevost and Hoeg (1975) methods are also very good.

All chamber pressuremeter test results presented in this report were interpreted using HSIMPLE. The technique can be adopted with minor modification for tests performed in situ. The differences between the results from HSIMPLE are entirely due to the $(\sigma_r - \sigma_0)$ relationships assumed in the method selected. Systematic errors which may be caused by different curve fitting techniques are therefore eliminated. Any interpretation technique can be incorporated within this scheme. For example the modification to the Prevost-Hoeg method described in the next chapter will be added to the program in the future.

CHAPTER 5

EFFECT OF DISTURBANCE

5.1 Introduction

During the boring process prior to a pressuremeter test, an annulus of soil around the borehole is softened, the strength of the soil in this annulus is reduced, and initial unloading of the soil may occur. The degree of softening depends on the sensitivity of the soil. The paradoxical effect of the presence of such a softened soil is to predict from the pressuremeter expansion curve an undrained strength larger than actually exists in situ (Baguelin, et al. 1978).

In this research, parametric studies were performed to evaluate the effect of a disturbed annulus, including initial unloading, in more detail. These studies were based on: (1) an analytical technique to predict pressuremeter expansion curves based on the strain path method and an anisotropic elastic-plastic soil model; and (2) a fitting technique to determine stress-strain curves from pressuremeter expansion curves. These two techniques are summarized first and their validity assessed from experimental results. Then, the results of the parametric studies are described. Experimental work which shows the potential of pore size distribution to determine the extent of disturbance is also presented.

5.2 Prediction of Pressuremeter Expansion Curve

It is assumed that the pressuremeter is very long so that the expansion takes place under axisymmetric, plane strain conditions. The cavity expansion

problem can be solved analytically if the soil is assumed to be elastic-perfectly plastic (Gibson and Anderson, 1961). However, when more sophisticated constitutive models are used to represent the soil behavior, numerical methods are required (e.g. Carter, et al., 1979). In this research, the Prevost model (1978) was chosen to represent the soil behavior.

The pressuremeter expansion curve is usually expressed as a relationship between the radial stress and the radial strain at the cavity boundary. If the constitutive model representing the soil behavior is known, then it is possible to calculate the strains knowing the applied stresses, and vice versa. Since the expansion of the pressuremeter is assumed to take place under axisymmetric, plane strain conditions, the strain field around the pressuremeter is fully defined in terms of the radial strain at the cavity wall. Therefore, it is convenient to calculate the stresses using the known strains. The following steps describe the method (Baligh, 1985) used to calculate the radial stress at the cavity boundary:

1. Calculate the incremental strains at selected points along a radial line;
2. Estimate initial stresses;
3. Compute the deviatoric stresses using a constitutive model;
4. Compute the total stresses from equilibrium conditions.

The four steps of the strain path method described above were incorporated into a computer program to analyze the expansion of a cylindrical cavity with a thin remolded annulus around it. A detailed description of the features of the program can be found in Prapaharan (1987).

The constitutive model (Prevost, 1978) used in this study can describe the anisotropic, elastic-plastic, path dependent, stress-strain behavior of clays

under undrained conditions. The model combines properties of isotropic and kinematic plasticity by introducing the concept of a field of plastic moduli which is defined in stress space by the relative configuration of yield surfaces. For any loading history, the instantaneous configuration is determined by calculating the translation and contraction (or expansion) of each yield surface. The model parameters required to characterize the behavior of any given clay can be derived entirely from conventional triaxial compression and extension test results. A detailed description of the model and the derivation of model parameters were given by Prapaharan (1987).

5.3 Determination of Stress-Strain Curve from Expansion Curve

The basic equation used in the interpretation method was derived independently by Baguelin, et al. (1972), Ladanyi (1972), and Palmer (1972), and is given by:

$$\tau = \frac{1}{2}\,\epsilon(1+\epsilon)(2+\epsilon)\,\frac{dP}{d\epsilon} \tag{5.1}$$

where, τ = shear stress

ϵ = circumferential strain at the cavity boundary

P = pressure at strain, ϵ

For small strains Eq. 5.1 can be reduced to:

$$\tau = \epsilon\,\frac{dP}{d\epsilon} \tag{5.2}$$

The stress-strain curve can be derived using Eq. 5.1 if the slope of the pressuremeter expansion curve ($dP/d\epsilon$) is known. In the past, attempts to calculate the slope graphically produced considerable scatter in the derived stress-strain curve. As a result, efforts were made to fit the pressuremeter expansion curve with curve fitting functions. Among the curve fitting equations which were considered (Prapaharan, 1987) the modified Prevost-Hoeg

equation (Ladd, et al., 1980) was the most promising since it can closely fit a curve and has a theoretical background. Nevertheless, it was found that it does not fit theoretical pressuremeter expansion curves with sufficient accuracy. Thus, we improved the Prevost-Hoeg equation to obtain a better fit for the theoretical pressuremeter expansion curves used in this study. The following equation is proposed:

$$P - P_0 = A \ln(1 + \epsilon^2) + B(\tan^{-1}(\epsilon + \hat{\epsilon})^n - \tan^{-1}\hat{\epsilon}^n) \tag{5.3}$$

The corresponding stress-stress strain relationship is:

$$\sigma_r - \sigma_\theta = (1 + \epsilon)(2 + \epsilon)\left[\frac{2A\epsilon^2}{1 + \epsilon^2} + \frac{nB(\epsilon + \hat{\epsilon})^{n-1}}{1 + (\epsilon + \hat{\epsilon})^{2n}}\right] \tag{5.4}$$

where, $\hat{\epsilon}$ is a small number. A value of 0.01 can be used for $\hat{\epsilon}$ to obtain an initial modulus comparable to those obtained with other curve fitting methods. Exclusion of $\hat{\epsilon}$ in the above equation results in infinitely large initial modulus. However, it is not desirable to use the initial modulus obtained by curve fitting methods for practical applications, as it is very sensitive to the type of equations used.

Evaluation of the Proposed Curve Fitting Equation -- The proposed curve fitting equation was evaluated by comparing the stress-strain curve derived using the equation with that obtained by the graphical method (numerical subtangent method) and the modified Prevost-Hoeg equation. Figs. 5.1 and 5.2 show that the proposed equation describes closely the stress-strain curve obtained by the numerical sub-tangent method whereas the modified Prevost-Hoeg equation fails to predict the correct stress-strain curve. The Prevost-Hoeg equation tends to give a flat post-peak response after a sharp pre-peak rise, and also the curve bends upwards at large strains if Eq.

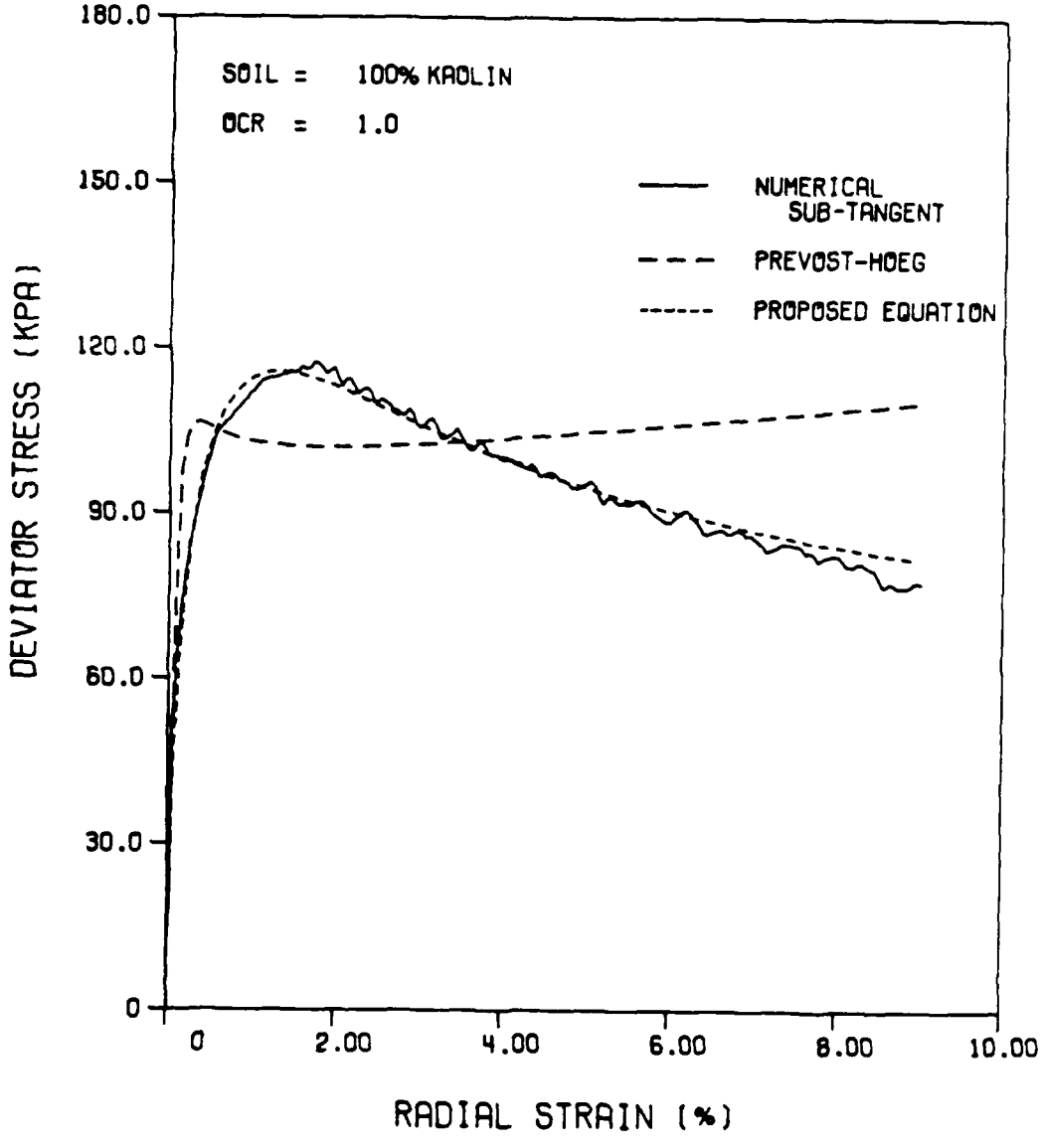

Figure 5.1 Comparison of stress-strain curves obtained by curve fitting the theoretical pressuremeter curves for 100% kaolin soil

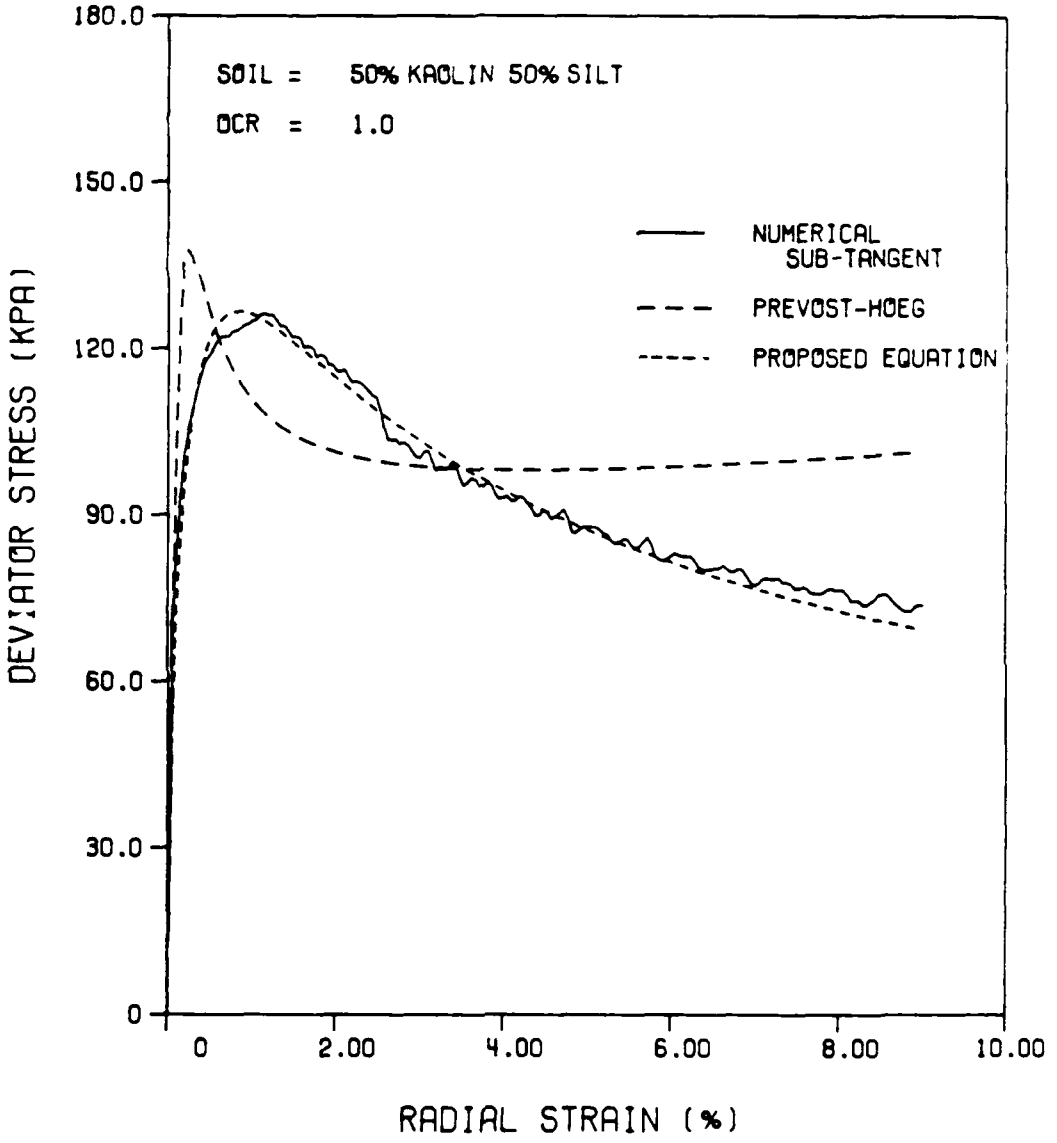

Figure 5.2 Comparison of stress-strain curves obtained by curve fitting the theoretical pressuremeter curves for 50:50 mixture of kaolin and silt

5.1 is used instead of Eq. 5.2.

5.4 Comparison to Experimental Results

The model described above was evaluated by comparing the predicted pressuremeter expansion curves with that obtained experimentally using a scale model pressuremeter in a calibration chamber (see Chapter 2 in this report). Fig. 5.3 compares the pressuremeter expansion curves obtained experimentally and that predicted theoretically for 50:50 mix of kaolin and silt. The stress-strain curve derived from the pressuremeter expansion curve is shown in Fig. 5.4. The stress-strain curves were obtained by the proposed curve fitting technique (Eqs. 5.3 and 5.4).

The model predicts the pressuremeter expansion curve and stress-strain curve reasonably well. The difference between the experimental results and the theoretical prediction is attributed to the following reasons, other than the assumptions made in the model itself:

— The inability to obtain the same K_o value in triaxial and calibration chamber tests.

— The presence of shear stress on the pressuremeter membrane due to the consolidation of soil around it.

Considering the above limitations, it is believed that the proposed model is reasonable enough to generate typical pressuremeter expansion curves, and thus to study the effect of disturbance on pressuremeter test results.

5.5 Disturbance Effects -- Parametric Study

The method described in the previous sections was used to analyze the effect of disturbance on the magnitude of the undrained strength derived from

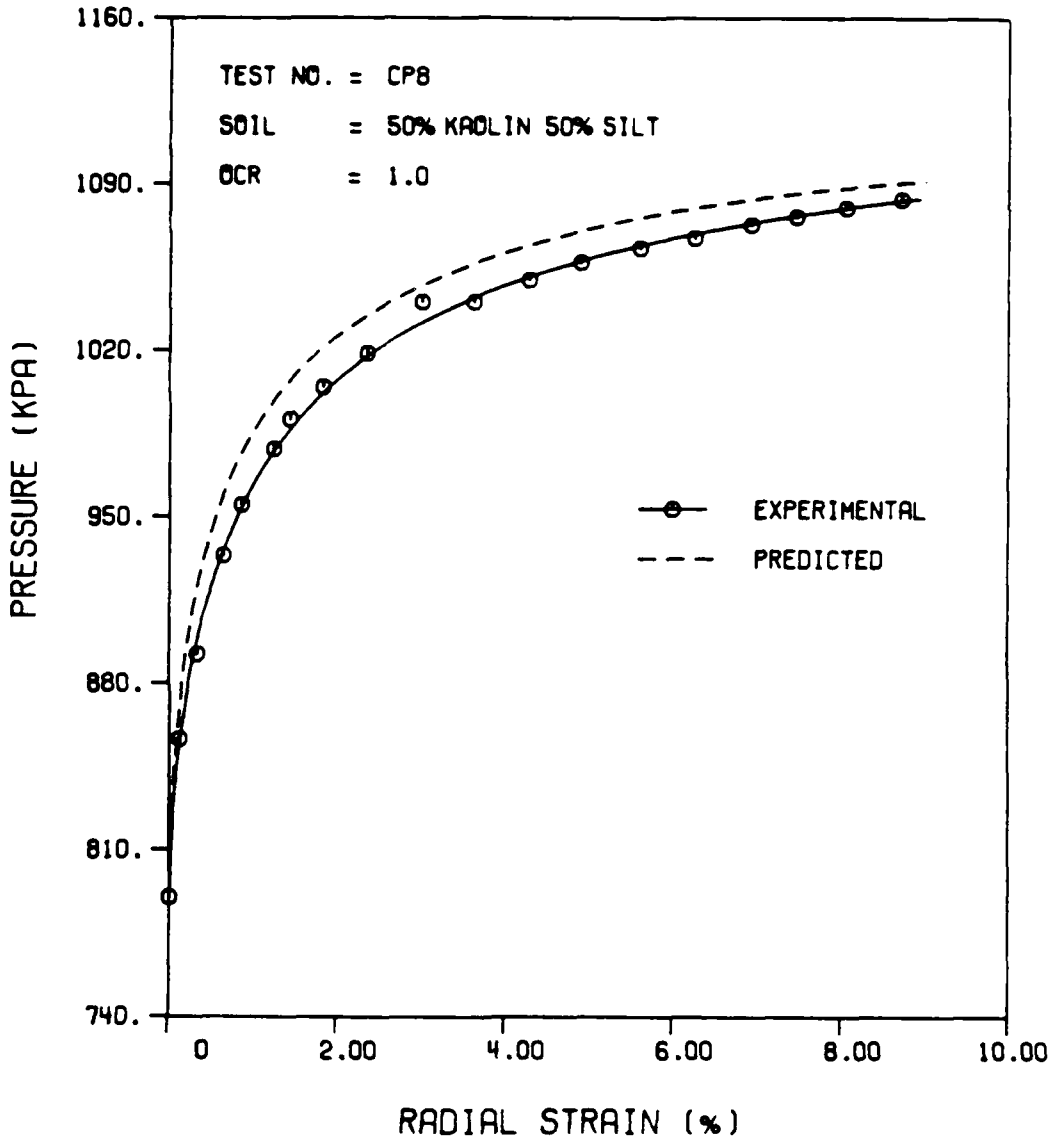

Figure 5.3 Comparison of experimental and predicted pressuremeter expansion curves for 50:50 mixture of kaolin and silt

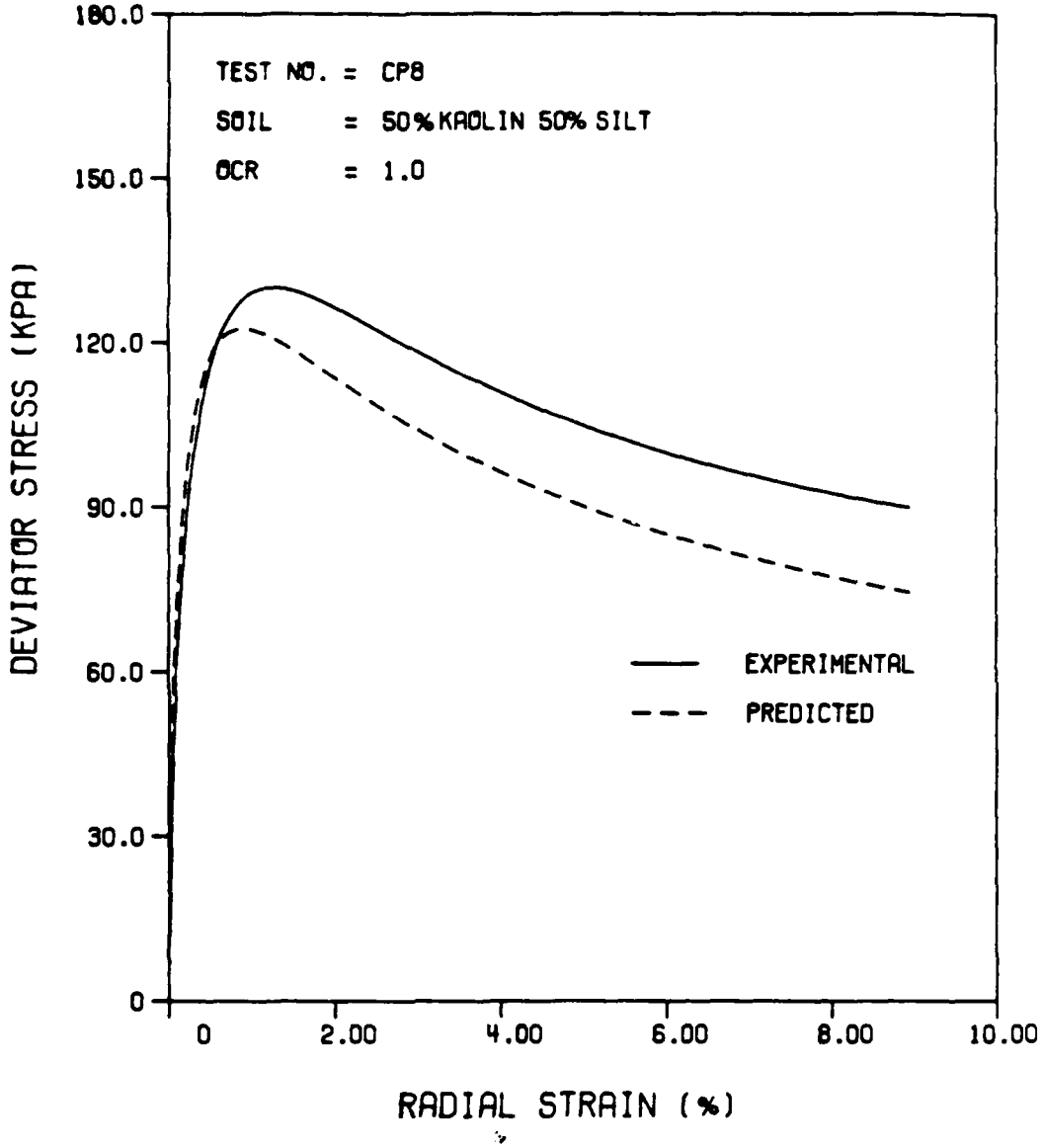

Figure 5.4 Comparison of experimental and predicted stress-strain curves for 50:50 mixture of kaolin and silt

pressuremeter tests. The thickness of the disturbed annulus was estimated by pore size distribution studies, and a hypothesis is presented to explain the effect of disturbance on undrained strength and modulus.

Thickness of the Disturbed Annulus -- An attempt was made to evaluate the use of pore size distribution studies to determine the extent of the disturbed annulus. The measurement of pore size allows one to obtain a quantitative measure of the fabric of soils. The fabric is likely to be different between disturbed and intact soil. So by comparing fabric, the thickness of the disturbed zone can be estimated.

A 10 cm cube block sample was obtained by isotropically consolidating kaolin in a true triaxial device (see Chapter 3 in this report). After consolidation, the applied stresses were released, the sample was removed from the apparatus and placed on a flat surface. A thin-walled stainless steel tube (37.7 mm dia.) was inserted about 25 mm into the sample and rotated 5 times to induce disturbance in the soil. Then, a wire cutter was used to cut 6 mm thick specimens from the soil surrounding the tube along the radial directions for pore size distribution studies. The upper dissected portion of the sample was then trimmed off, and the tube was pushed in another 25 mm and rotated 15 times to cause more severe disturbance. Once again 6 mm thick specimens were cut along radial directions.

The specimens cut from the block sample were then labeled and freeze dried for pore size measurements. A detailed description of the freeze drying method and of the mercury intrusion technique used to find the pore size distribution of the specimen have been presented by Prapaharan (1982).

The data from mercury porosimetry is presented in the form of cumulative and differential pore size distribution curves. With cumulative

distribution curves, the pore size distribution data are normally expressed in terms of the cumulative volume of the pore space intruded as a function of pore diameter. At a given diameter the volume intruded is normalized to 100% of the total pore volume and plotted against the logarithm of diameter. The differential distribution curves are obtained by plotting the derivative of the cumulative distribution curve against the pore diameter.

Figs. 5.5 through 5.8 show the cumulative and differential pore size distribution curves for varying amounts of induced disturbance. The differential distribution curves exhibit single modal characteristic. The effect of disturbance is clearly seen in Fig. 5.8; the magnitude of the peak decreases and the associated pore diameter increases with the distance from the tube wall. This trend is reasonable since, in other studies, disturbance was shown to decrease the number of voids. The degree of disturbance caused by the rotation of the tube decreases with distance from the tube wall. Comparison of Figs. 5.6 and 5.8 shows that the five rotations of the steel tube were not sufficient to create any significant disturbance, since the porosity density functions are essentially unchanged.

Pore size distribution studies have the potential to provide estimates of the thickness of the disturbed annulus. For example, Fig. 5.8 indicates that the disturbed annulus could be more than 64% of the radius of the cavity. It is not possible to compare the thickness of the disturbed zone in the field to that obtained in this study as the fabric, kind, and amount of disturbance are different in both cases. However, it has been demonstrated that pore size distribution studies can be used as a tool to estimate the thickness of the disturbed zone. The degree of disturbance is difficult to establish at present. The previous studies conducted at Purdue University (e.g., White, 1980; Altschaeffl

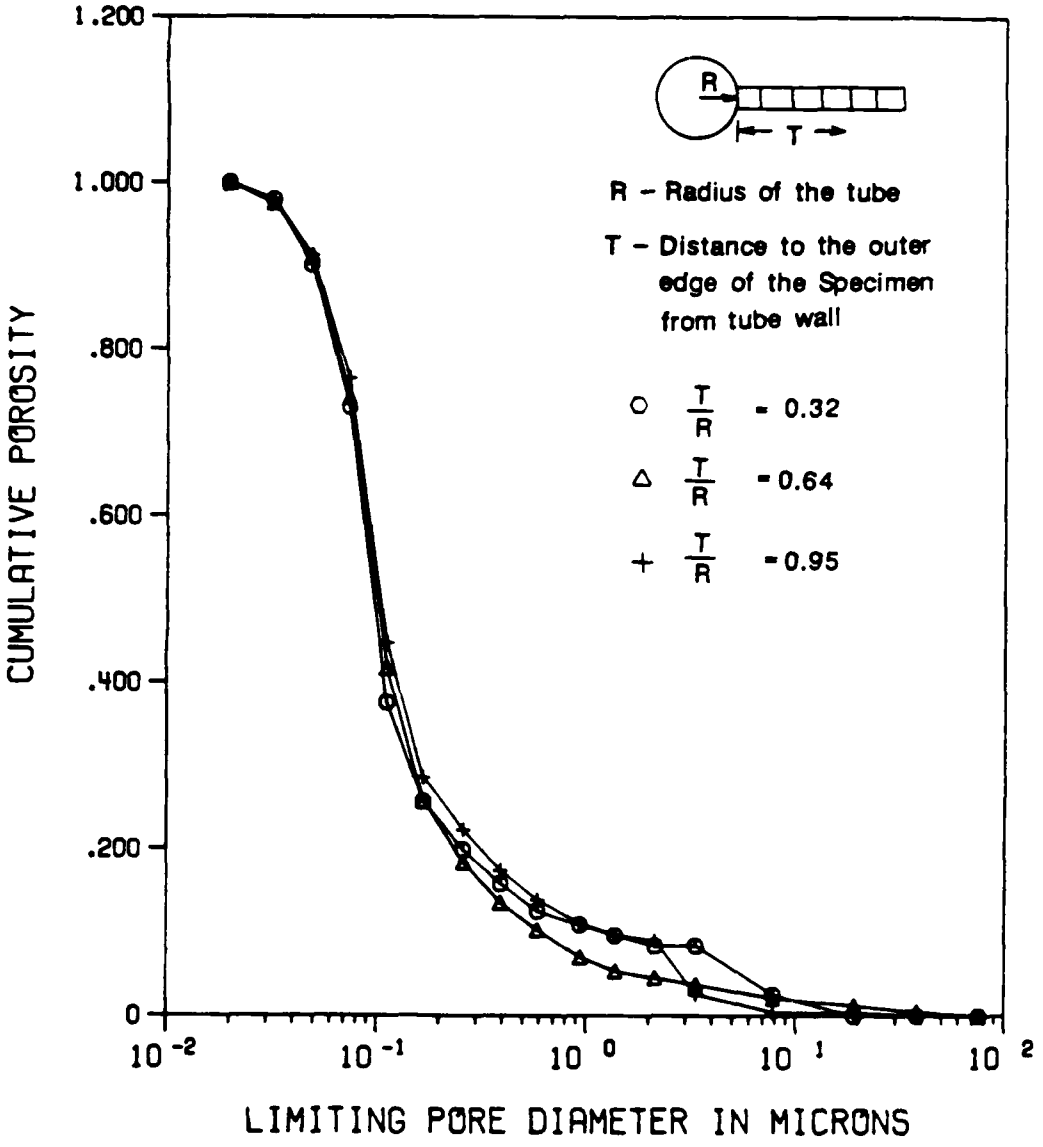

Figure 5.5 Cumulative pore size distribution curves for specimens associated with 5 rotations of the disturbing tube

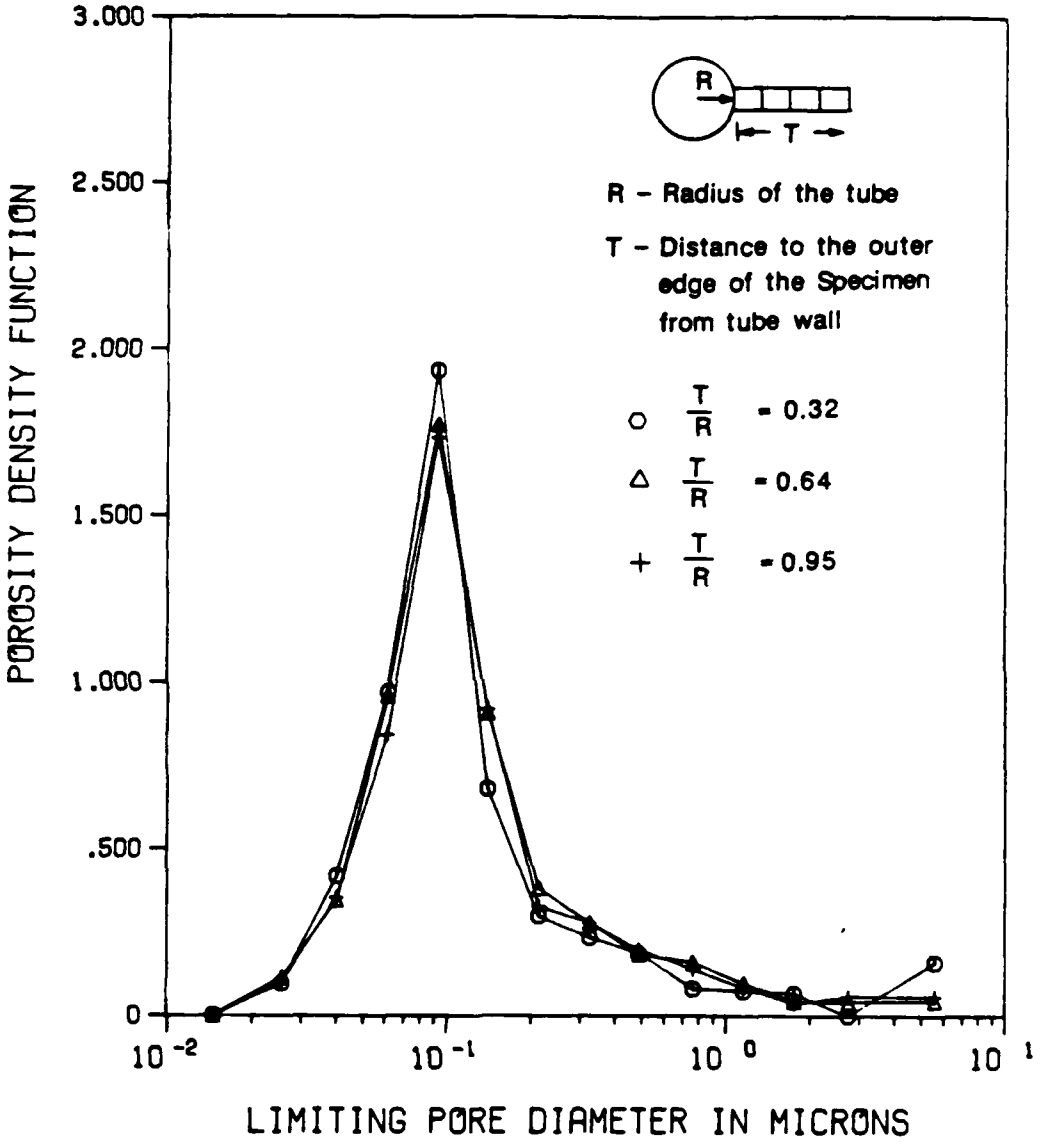

Figure 5.6 Differential pore size distribution curves for specimens associated with 5 rotations of the disturbing tube

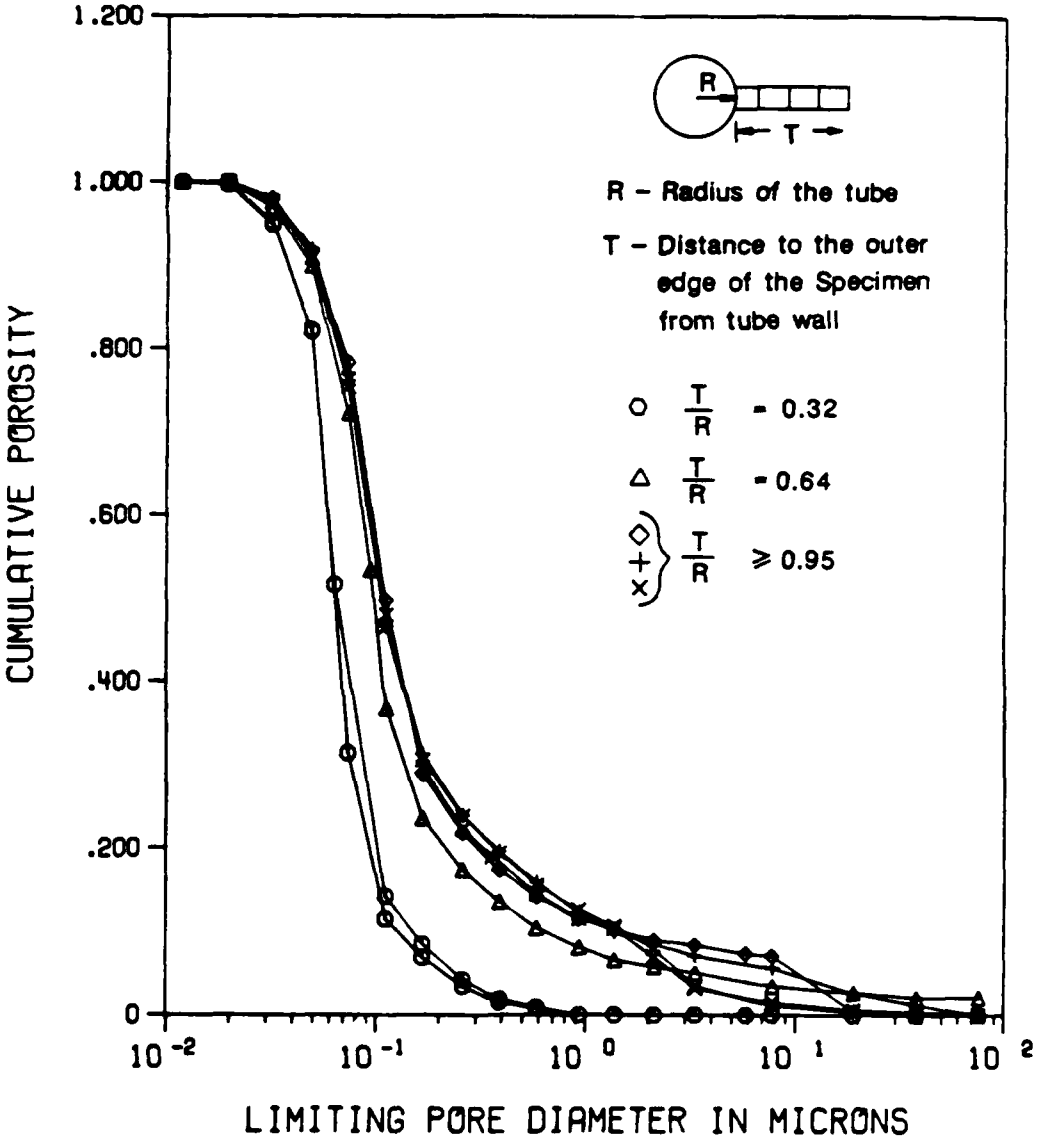

Figure 5.7 Cumulative pore size distribution curves for specimens associated with 15 rotations of the disturbing tube

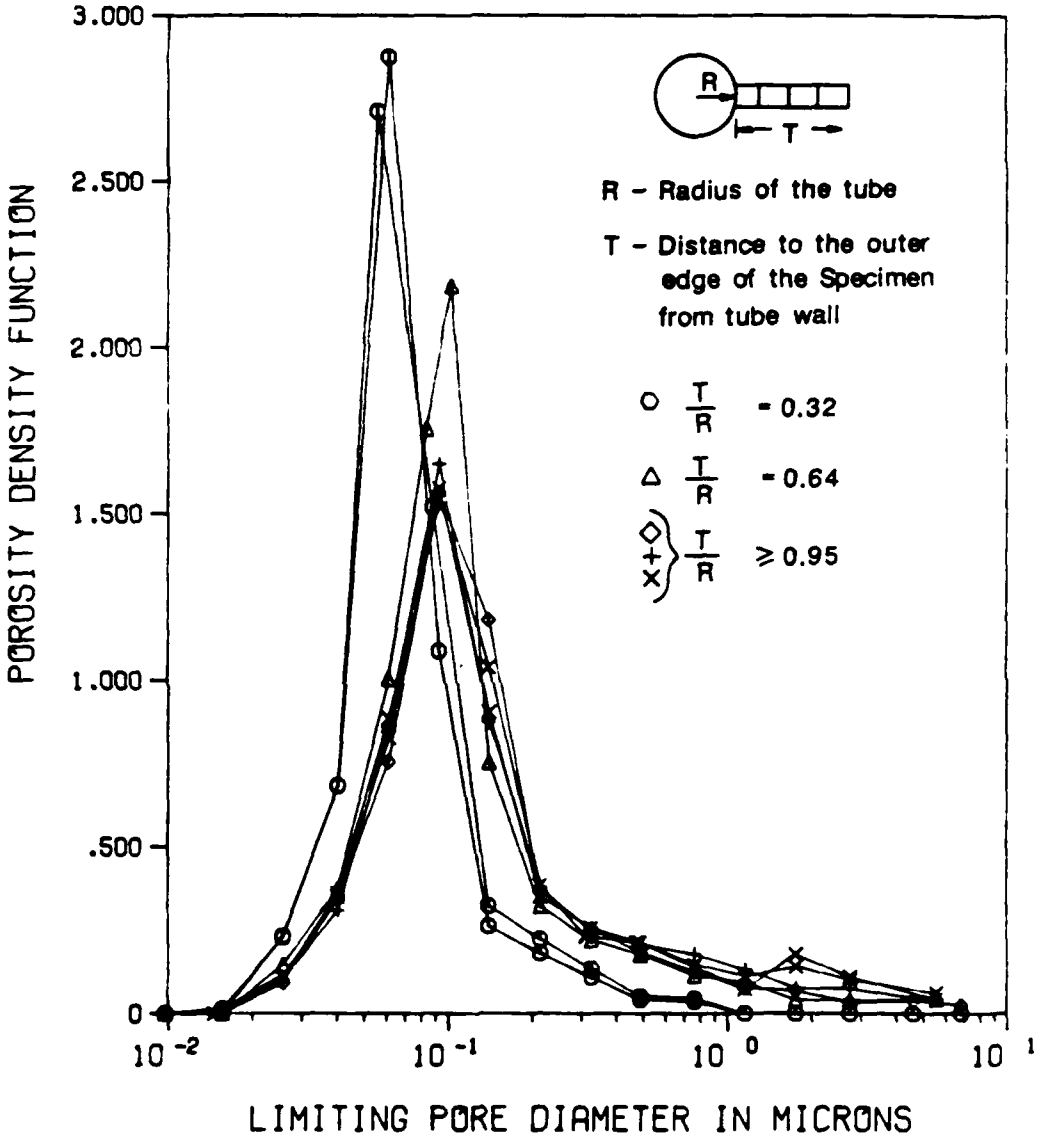

Figure 5.8 Differential pore size distribution curves for specimens associated with 15 rotations of the disturbing tube

and Lovell, 1983) have shown that compaction variables can be correlated with pore size descriptors and strength parameters. Therefore, it is possible to correlate pore size descriptors with strength parameters. If further research can establish such a relationship, then it will be possible to predict the strength and modulus of the soil in the disturbed annulus.

Parameters for Parametric Analysis -- Two different soils were used in the parametric study: a) 100% Kaolin, and b) Boston Blue Clay. The triaxial compression and extension curves for K_o-consolidated Kaolin were obtained by Huang (1986) and were presented in Chapter 2 of this report. The stress-strain curves for resedimented K_o-consolidated Boston Blue Clay were obtained by Ladd and Varallyay (1965). The stress-strain curves for both soils are shown in Figs. 5.9 and 5.10.

It is difficult to obtain the stress-strain curves for the disturbed soil experimentally, as the kind and amount of disturbance caused by the pressuremeter installation is not known. However, it is known that disturbance reduces the peak strength and increases the failure strain for brittle soils. For ductile soils, the stress-strain curve for the disturbed soil falls under that for undisturbed soils. The tangent modulus is reduced considerably for both soil types regardless of the sensitivity (Broms, 1980). The stress-strain curves for the disturbed soils used in this study (Figs. 5.9 and 5.10) were selected based on the above observations. Since the peak strength of the soil decreases with disturbance, it was chosen as low as possible in order to produce a large error in the undrained strength derived from the pressuremeter expansion curve. The effect of disturbance on extension test results is not known. It was decided to use a stress-strain curve that falls well under that for undisturbed soil.

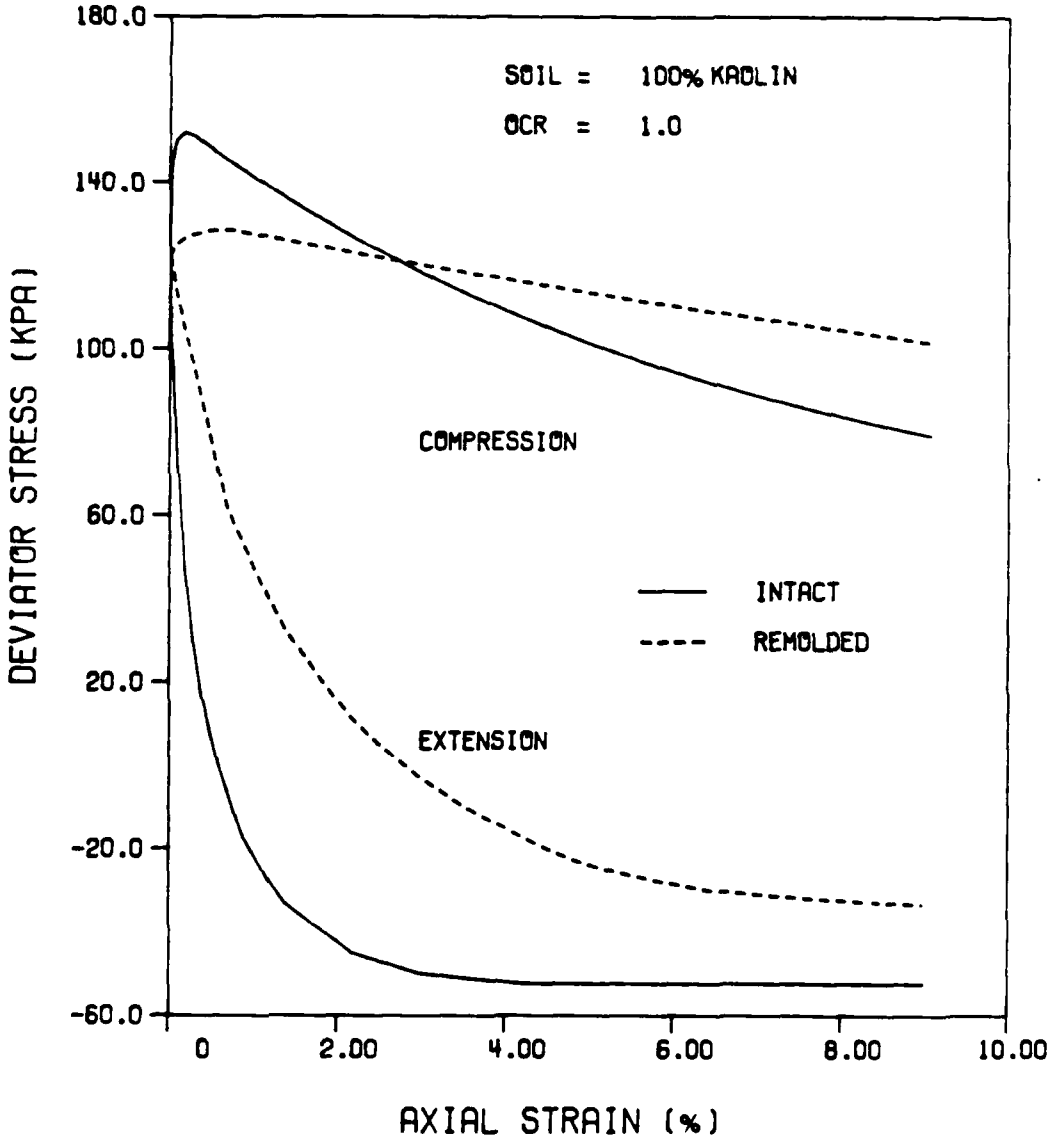

Figure 5.9 Triaxial stress-strain curves for 100% kaolin soil

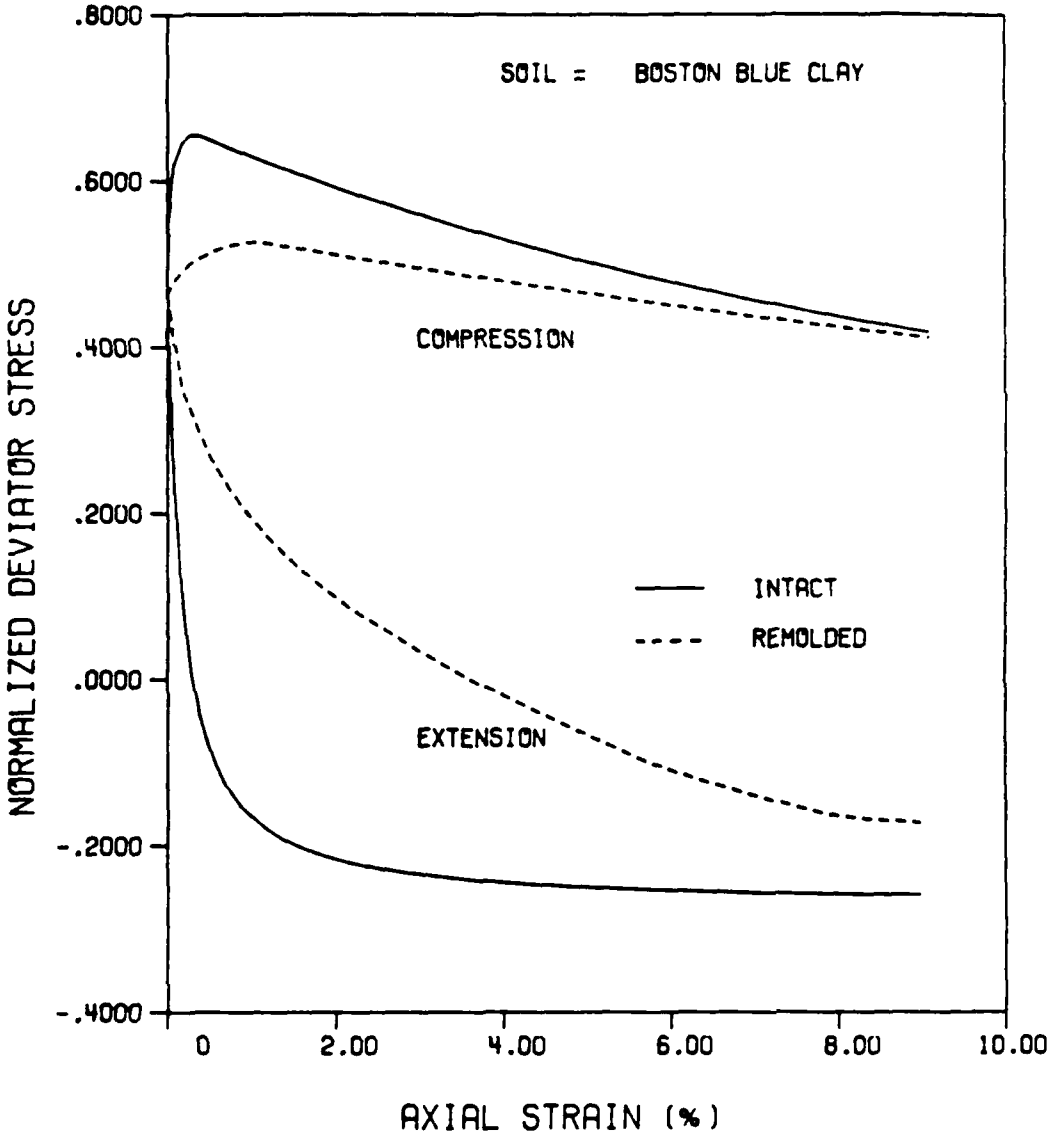

Figure 5.10 Triaxial stress-strain curves for resedimented K_o-consolidated Boston Blue Clay (after Ladd and Varallyay, 1965)

The model parameters required to predict the pressuremeter expansion curves were derived from the triaxial compression and extension curves for the intact and remolded soils.

Results and Discussion -- The pressuremeter expansion curves predicted for kaolin with different thicknesses of disturbed zone are shown in Fig. 5.11. The stress-strain curves derived from the pressuremeter expansion curves shown in Fig. 5.11 are given in Fig. 5.12. The predicted undrained strength increases with the thickness of the disturbed zone. The results for Boston Blue Clay show trends similar to those observed for kaolin (Figs. 5.13 and 5.14).

The error in undrained strength and modulus due to the presence of a disturbed annulus is plotted against the thickness of the annulus in Fig. 5.15 and 5.16 for both soils. The error is calculated with reference to the strength and modulus values obtained for undisturbed soil. The modulus used in this parametric study is the secant modulus at 50% of the peak stress level (i.e. G_{50}). If the thickness of the disturbed annulus is half the radius of the cavity, then the undrained strength will be overestimated by 11-15%, and the modulus will be underestimated by 40%. It should be remembered that the reference strength used to calculate the error is the undrained strength derived from the pressuremeter expansion curve obtained for soils with no disturbed zone.

For Boston Blue Clay, Fig. 5.17 (Ladd, et al., 1980) shows that the undrained strength obtained from selfboring pressuremeter tests exceeds the SHANSEP peak $C_u(V)$ by as much as 100% and does not lie between the SHANSEP curves except at rather shallow test elevations. It is therefore apparent from results given in Figs. 5.11 to 5.16, that the presence of a dis-

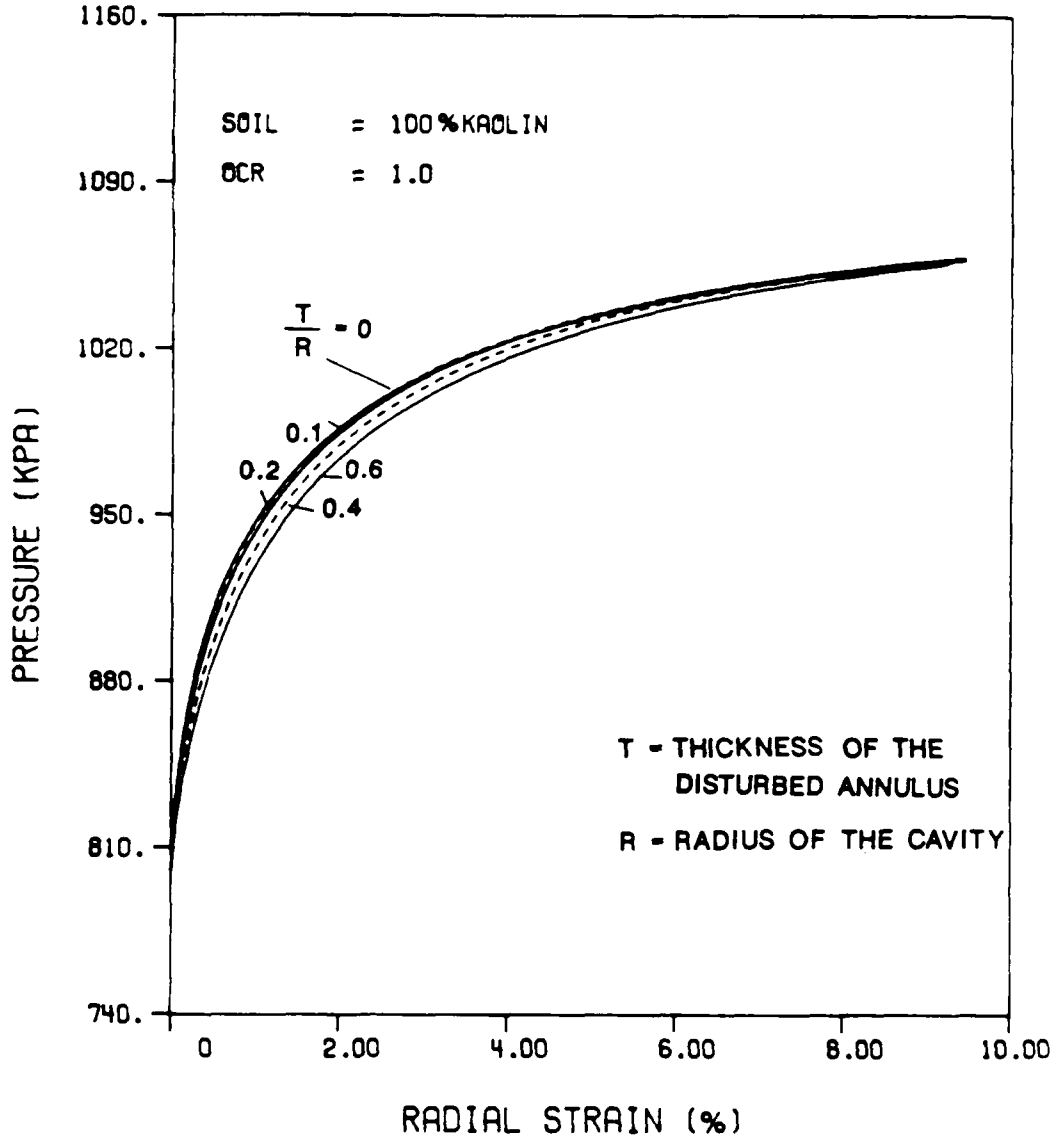

Figure 5.11 Predicted pressuremeter curves for kaolin with different disturbed annuli

AD-A181 428 FUNDAMENTAL ASPECTS OF PRESSUREMETER TESTING(U) PURDUE 2/2
UNIV LAFAYETTE IN SCHOOL OF CIVIL ENGINEERING
J L CHAMEAU ET AL 30 APR 87 AFOSR-TR-87-0777
UNCLASSIFIED AFOSR-84-0330 F/G 8/10 NL

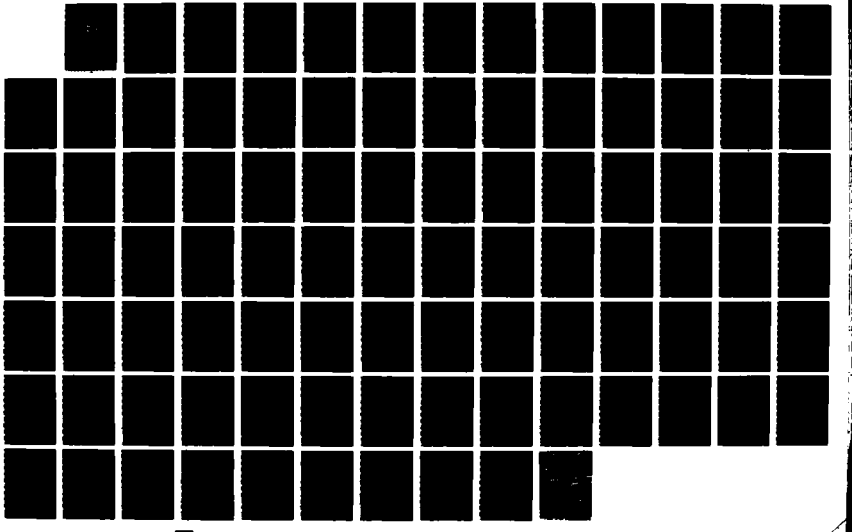

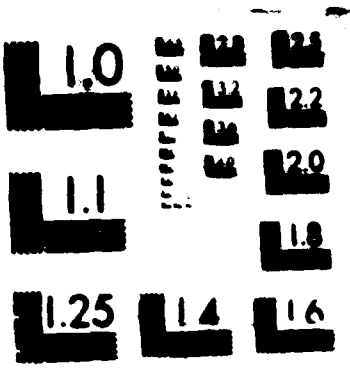

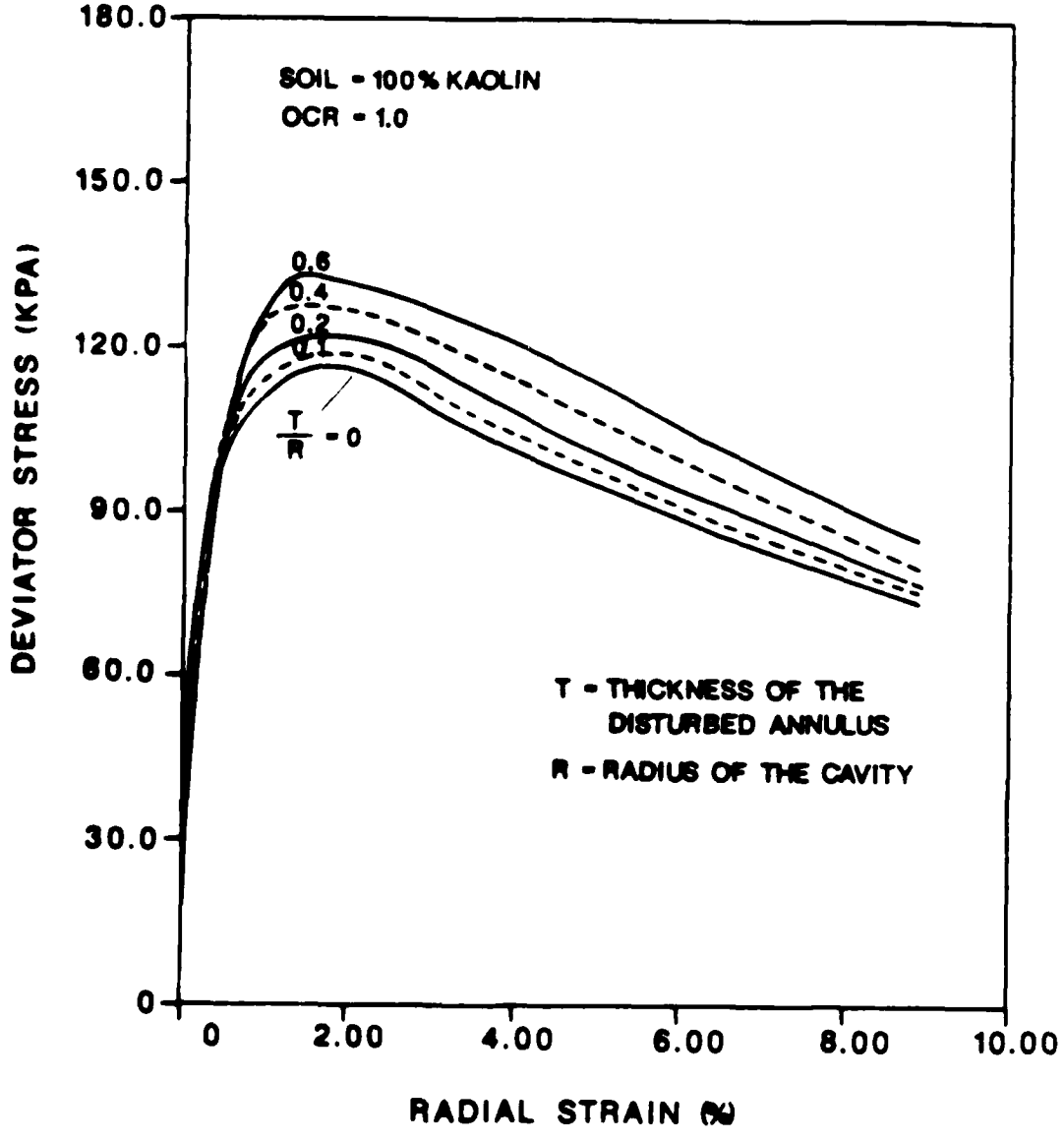

Figure 5.12 Derived stress-strain curves for kaolin with different disturbed annuli

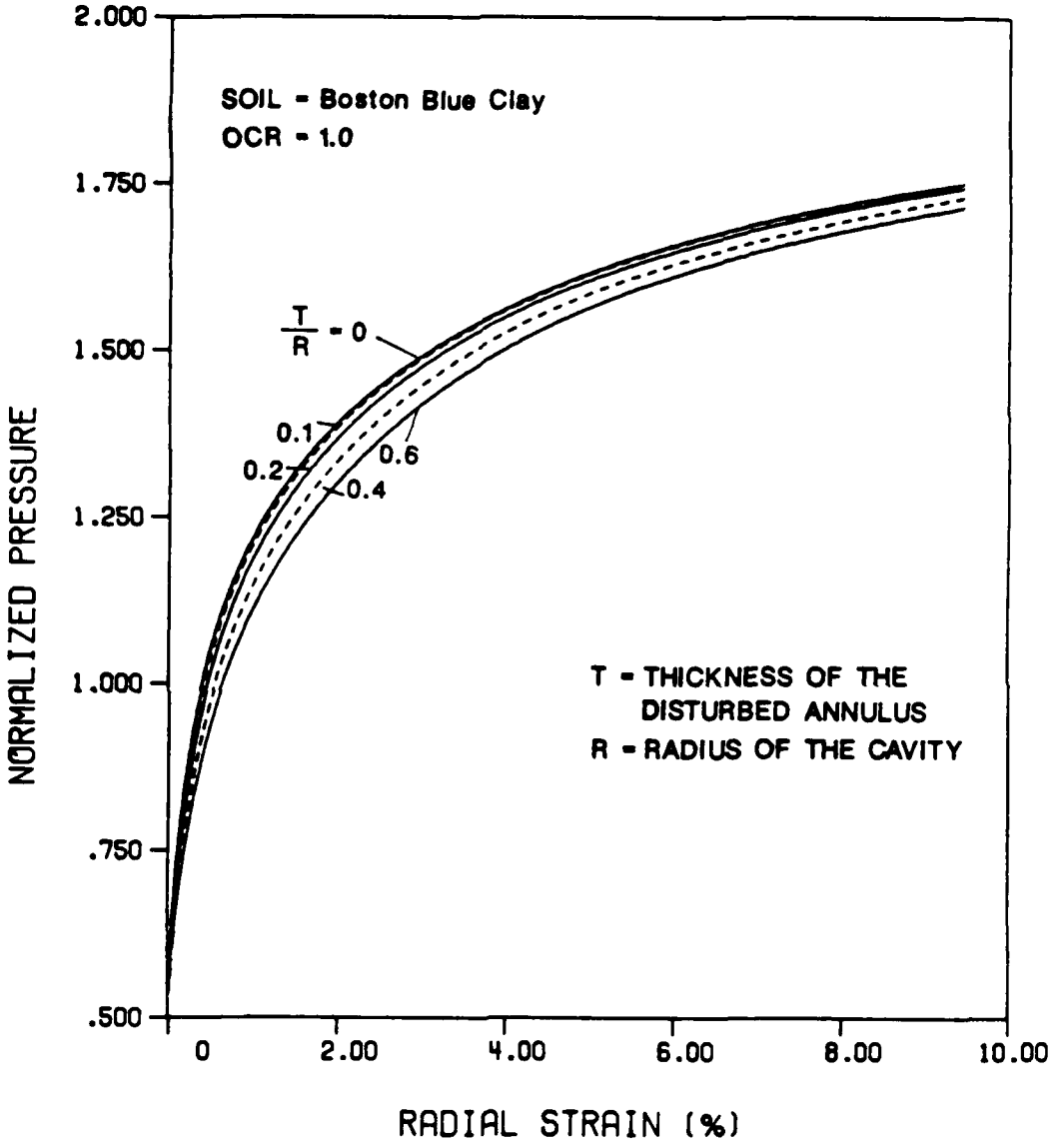

Figure 5.13 Predicted pressuremeter curves for resedimented Boston Blue Clay with different disturbed annuli

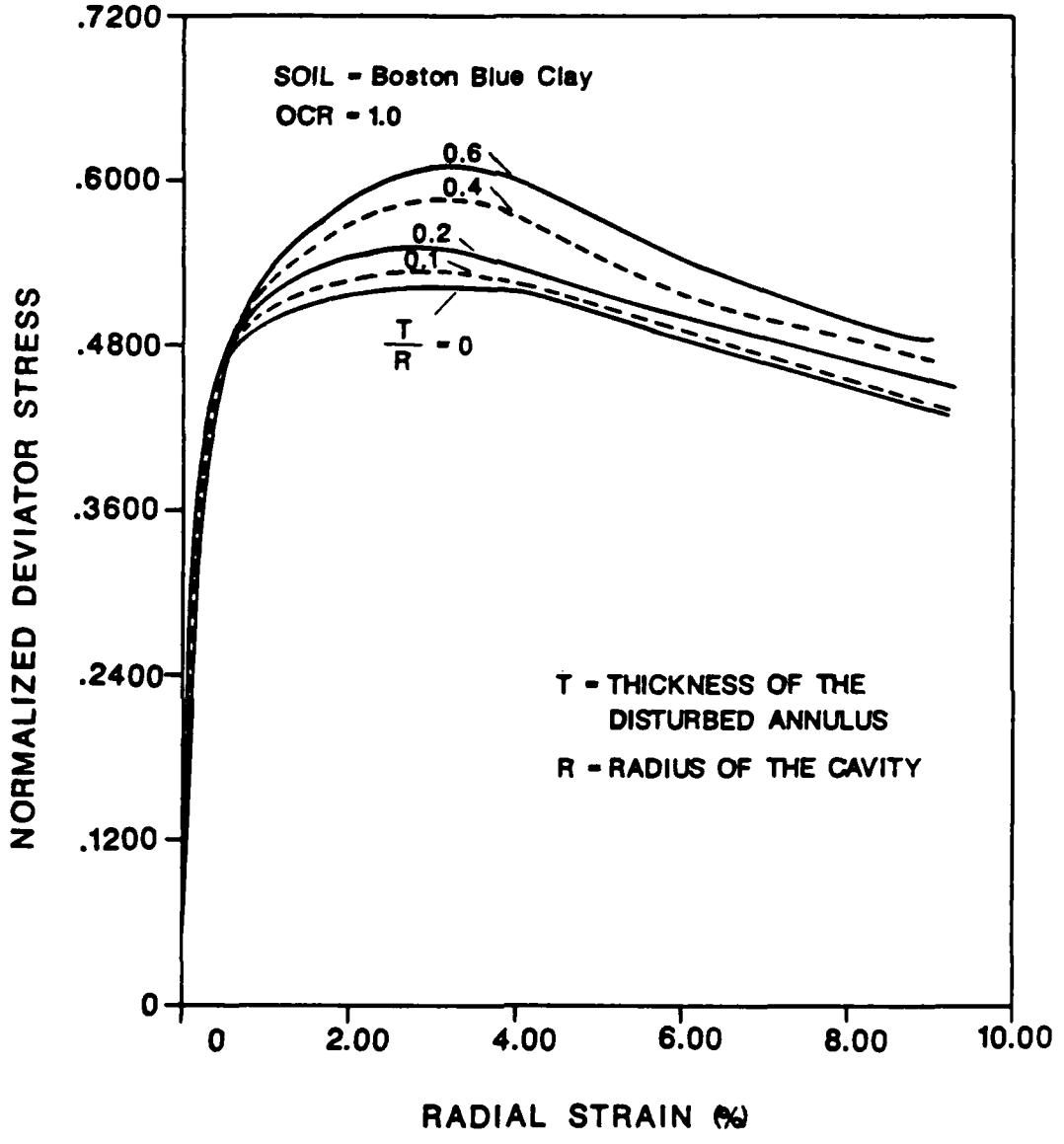

Figure 5.14 Derived stress-strain curves for Boston Blue Clay with different disturbed annuli

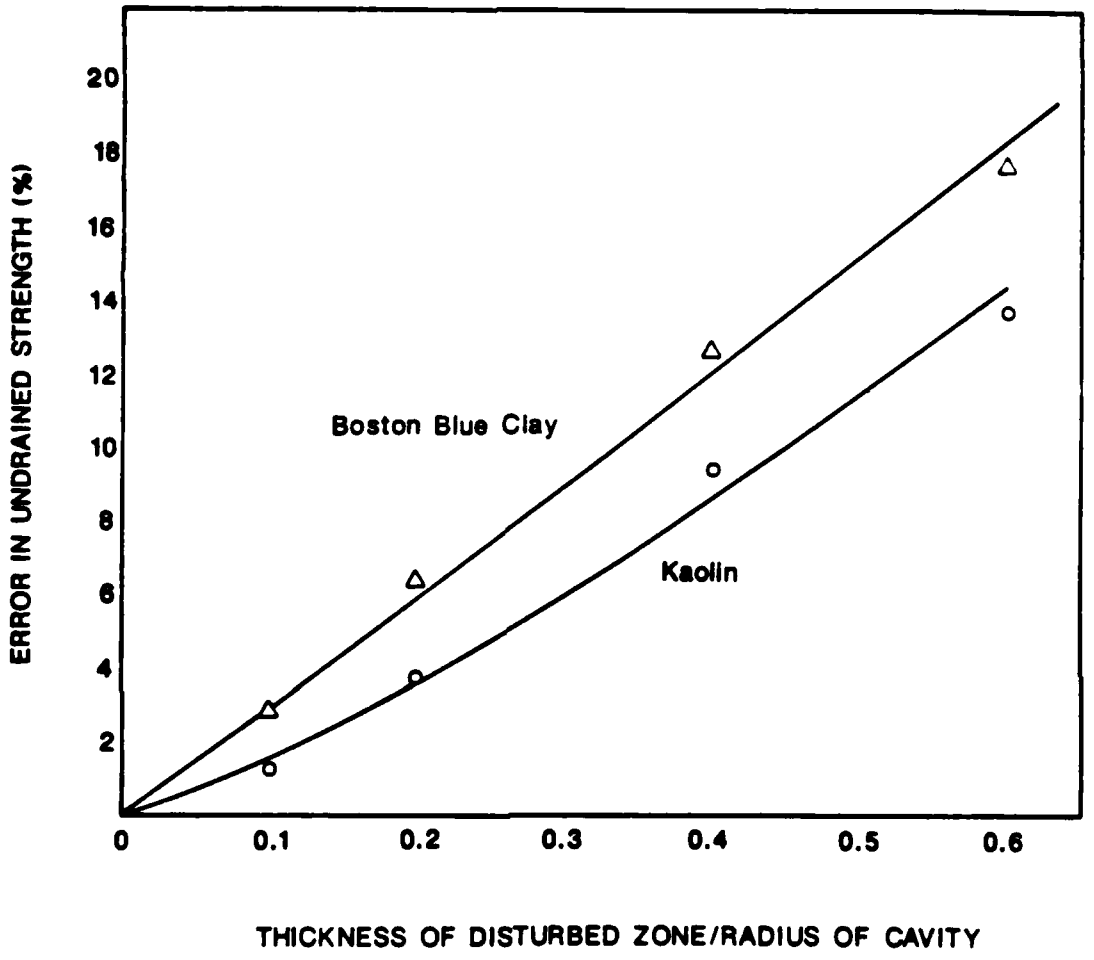

Figure 5.15 Error in predicted undrained strength vs Thickness of the disturbed annulus

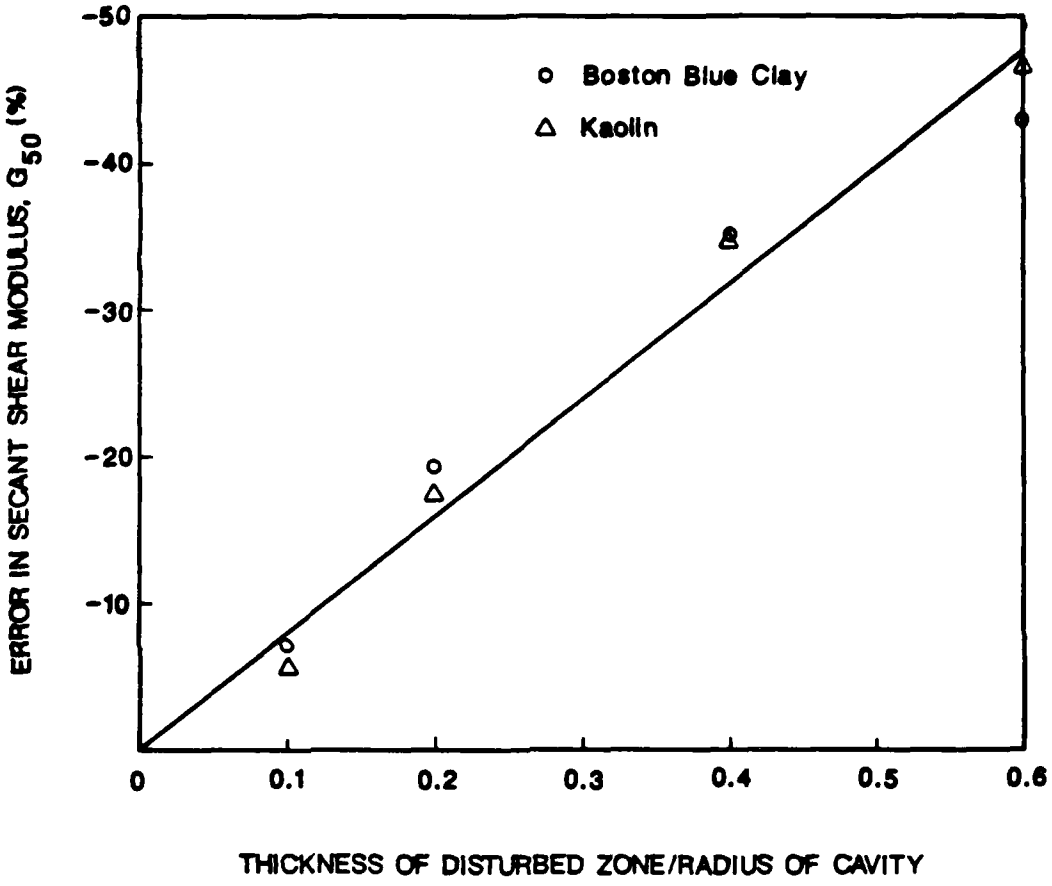

Figure 5.16 Error in modulus vs thickness of the disturbed annulus

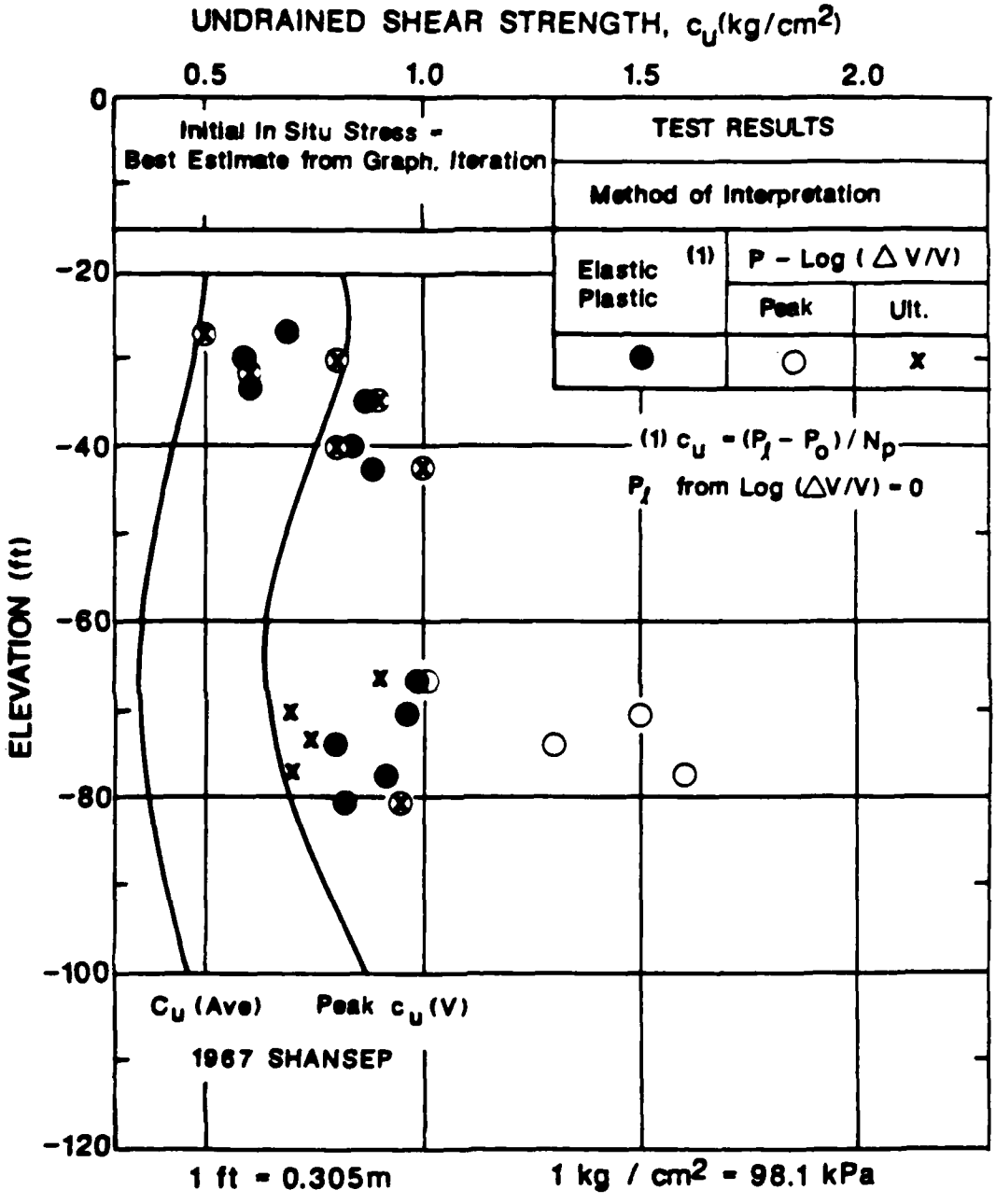

Figure 5.17 Elastic-plastic and derived undrained shear strengths from camkometer tests in Boston Blue Clay (after Ladd et al., 1980)

turbed annulus alone could not have resulted in such a large error. The other possible factors which could significantly influence the results are strain rate, partial drainage, and initial unloading of the soil. The effect of strain rate and partial drainage on undrained strength is discussed in Chapter 6, where it is shown that the error due to strain rate effects could not be more than 15%, and that the pressuremeter curve and hence the derived undrained strength is not affected significantly by partial drainage. Thus, it can be concluded that initial unloading must be the critical effect.

The amount of the initial unloading is difficult to estimate as it depends on the sensitivity of the soil, the cutter position in the cutting shoe, the cutting rate, and the size of the cutting shoe relative to the probe membrane. It is difficult to show experimentally that initial unloading takes place during a self boring pressuremeter test. A close examination of the results reported in the literature reveals that the pressuremeter tests in highly anisotropic and strain softening soils yield undrained strengths considerably larger than the reference strengths (Prapaharan, 1987). The following hypothesis is proposed to explain the high strengths obtained with the self boring pressuremeter in these soils.

During the self boring process, the lateral stress in the soil element close to the cutter shoe is reduced. If the resulting deformation exceeds the peak failure strain then plastic flow will occur. The soil that flows into the cutter shoe will be removed by the water circulating through the probe. This scenario results in unloading of the soil at the cavity face thus reducing the lateral earth pressure. Furthermore, only a very small movement is necessary to cause 1% strain in the element close to the probe (e.g. 0.4mm for 8cm dia. probe). It has been reported that a 20% reduction in lateral earth pressure

results in overestimation of undrained strength by 60-100% (Benoit and Clough, 1986).

The effect of initial unloading on the pressuremeter test results can be studied theoretically using the method described earlier in this chapter. Fig. 5.18 shows the pressuremeter curves for kaolin for initial unloading and subsequent reloading, and Fig. 5.19 gives the respective stress-strain curves derived from the pressuremeter curves in Fig. 5.18, assuming the unloaded state as the initial state. The undrained strength increases with the amount of initial unloading. Similar curves were obtained for Boston Blue Clay, and for various thicknesses of disturbed annulus (Prapaharan, 1987).

The average values of error induced in the undrained strength and the modulus for both soils due to initial unloading are plotted versus the thickness of the remolded annulus for various amounts of initial unloading in Figs. 5.20 and 5.21. These figures clearly illustrate the relative effects of initial unloading and disturbance on both strength and modulus. For small amounts of initial unloading (i.e. initial strain less than 0.1 to 0.2%), the remolded annulus has the strongest influence on strength estimates, however the error in undrained strength will be less than 20%. For large amount of unloading, the initial strain due to unloading overwhelms the effect of the remolded annulus, and the undrained strength can be overestimated by as much as 100% for an initial strain of 1%. The modulus, however, is affected by the size of the disturbed annulus as well as the amount of initial unloading, and can be under estimated by as much as 40%.

Prevost (1979) suggested a method to correct the field pressuremeter curve for initial unloading if the amount of initial unloading of the borehole is known. However, it is not possible in practice to know the amount of initial

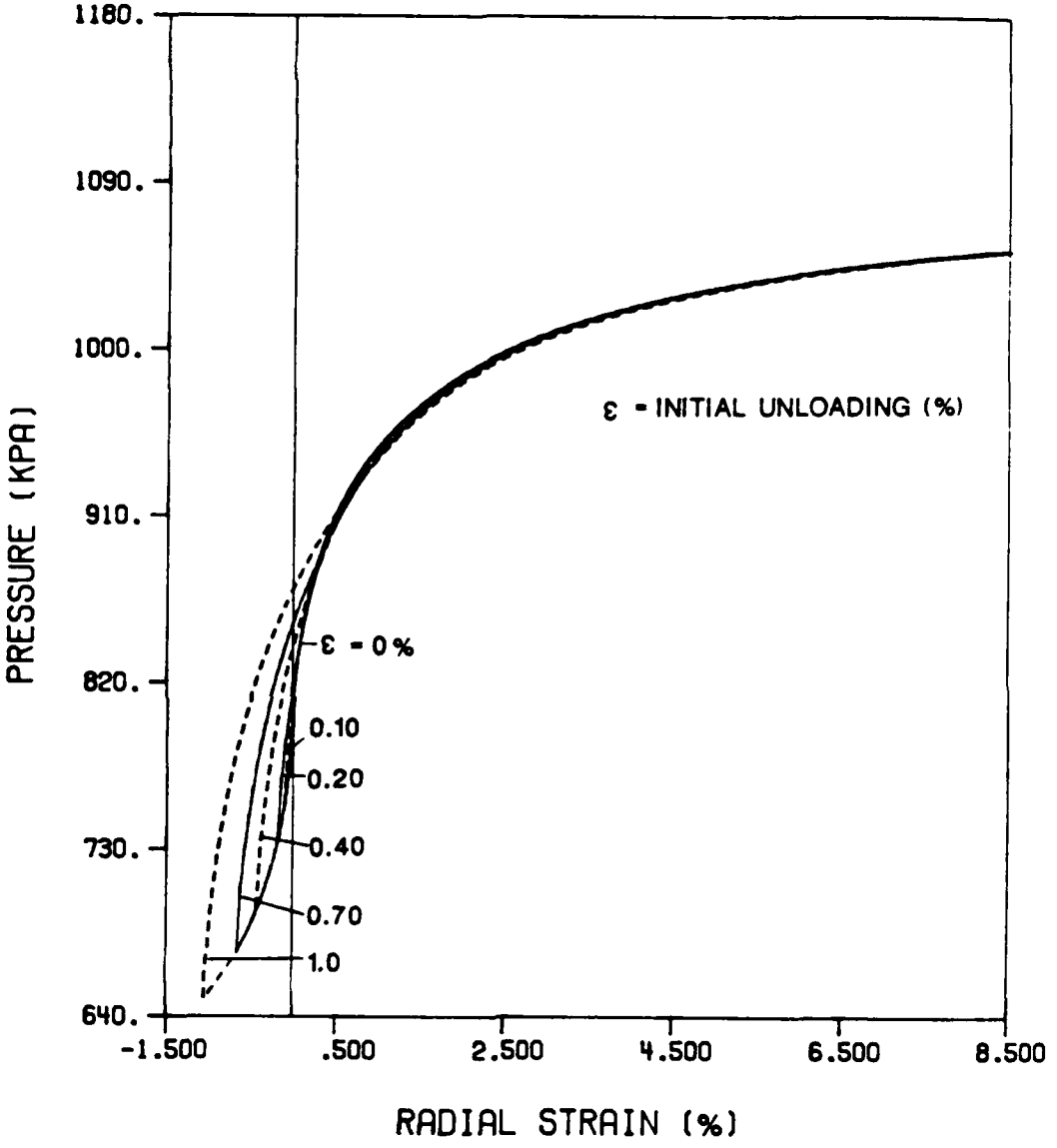

Figure 5.18 Predicted pressuremeter curves for kaolin for initial unloading and reloading: no disturbed annulus

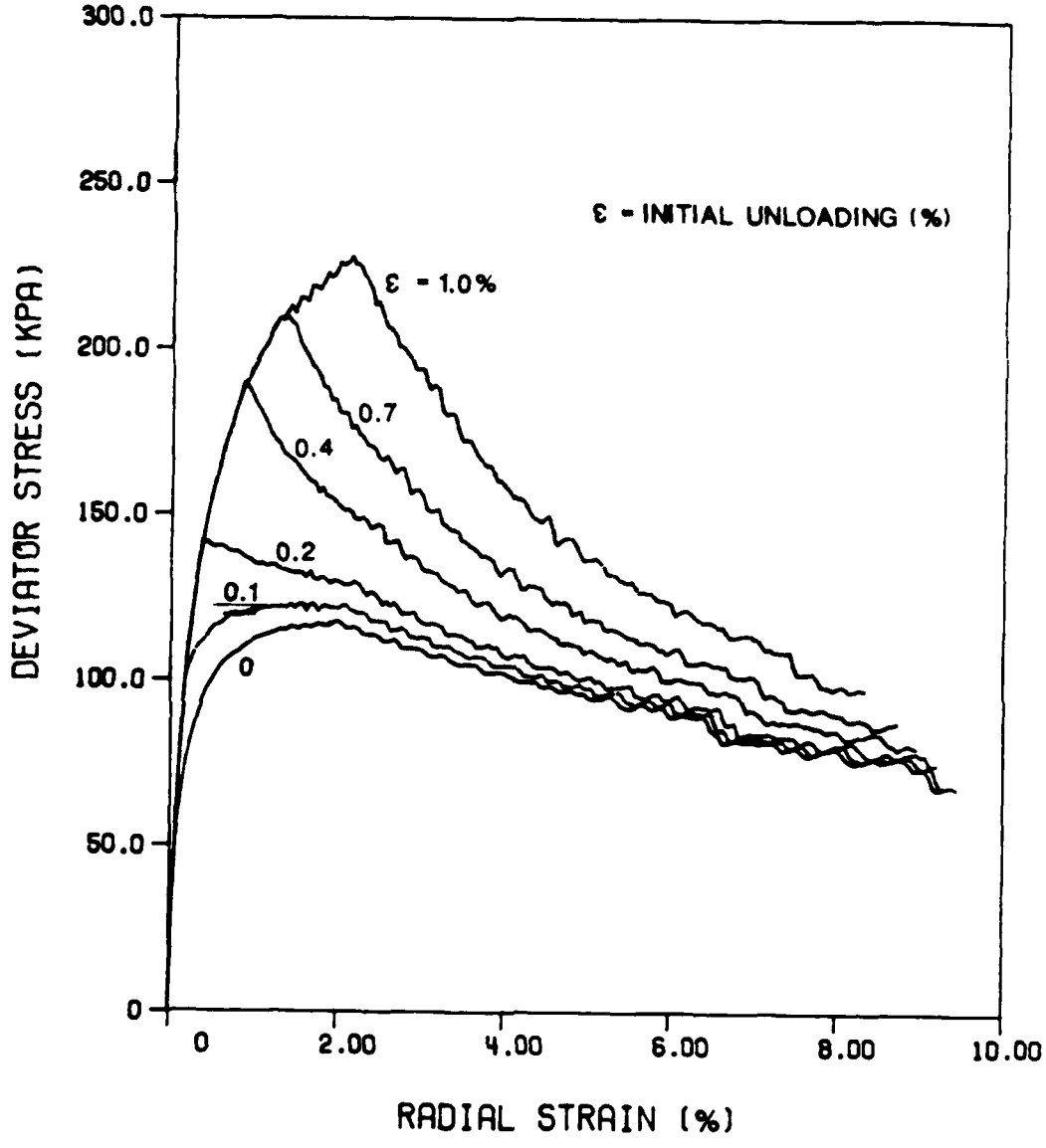

Figure 5.19 Predicted stress-strain curves for kaolin: no disturbed annulus

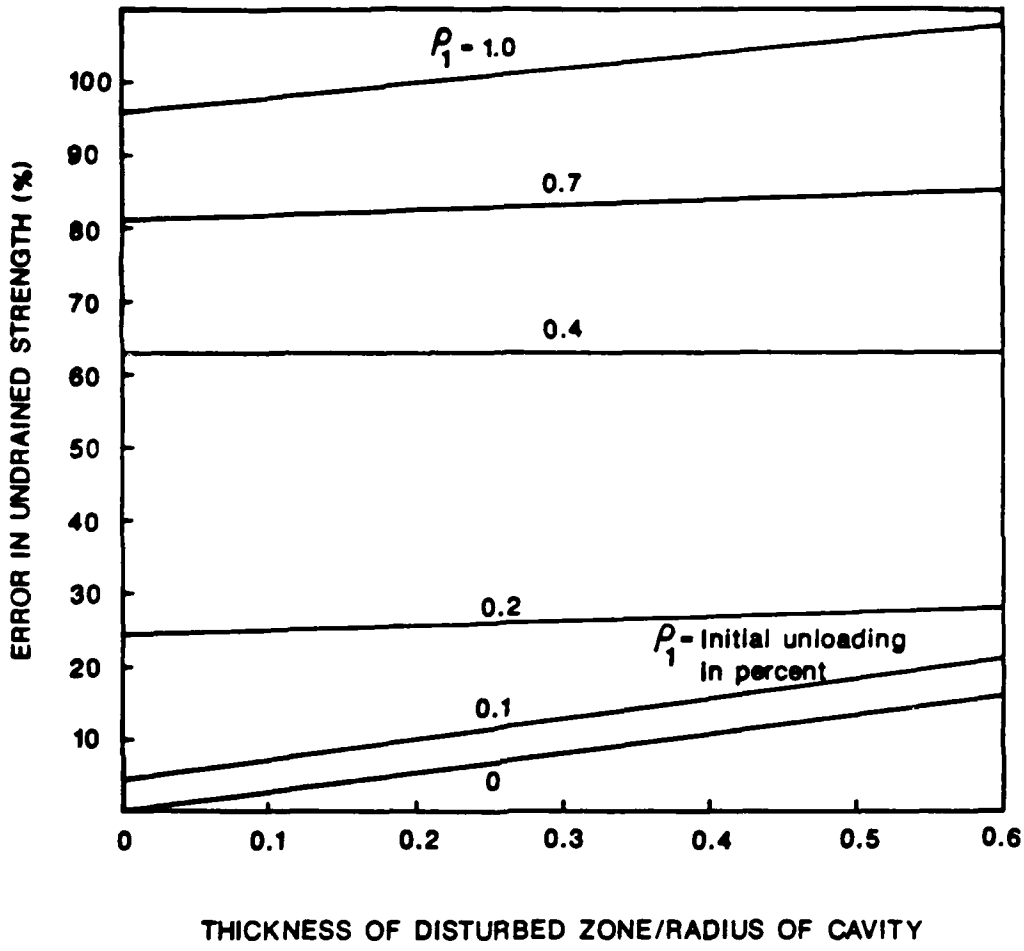

Figure 5.20 Error in undrained strength due to disturbance

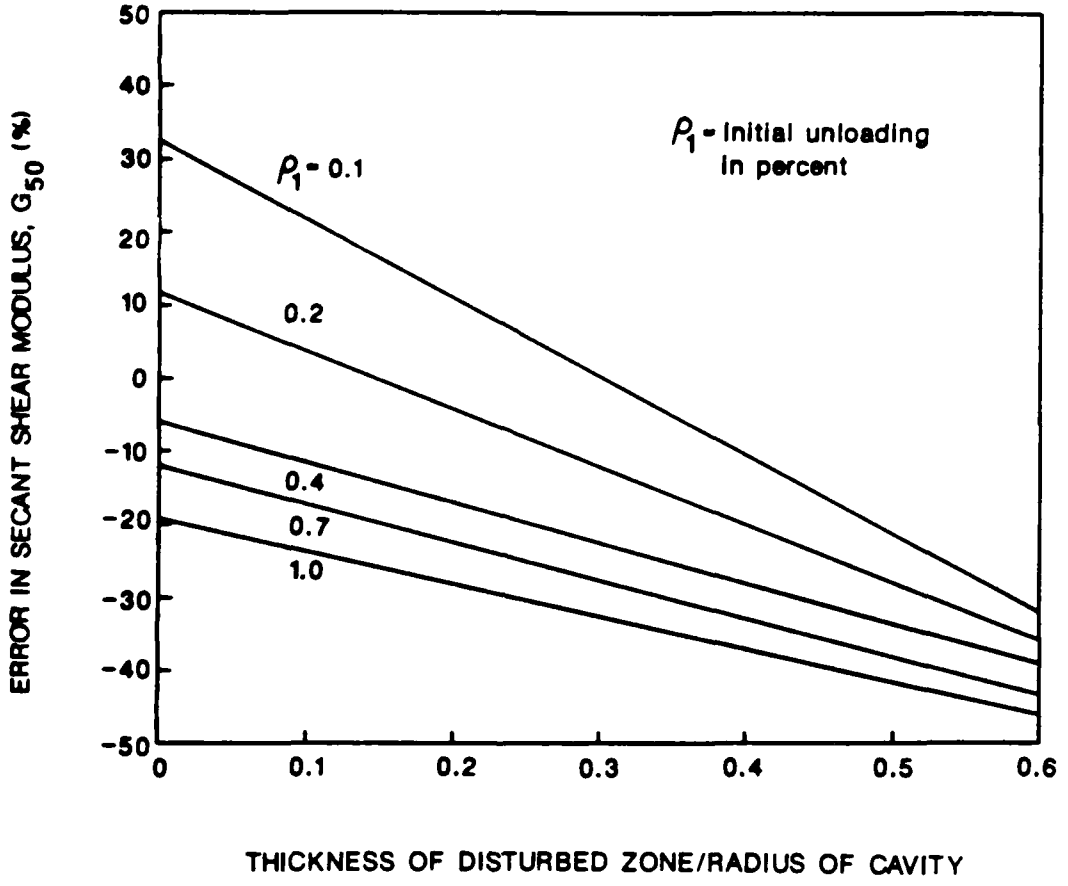

Figure 5.21 Error in modulus due to disturbance

unloading and also it will be different for different soils. Furthermore, the effect of stress relaxation also will have to be taken into consideration. It appears that without fully understanding the influence of all the factors involved in the interpretation of test results, it may not be possible to use the current interpretation procedures for highly strain softening soils. At present, it may be worthwhile to simply use an interpretation procedure based on limit pressure (Baguelin, et al., 1978).

5.6 Conclusions

It has been shown that pore size distribution analyses can provide the means to estimate the size of the disturbed annulus around the probe. It is recommended that field samples be obtained and analyzed with this technique to study the extent of the disturbed zone in the field. The presence of a remolded annulus can result in an overestimation of undrained strength by 15% and underestimation of modulus by 40%. However, The unloading of the borehole due to drilling overwhelms the effect of the presence of a disturbed annulus, and can result in overestimation of the undrained strength by as much as 100%. The modulus, however, is affected by both the unloading and the size of the disturbed annulus. A hypothesis is proposed to explain the mechanism involved in the unloading of the soil during the self-boring process. Highly anisotropic and strain softening soils are shown to be affected most by the disturbance (or initial unloading) caused during the drilling process and therefore it is not advisable to use self-boring pressuremeter tests in such soils with the currently available interpretation procedures.

It is possible to correct the pressuremeter expansion curve for the initial unloading if the amount of initial unloading is known. Further research is needed to establish typical values of initial unloading for different soils and

different drilling procedures. The description of the strain-softening behavior of soils by the model needs improvement, since, at present it employs a curve fitting technique to describe post-peak behavior. Further, the model does not consider strain rate effects. Since the strain rate in a pressuremeter test varies with the radius across the soil mass, it is believed that a strain space based constitutive model would better accommodate the strain rate effects as well as the post peak behavior.

CHAPTER 6

EFFECTS OF STRAIN RATE AND PARTIAL DRAINAGE

The strain rate used in the pressuremeter test is generally one to two orders of magnitude larger than the strain rate used in ordinary laboratory strength tests. Since the undrained strength increases with the strain rate, the pressuremeter is bound to yield a larger undrained strength. A reduction of strain rate will result in drainage during the test. This chapter examines the effects of strain rate and partial drainage on the undrained strength derived from pressuremeter tests in clay. More detailed discussion on the derivation of the equations used in this chapter can be found in Prapaharan (1987).

6.1 Effect of Strain Rate

The effect of strain rate on undrained strength determined from pressuremeter test results using conventional interpretation methods was studied. In this section, the kinematics of deformation are considered first, and the radial stress at the cavity boundary is calculated by integrating the equilibrium equation. Then an equation is derived to calculate the variation of strain rate with distance from the center of cavity. A relationship between undrained strength and strain rate is proposed to be used in the analysis. Finally, the results of a parametric study are presented.

Cavity Expansion -- In this analysis, it is assumed that the undrained expansion of a cavity takes place under conditions of plane strain and axisymmetry. Tensile stresses are taken as positive. At each point in the soil, the principal directions are the local radial, circumferential, and axial direc-

tions, and cylindrical coordinates (r, θ, z) are used. In the initial state, the applied radial pressure, P_o, is assumed to be equal to the initial in situ horizontal stress, σ_h. Initially, the cavity radius is a_o, and a generic material point in the soil located at a radial distance r-u is considered. When the cavity radius increases from a_o to a_o+u_o, this point moves from r-u to r. It can be shown that the circumferential strain, ϵ_θ, is given by the equation:

$$\epsilon_\theta = -1 + \left[1 - \frac{u_o(2a_o + u_o)}{r^2}\right]^{-\frac{1}{2}} \tag{6.1}$$

and is positive. Since there is no volume change and the axial strain is zero, the radial strain, ϵ_r, is related to ϵ_θ by:

$$(1 + \epsilon_r)(1 + \epsilon_\theta) = 1 \tag{6.2}$$

In the initial state, the radial and circumferential stresses are equal and uniform, and equal to the in situ horizontal stress, σ_h. As the radius of the hole is increased, the circumferential extension, ϵ_θ, is positive and the radial extension, ϵ_r, is negative. The corresponding shear strain induces a difference between the circumferential and radial effective stresses σ'_θ and σ'_r, a difference which is a function of the difference in principal strains and therefore a function of ϵ_θ and the strain rate $\dot{\epsilon}_\theta$ (the majority of commonly available constitutive models do not consider the effect of strain rate and the model used in Chapter 5 is no exception):

$$\sigma'_r - \sigma'_\theta = \sigma_r - \sigma_\theta = q(\epsilon_\theta, \dot{\epsilon}_\theta) \tag{6.3}$$

The radial equilibrium equation is:

$$\frac{\partial \sigma_r}{\partial r} + \frac{\sigma_r - \sigma_\theta}{r} = 0 \tag{6.4}$$

Substituting Eq. 6.3 into Eq. 6.4:

$$\frac{\partial \sigma_r}{\partial r} = -\frac{1}{r}\, q(\epsilon_\theta, \dot{\epsilon}_\theta) \tag{6.5}$$

As r tends to infinity, σ_r tends to σ_h, which is independent of time. At the inside boundary, σ_r is equal to the applied pressure which is the measured function, P, of the circumferential strain, ϵ_o, at the cavity wall and strain rate, $\dot{\epsilon}_o$, for strain controlled expansion. Integrating Eq. 6.5 from infinity to the cavity boundary at $r=a_o+u_o$ yields:

$$P(\epsilon_o, \dot{\epsilon}_o) - \sigma_h = \int_{\infty}^{a_o+u_o} -\frac{1}{r}\, q(\epsilon_\theta, \dot{\epsilon}_\theta)\, dr \tag{6.6}$$

The integration variable r can be eliminated from Eq. 6.6 using Eq. 6.1 (for convenience of notation, ϵ_θ is replaced by ϵ in the following):

$$P(\epsilon_o, \dot{\epsilon}_o) - \sigma_h = \int_0^{\epsilon_o} \frac{1}{\epsilon(1+\epsilon)(2+\epsilon)}\, q(\epsilon, \dot{\epsilon})\, d\epsilon \tag{6.7}$$

If the function $q(\epsilon, \dot{\epsilon})$ is known, the above equation can be numerically integrated to obtain the strain rate dependent pressuremeter expansion curve. In the conventional interpretation method, it is assumed that the stress-strain curve is not affected by strain rate, i.e. $q(\epsilon, \dot{\epsilon}) = q(\epsilon)$. Thus, differentiating Eq. 6.7 leads to:

$$q(\epsilon_o) = \epsilon_o(1+\epsilon_o)(2+\epsilon_o)\, \frac{dP}{d\epsilon_o} \tag{6.8}$$

which is same as the equation derived by Palmer (1972). Eq. 6.8 can be used to derive the stress-strain curve from the pressuremeter expansion curve obtained using Eq. 6.7, and the resulting curve can be compared with the material stress-strain curve, $q(\epsilon, \dot{\epsilon})$, which includes strain rate effects.

Variation of Strain Rate within the Soil Mass -- The strain rate can be obtained by differentiating Eq. 6.1 with respect to time. It can be shown (Prapaharan, 1987) that the strain rate is related to the strain by the following equation:

$$\dot{\epsilon} = \dot{\epsilon}_o \frac{(1+\epsilon_o)}{\epsilon_o(2+\epsilon_o)} \frac{\epsilon(2+\epsilon)}{(1+\epsilon)} \tag{6.9}$$

The above equation d scribes the variation of strain rate within the soil mass for a given strain, ϵ_o, and strain rate, $\dot{\epsilon}_o$, at the cavity wall.

Variation of Undrained Strength with Strain Rate -- The undrained shear strength has been shown experimentally to increase linearly with the logarithm of strain rate (e.g. Bjerrum, 1972; Vaid and Campanella, 1977; Nakase and Kamei, 1986). All the results obtained by these researchers are plotted in Fig. 6.1. In order to compare the results, the shear stresses were normalized with respect to the shear stress at a strain rate of 0.01% per min. It can be seen that the shear strength increases by 8-10% for a 10 fold increase in strain rate. In this study, it was decided to use the relationship shown in Fig. 6.1 (dashed line) to study the strain rate effect on pressuremeter test results. The upper yield strength is assumed to occur at a strain rate of 0.001% per *min*. It is believed that the chosen relationship is a realistic one, and thus valuable insight can be gained about the effect of strain rate on undrained strength derived from pressuremeter tests using conventional interpretation methods.

The proposed relationship (Fig. 6.1) between undrained strength and strain rate can be expressed as:

$$q_u = q_a \, (1 + M \log_{10}(\dot{\epsilon}/a)) \tag{6.10}$$

where, q_u = strength at strain rate $\dot{\epsilon}$.

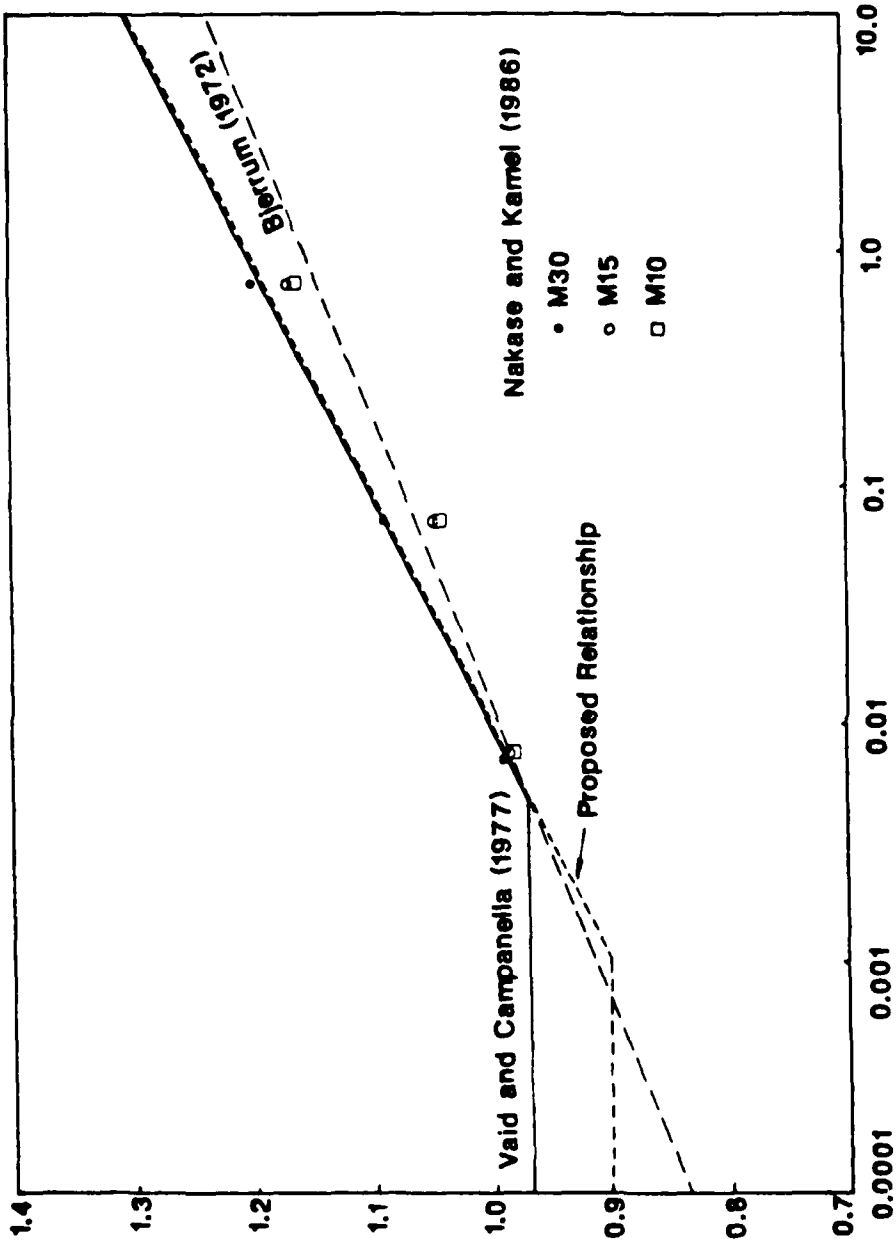

Figure 6.1 Normalized shear strength Vs Strain rate

q_a = undrained strength at reference strain rate, a.

M = Slope of strength vs. logarithm of strain rate relationship.

The parametric study can be conducted for both strain hardening and strain softening soils. The forms of the stress-strain curves that were used are given below.

a) Strain Hardening

An hyperbolic relationship was used for strain hardening soils:

$$q = \frac{\epsilon}{\lambda + \epsilon} q_u \tag{6.11a}$$

where, q_u = ultimate strength

λ = constant

b) Strain Softening

The stress-strain relationship of strain softening materials was represented by the relationship proposed by Prevost and Hoeg (1975):

$$q = A \frac{(B\epsilon^2 + \epsilon)}{1 + C\epsilon^2} \tag{6.11b}$$

where A, B, and C are constants. It can be shown that the peak strain $\epsilon_f = (B+\sqrt{B^2+C})/C$, the slope at zero strain is A, and the residual strength q_{res} is AB/C.

Combining Eqs. 6.7, 6.10, and 6.11a leads to:

$$P(\epsilon_o, \dot{\epsilon}_o) - \sigma_h = \int_0^{\epsilon} \frac{q_a(1 + M \log_{10}(\dot{\epsilon}/a))}{(1+\epsilon)(2+\epsilon)(\lambda+\epsilon)} d\epsilon \tag{6.12a}$$

Combining Eqs. 6.7, 6.10, and 6.11b yields:

$$P(\epsilon_o, \dot{\epsilon}_o) - \sigma_h = \int_0^{\epsilon} \frac{A(1+B\epsilon)\,(1 + M\log_{10}(\dot{\epsilon}/a))}{(1+\epsilon)(2+\epsilon)(1+C\epsilon^2)}\, d\epsilon \qquad (6.12b)$$

The strain rate, $\dot{\epsilon}$, in Eqs. 6.12a and 6.12b is a function of strain, ϵ, and can be calculated from Eq. 6.9. The mathematical formulation is now complete, and Eq. 6.12 can be numerically integrated to generate a pressuremeter expansion curve. The conventional interpretational method (Eq. 6.8) can be used to derive the undrained strength from this pressuremeter expansion curve.

Parameters for the Analysis -- In order to obtain the pressuremeter expansion curve from Eq. 6.12, the parameters q_a, a, $\dot{\epsilon}_o$, M, and the parameters describing the stress-strain curves (Λ, A, B, and C) are needed. The values assigned to these parameters are:

q_a - The derived stress-strain curve is normalized with respect to the reference strength, q_a, thus its absolute value is not needed in the analysis.

a - The reference strain rate a is taken as 0.01% per min as it is the rate commonly used in laboratory tests.

$\dot{\epsilon}_o$ - Two strain rates are used: (a) 1% per min (The strain rate usually used in the pressuremeter test.) (b) 0.1% per min.

M - The slope is assumed to be 0.1 from Fig. 6.1.

Strain Hardening Soil -- A realistic value of Λ has to be chosen for the proper representation of the material stress-strain curve. Typical values of Λ range from 1/300 to 1/1000. In this study, a value of 1/500 was used for Λ.

Strain Softening Soils -- In selecting the stress-strain curve for the strain softening soil, the peak strain was assumed to be unaffected by the strain rate. It is believed that the relative change in strength due to strain

rate effect is more important than the actual form of the stress-strain curve, and therefore the results obtained using this curve will be general in nature. The following values (Prapaharan, 1987) were assigned to the parameters A, B, and C describing the stress-strain curve at the reference strain rate a (i.e. 0.01% per min):

$$A = 185.3 \text{ KPa}, B = 2.308, C = 3.9$$

Therefore, at the reference strain rate:

$$q_{peak} = 127.0, \quad \epsilon_f = 1.39\%$$

Results and Discussion -- The results of the parametric study are shown in Figs. 6.2 and 6.3. The solid lines in these figures represent the material stress-strain curves obtained for different strain rates (Eqs. 6.11a and 6.11b). The dashed lines show the stress-strain curves derived from the pressuremeter expansion curves (using the conventional Eq. 6.8, i.e. neglecting stress rate effect) corresponding to two different expansion rates. The following observations can be made from Figs. 6.2 and 6.3:

a. Strain Hardening Soils

- The derived stress-strain curve tends to strain soften mildly at large strain
- The peak strength at 1.0% per min strain rate is approximately equal to the ultimate strength of the material from the stress-strain curve for the reference strain rate (0.01% per min), whereas the peak strength at the 0.1% per min strain rate is about 6% less than the reference strength
- The form of the material stress-strain curve at the reference strain rate is different from that obtained from pressuremeter tests. How-

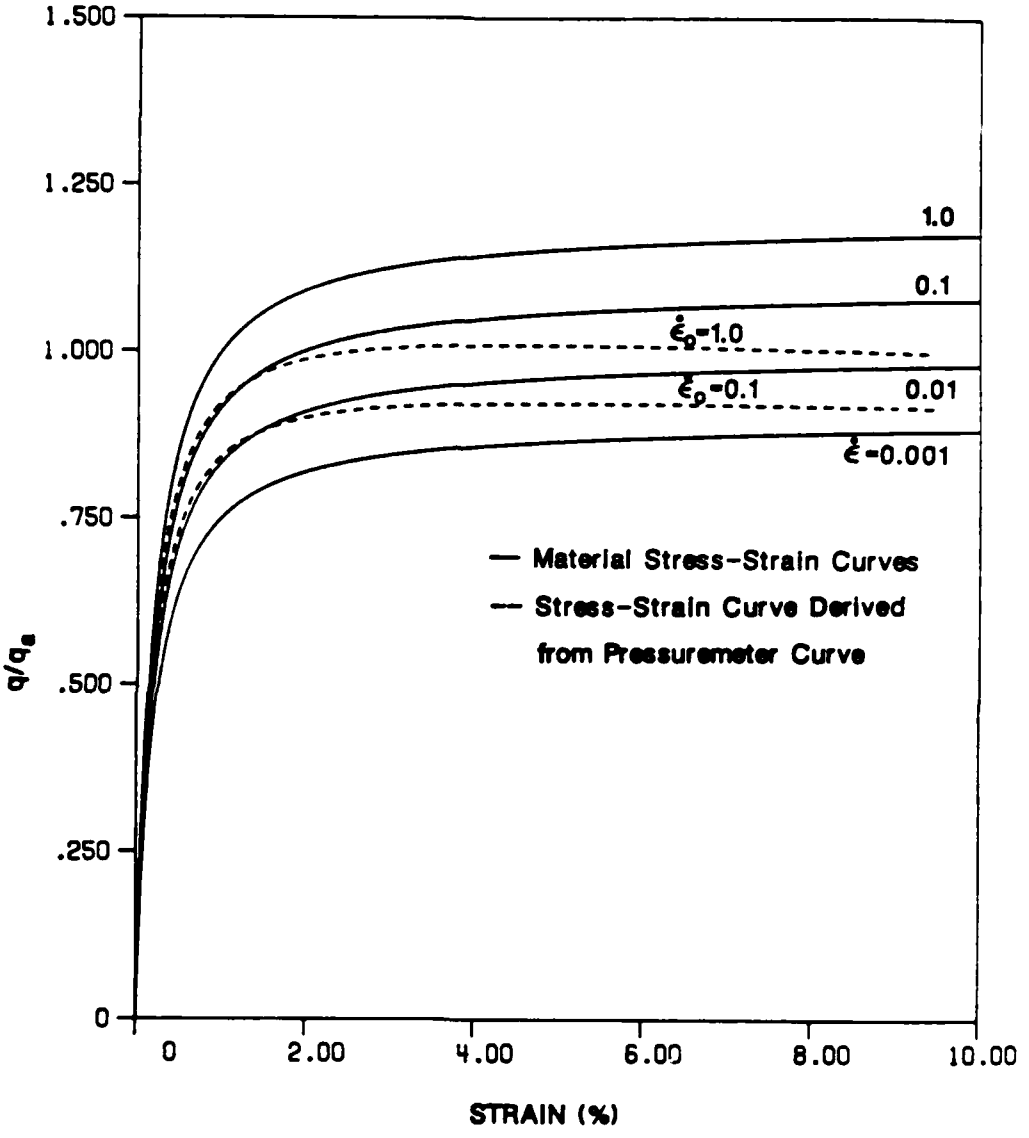

Figure 6.2 Effect of strain rate on undrained strength derived from pressuremeter test: Strain hardening soils

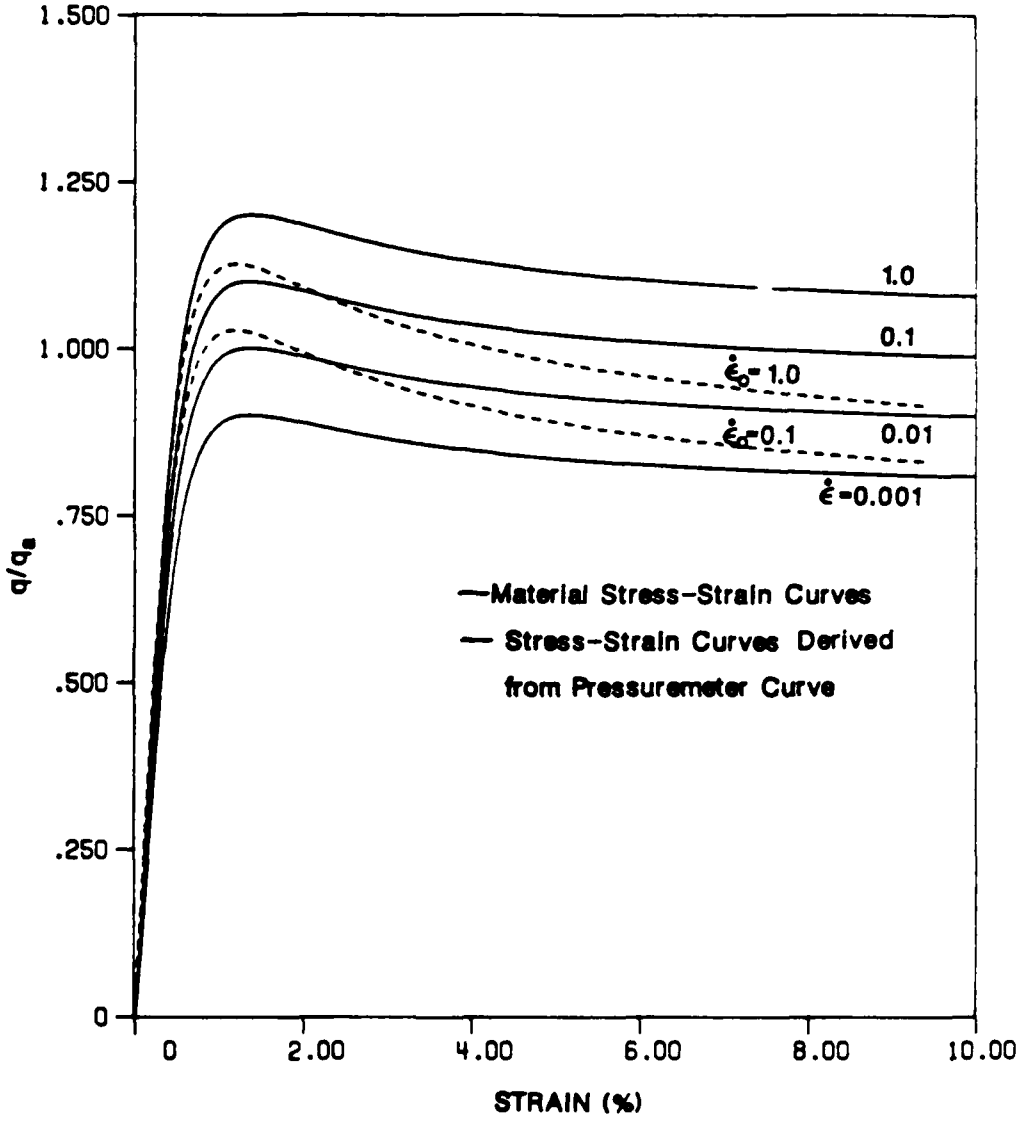

Figure 6.3 Effect of strain rate on undrained strength derived from pressuremeter test: Strain softening soils

ever, the maximum value of strength is not affected significantly.

b. Strain Softening Soils

- The derived stress-strain curves exhibit more pronounced strain softening characteristics as compared to the material stress-strain curve.
- The peak stress at 1.0% per min strain rate is 12.6% larger than the reference strength whereas the peak stress at 0.1 per min strain rate is about 2.6% larger than the reference strength.

It can be concluded that, regardless of whether strain hardening or strain softening is involved, not considering strain rate effects causes different stress-strain curves and strengths to be predicted from pressuremeter expansion curves than if they are included. If laboratory results are the reference (lower strain rates), then the usual pressuremeter test creates an overestimate of the undrained strength. In these parametric studies, for the pressuremeter strain rate, the strength was overestimated by about 13% for strain softening soils. For strain hardening soils, even though the form of the stress-strain curve was different, the maximum value of strength was not affected significantly.

6.2 Effect of Partial Drainage

A typical pressuremeter test takes about 20 to 60 min depending upon whether it is a stress or strain-controlled test, thus some drainage will inevitably occur during this period. The degree of pore pressure dissipation depends on the consolidation characteristics of the soil and, since the coefficient of permeability in the horizontal direction is often greater than that in the vertical direction, significant dissipation of pore pressures could be

expected. The volume change associated with drainage during the test is usually ignored in the interpretation of test results.

In this section, the effect of partial drainage on the pressuremeter expansion curve is studied and the results are discussed. The soil skeleton is assumed to behave as a linear-elastic material.

Method of Analysis -- Soil consolidation is a process by which the applied stresses are gradually transferred to the soil skeleton following the dissipation of excess pore pressure. There are two main categories of consolidation theories. One is called the Terzaghi-Rendulic method or the uncoupled approach, where it is assumed that the total stress remains constant everywhere so that strains are caused only by the change in effective stress. The second is the coupled approach by Biot (1941) in which the continuing interaction between skeleton and pore water is included in the formulation. This generally leads to more complex equations.

Sills (1975) showed that for a linear elastic soil, radial consolidation around a spherical cavity is an inherently uncoupled problem. The same results apply to radial consolidation around a cylindrical cavity. This means that the Biot's equation can be reduced to the Terzaghi-Rendulic equation for a linear elastic soil model.

Consolidation Equation -- The governing equation for consolidation around a cylindrical cavity is:

$$\frac{\partial u}{\partial t} = C \left[\frac{\partial^2 u}{\partial r^2} + \frac{1}{r} \frac{\partial u}{\partial r} \right] \tag{6.13}$$

where, u = pore pressure

C = coefficient of consolidation

r = radial coordinate

t = time

The boundary conditions for consolidation during the pressuremeter expansion test are as follows:

$$\begin{aligned}
&\text{a.}\quad u = u_0(r) \quad \text{at} \quad t = 0 \quad \text{for} \quad r \geq r_0 \\
&\text{b.}\quad u \longrightarrow 0 \quad \text{as} \quad t \longrightarrow \infty \quad \text{for} \quad r \geq r_0 \\
&\text{c.}\quad u = 0 \quad \text{at} \quad r = r^* \quad \text{for} \quad t \geq 0 \\
&\text{d.}\quad \frac{\delta u}{\delta r} = 0 \quad \text{at} \quad r = r_0 \quad \text{for} \quad t \geq 0
\end{aligned} \tag{6.14}$$

where, r_0 = radius of borehole.

r^* = distance sufficiently far from the wall so that excess pore pressure is zero.

The approach used by Randolph and Wroth (1979) to solve the consolidation equations for consolidation around a cylindrical pile was used in this study. However, it was extended to different boundary conditions, since in the pressuremeter test there is displacement at the cavity face during consolidation, whereas no displacement occurs at the pile wall. It is assumed that the boundary between the pressuremeter membrane and the soil is impermeable and drainage takes place radially away from the membrane. Furthermore, at the end of expansion and before consolidation has started, the excess pore pressure distribution will be of the form shown in Fig. 6.4. For $r_0 \leq r \leq R$ (where r_0 is the radius of the expanded cavity and R the radius of the plastic zone) the excess pore pressure, $u_0(r)$, is non-zero, whereas for $r > R$, $u_0(r)$ is equal to zero. The initial distribution of pore pressure is obtained by assuming that the soil behaves as elastic-perfectly plastic material, and expressed as (Fig. 6.4):

$$u_0(r) = 2\, c_u \ln\left[\frac{R}{r}\right] \qquad r_0 \leq r \leq R \tag{6.15}$$

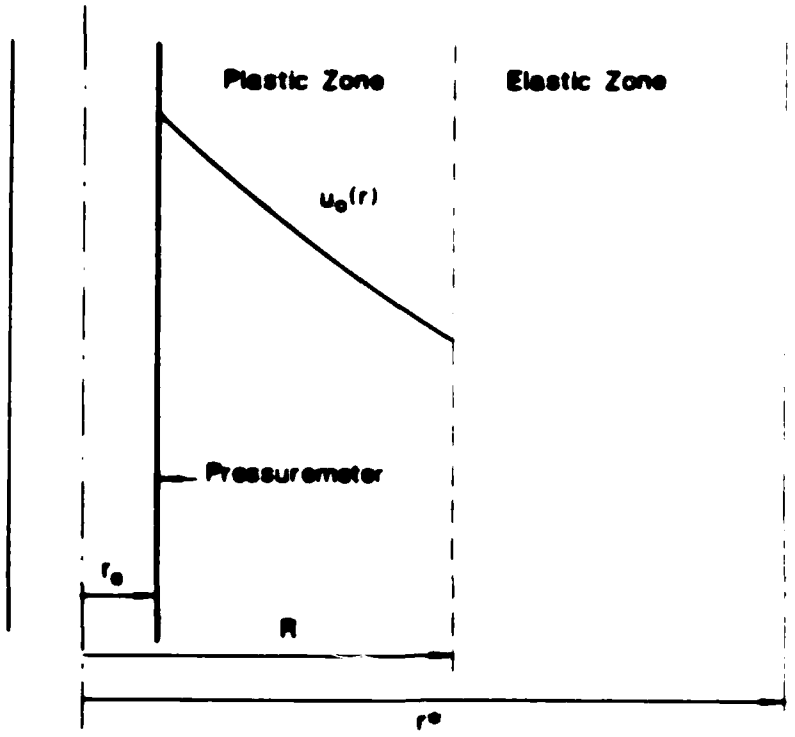

Figure 6.4 Diagram of soil around pressuremeter showing features of consolidation

$$u_0(r) = 0 \qquad R < r \leq r'$$

where, c_u = undrained strength.

It will be shown later that the above initial distribution is reasonable in predicting the pore pressure generated during pressuremeter expansion in a calibration chamber. A complete solution to Eq. 6.13 can be obtained by a technique based on separation of variables (details can be found in Prapaharan (1987), and expressed as:

$$u = \sum_{n=1}^{\infty} A_n e^{-\lambda_n^2 T} \left[J_0(\lambda_n r) + \gamma_n Y_0(\lambda_n r) \right] \tag{6.16}$$

where A_n, γ_n, λ_n, and λ_n are constants which can be determined from boundary conditions, and

$J_0(\lambda r)$ = Bessel function of order zero and kind one.

$Y_0(\lambda r)$ = Bessel function of order zero and kind two.

$$\lambda_n = \left[\frac{\omega_n^2}{C} \right]^{1/2}$$

Eq. 6.16 can be used to calculate the pore pressure distribution and its dissipation with time at any point in the soil mass.

Calculation of Displacement at the Cavity Face Due to Consolidation -- The change in volume of the cavity with time, at constant cavity stress, can be calculated if the distribution and dissipation of the pore pressure with time are known. In the following analysis, it was assumed that the cavity expanded to a radius, r_o, under undrained conditions, and the pore pressure dissipation and volume change took place only after the expansion is completed. It is recognized that this assumption is limited, since during the

pressuremeter expansion test, some drainage takes place and the volume of the cavity increases; however it is believed that the parameters thus calculated constitute an upper bound solution (e.g. an upper bound of the effect of partial drainage on the pressuremeter expansion curve). The displacement, s(t), at the cavity boundary due to consolidation is (Prapaharan, 1987):

$$s(t)=\frac{1-2\nu'}{2G(1-\nu')}\sum A_n(e^{-(\lambda_n r_0)^2 Ct/r_0^2}-1)(F(\lambda_n r^*)-F(\lambda_n r_0)) \qquad (6.17)$$

where,

G = shear modulus

ν' = Poisson's ratio

$$F(\lambda r) = r\left[J_0(\lambda r) + \frac{\pi}{2}\left[J_1(\lambda r)H_0(\lambda r) - J_0(\lambda r)H_1(\lambda r)\right]\right] +$$

$$\mu r\left[Y_0(\lambda r) + \frac{\pi}{2}\left[Y_1(\lambda r)H_0(\lambda r) - Y_0(\lambda r)H_1(\lambda r)\right]\right]$$

H_0 = Struve function of order zero

H_1 = Struve function of order one

Calculation of Change in Volume of the Cavity Due to Consolidation -- The total volume change, ΔV, per unit height of the cavity due to consolidation (for small displacements) is given by:

$$\Delta V = 2\pi r_0 s(t)$$

and

$$\frac{\Delta V}{V_0} = 2\left[\frac{r_0}{a^2}\right]s(t) \qquad (6.18)$$

where, $V_0 = \pi a^2$ is the initial volume of the cavity.

Results and Discussion -- Computer programs were written to perform all the above calculations and the methodology developed in the previous sections was used to predict the pore pressure distribution measured during

pressuremeter expansion tests performed in a kaolin clay in the calibration chamber (Chapter 2). The pore pressure distribution was measured after the pressuremeter was expanded to a radial strain of 10%.

The strength parameters for kaolin were obtained from the pressuremeter test. Since the soil was assumed to be elastic-perfectly plastic in the analysis, the interpretation procedure by Gibson and Anderson (1961) was used to derive the strength parameters from the pressuremeter expansion curve. The values of G/c_u and c_u were found to be 250 and 62 KPa, respectively. The coefficient of consolidation for kaolin in the horizontal direction was obtained by Huang (1986), and is equal to 7.4 m^2/yr.

During the pressuremeter expansion test, both generation and dissipation of pore pressures take place. Some simplifying assumptions are necessary in order to use closed form solutions for strain-controlled expansion. Initially, it is assumed that no dissipation of pore pressure takes place until the pressuremeter is expanded to a certain strain (ϵ_1), and the probe pressure is then held constant. The pore pressure generated during the expansion, $u_o(r)$, is calculated using Eq. 6.15. The actual pore pressure will be less than that given by Eq. 6.15 as some dissipation takes place during expansion. The dissipation of pore pressure with time after the expansion is calculated using Eq. 6.16. If the time taken to reach the strain ϵ_1 is t_1, it will be assumed that the pore pressure dissipated during expansion is equal to that dissipated after the expansion during the time interval t_1. Obviously, this is an upper bound solution. A similar approach can be used to calculate the change in volume of the cavity due to consolidation during expansion.

Fig. 6.5 shows the distribution of pore pressure with time after the pressuremeter has been expanded to 10% strain. The predicted and the measured

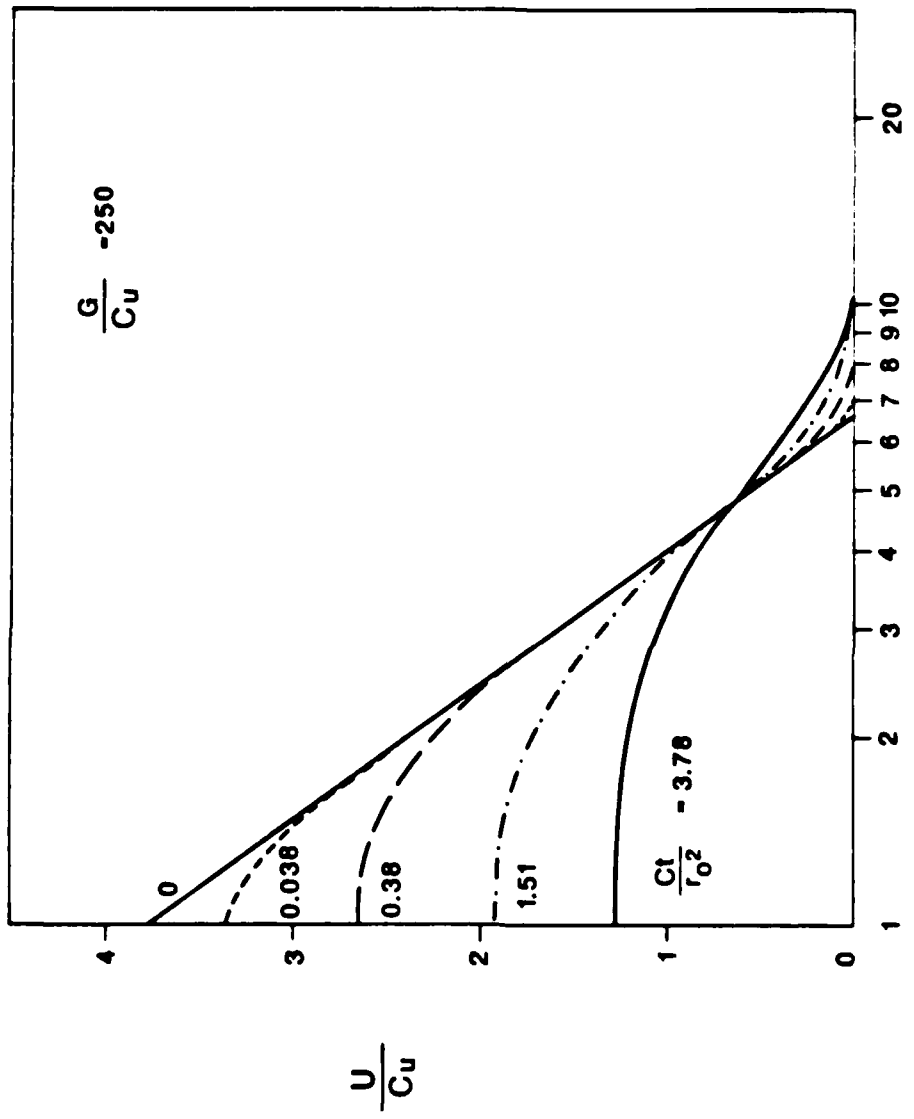

Figure 6.5 Variation of radial distribution of pore pressure with time (after expansion to 10% strain)

pore pressure distribution curves for the pressuremeter expansion test in the calibration chamber are shown in Fig. 6.6. The pore pressure distribution was obtained after the pressuremeter was expanded to 10% strain at a strain rate of 0.73%/min. The predicted curves were obtained by two methods. In the first method (discussed previously), it is assumed that no drainage takes place until the pressuremeter is expanded to 10% strain. The pore pressure dissipated during the expansion is assumed to be equal to that dissipated after the expansion for a time interval equal to that taken to reach 10% strain. In the second method, it is assumed that 10% strain is reached in 4 increments. The distribution of pore pressure after the first increment is calculated using the method mentioned above. The pore pressure increase during the second increment is added to the pore pressure obtained after the first increment. The resulting distribution is approximated by a linear distribution with the logarithm of radius, and used as the initial pore pressure distribution at the end of second increment. This procedure is repeated until 10% strain is reached.

Fig. 6.6 shows that the theoretical pore pressure distribution curves obtained by both methods do not differ considerably. The shapes of the predicted and experimental curves are similar, and the agreement between both curves are excellent. It shows that linear solutions can be used to predict the distribution of pore pressures around the pressuremeter.

The effect of the change in volume of the cavity due to partial drainage on the pressuremeter expansion curve is shown in Fig. 6.7. The undrained pressuremeter expansion curve was obtained from solutions for cavity expansion in an elastic-perfectly plastic medium (Gibson and Anderson, 1961). The expansion curve with partial drainage was determined by adding the additional strain caused by partial drainage to the strain obtained for undrained

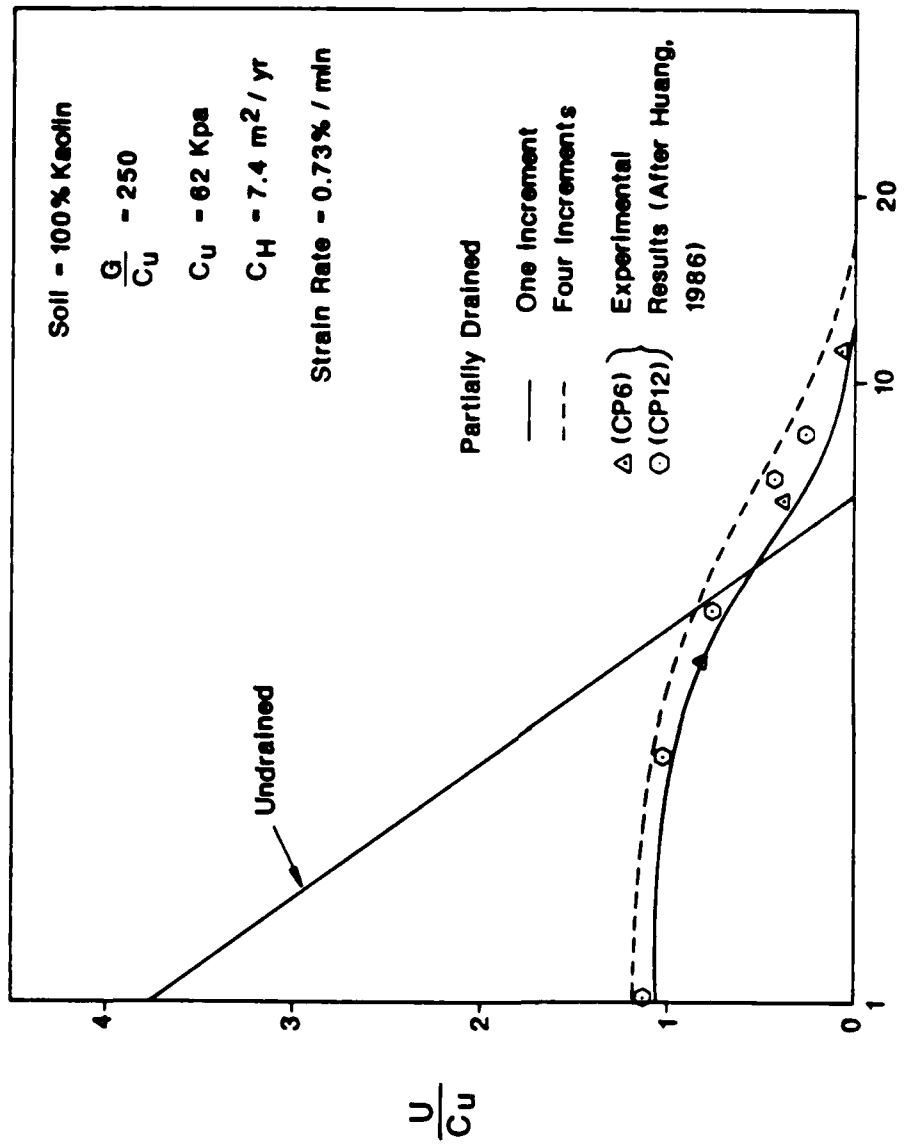

Figure 6.6 Predicted and measured pore pressure distribution around pressuremeter at 10% radial strain

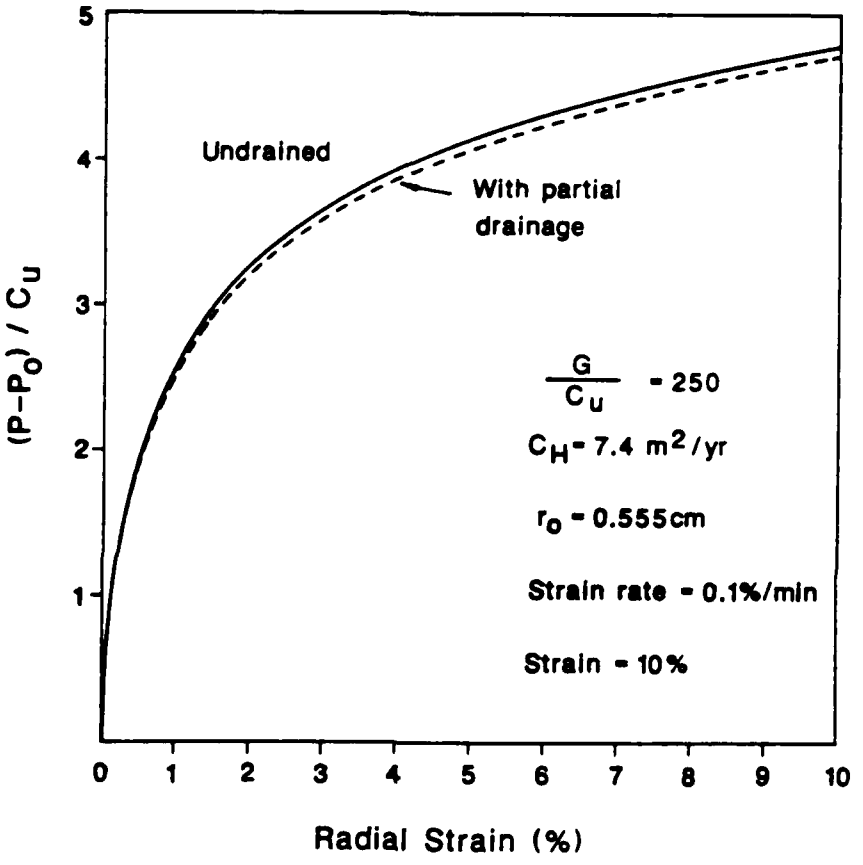

Figure 6.7 Effect of consolidation on expansion curve $\frac{G}{C_u}$ = 250

expansion. Although considerable dissipation of pore pressure occurs during expansion (Fig. 6.6), the pressuremeter expansion curve is not altered significantly, especially at small strains. In this analysis, the increase in strength of the soil due to consolidation was not considered, and any increase in strength would have resulted in a smaller volume change at large strains.

It is not possible to obtain experimentally the undrained expansion curve shown in Fig. 6.6 in the calibration chamber as dissipation of pore pressure occurred even at the highest strain rates (e.g., 0.73%/min) used in the test (Chapter 2). It is believed that the pressuremeter expansion curve obtained for kaolin in the calibration chamber was not affected significantly by partial drainage as the derived undrained strength was very close to that predicted from triaxial compression and extension test results (Table 6.1).

The dissipation of pore pressure, and hence the change in volume of the cavity during the pressuremeter test, will be smaller if a larger pressuremeter probe is used; this is illustrated in Figs. 6.8 and 6.9. The pressuremeter curves with partial drainage in these figures were obtained for a strain rate of 0.2%/min and a probe diameter of 8.0 cm. It was also found that at the standard strain rate of 1%/min, almost no influence of partial drainage was detected on the pressuremeter expansion curve.

6.3 Conclusions

The comparison of results from analytical and experimental studies using a model pressuremeter show that linear analysis can be used to predict the pore pressure generated during pressuremeter expansion. The partial drainage that takes place during the pressuremeter test was shown to affect the generation of pore pressures. However, the pressuremeter expansion curve was not altered significantly by partial drainage.

Table 6.1 Experimental and predicted undrained strength values

Soil	OCR	c_u^1	Strain Rate	
			0.1%/min	0.73%/min
			c_u^2	c_u^2
50% Kaolin 50% Silt	1.0	64	65	63
100% Kaolin	1.0	59	-	62

c_u^1 - Undrained strength predicted from triaxial compression and extension test results.

c_u^2 - Undrained strength derived from pressuremeter tests in a calibration chamber.

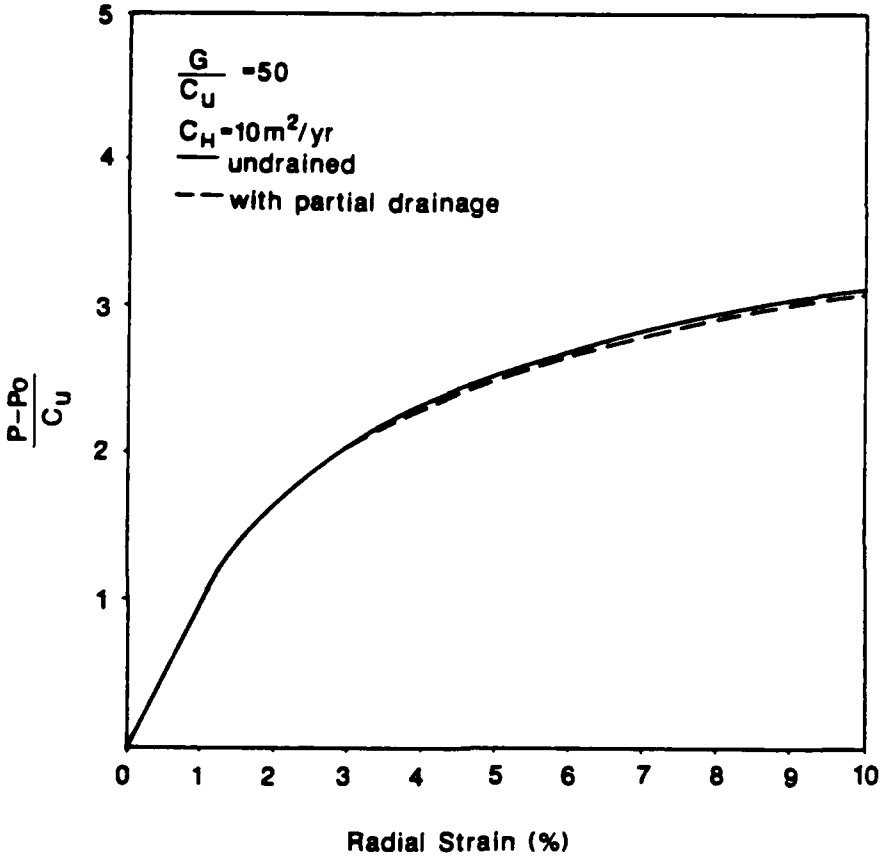

Figure 6.8 Effect of consolidation on expansion curve: $G/c_u = 50$

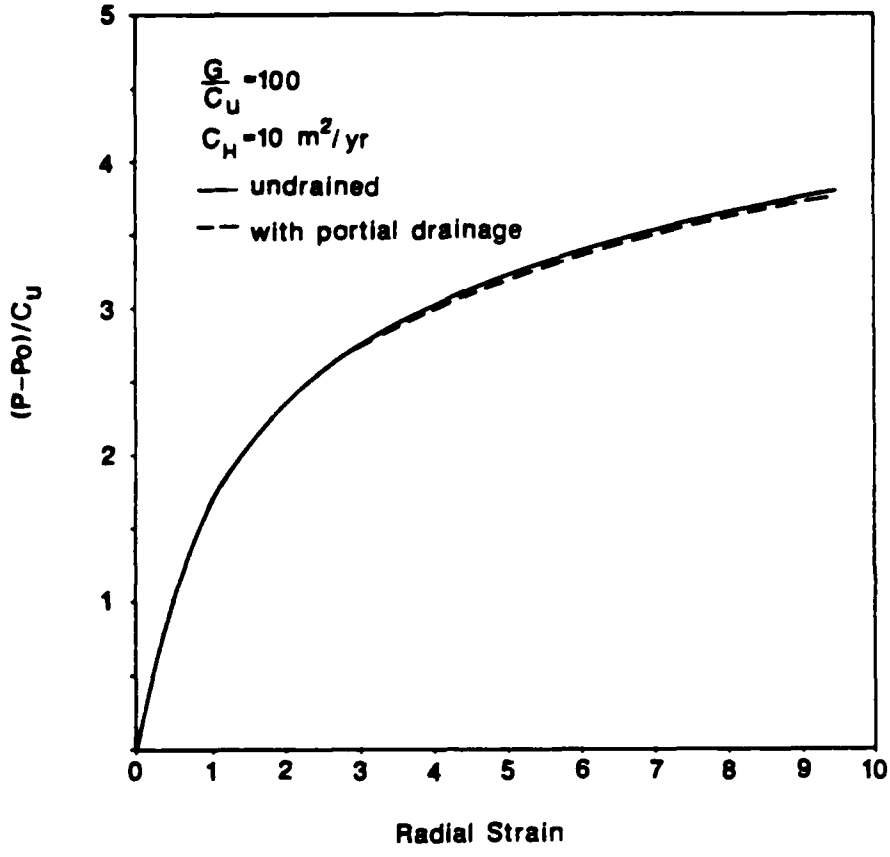

Figure 6.9 Effect of consolidation on expansion curve: G/c_u = 100

The analytical studies indicate that the pressuremeter expansion curve obtained using commercially available probe with a standard strain rate of 1%/min is not significantly affected by partial drainage. As a result, the interpretation methods developed to derive stress-strain curve from undrained pressuremeter expansion curve can still be used, even if the expansion is not perfectly undrained.

CHAPTER 7

THEORETICAL STUDY OF ANISOTROPY AND STRESS PATH

7.1 Introduction

A theoretical study was made of two factors which influence the laboratory and field tests: undrained strength anisotropy and the stress path. The effects of intermediate principal stress in plane strain compression (e.g., pressuremeter test) were also studied (Sivakugan, 1987). Although the study was initiated as part of our research program on the pressuremeter testing in clays, it provides a strong theoretical basis for the shear strength of clays in general.

7.2 CK_0UC Tests versus CIUC Tests

In conventional laboratory triaxial testing the test specimens are isotropically or hydrostatically consolidated (CIUC Tests) primarily because of convenience and simplicity in the testing procedures. Non-hydrostatic or anisotropically consolidated (CAUC) tests are more complicated, requiring some form of servo system to perform K_0 consolidation. Therefore, it is highly desirable to have some means of predicting the CK_0UC shear strength simply from CIUC test results.

Based on Skempton's (1954) pore pressure equation, a simple procedure was developed to predict CK_0UC (K_0 consolidated undrained compression) shear strength from CIUC tests. The procedure was validated with experimental data available in the literature. This technique has a sound theoretical basis and it will very likely be useful in future interpretation of both field and

laboratory tests. The reader is referred to the paper by Sivakugan et al (1987) for details. One of the parameters required in the predictions was A_f, the Skempton's A-parameter at failure for K_o consolidated soils. It was shown that even a "crude estimate" of A_f is sufficient for a reasonably good prediction of CK$_o$U shear strength. Such an estimate of A_f can be obtained from the extended Cam Clay or extended Modified Cam Clay model proposed by Sivakugan (1987). These models are briefly described below, since not only can they be used to estimate A_f, but also to model the in situ behavior of normally consolidated clays. It is believed that they will prove to be useful to researchers in the future.

7.3 Triaxial Shear Model for Normally Consolidated Clays

The need to develop better constitutive models for soils to predict stress-strain behavior was realized in the early 1960s with the evolution of the critical state soil models. The Cam Clay (Roscoe et al., 1963) and the modified Cam Clay (Roscoe and Burland, 1968) are the most widely accepted critical state models. They have undergone several modifications over the past two decades (Egan, 1977; Pender, 1978; van Eekelen and Potts, 1978).

The critical state model gives a simple qualitative view of soil behavior but, at the same time, it purports to give a complete mathematical model for saturated clays. It describes well commonly observed features of soil behavior. The strength, effective stress, and water content are linked together in a rational way. As a framework for teaching, understanding and communicating the fundamentals of soil mechanics, critical state soil mechanics is highly recommended (Atkinson, 1983). However, the Cambridge soil models were developed essentially for isotropically consolidated clays, although most soil deposits encountered in nature are one-dimensionally consolidated with K_o

lateral deformation. Therefore, it is more appropriate to study the triaxial shear behavior of clays consolidated with no lateral strains.

In this research, the Cam Clay and the modified Cam Clay models were extended to consider a K_o consolidated initial state. A new state parameter, the spacing ratio, was introduced to simplify the analysis. Expressions were developed for $A_{f_{K_o}}$ and undrained shear strength. A brief summary of this study and the final conclusions are given below. The details of derivations are given in Sivakugan (1987).

7.3.1 Extension of Critical State Models to K_o UC Tests

The state boundary surface according to the Cambridge soil models is shown in the p – q – v space (Fig. 7.1). p and q are the mean effective stress and the deviatoric stress respectively. v is the specific volume defined as

$$v = 1 + e \tag{7.1}$$

where e is the void ratio.

In the Cambridge soil models, it was hypothesized that the K_o consolidation line (K_o CL) in the p – q – v space lies on the state boundary surface between the critical state line (CSL) and the isotropic consolidation line (ICL) (Atkinson and Bransby, 1978, Roscoe and Poorooshasb, 1963). Furthermore, ICL, K_o CL and CSL are assumed to be three parallel lines with a negative slope of λ in the v – ln p plane, as shown in Fig. 7.2 (Atkinson and Bransby, 1978). In the v – ln p plane, ICL, K_o CL and CSL are given by the following equations respectively.

$$v = N - \lambda \ln p \tag{7.2a}$$

$$v = N_{K_o} - \lambda \ln p \tag{7.2b}$$

$$v = \Gamma - \lambda \ln p \tag{7.2c}$$

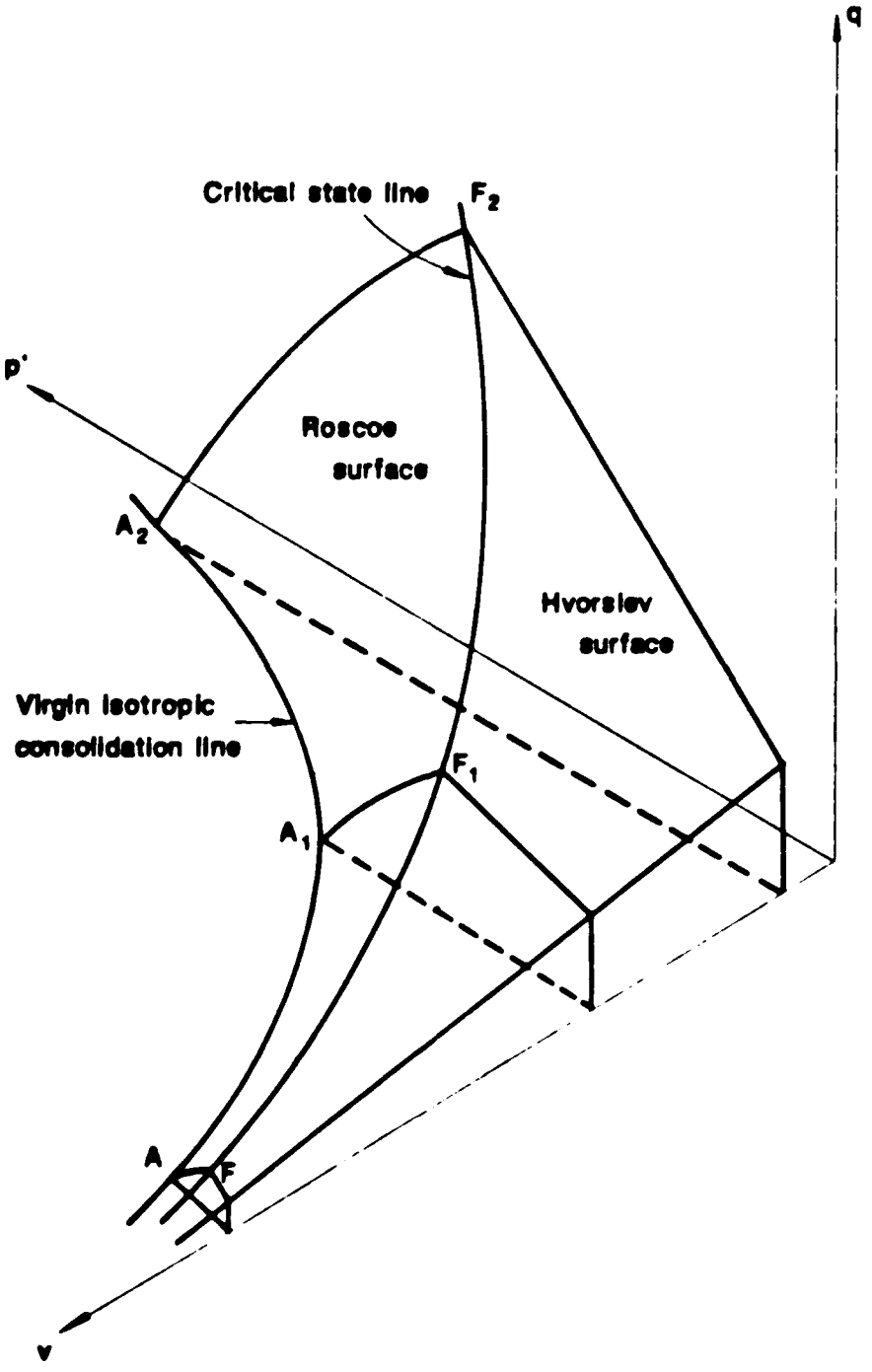

Figure 7.1 State Boundary Surface in p' - q - v Space

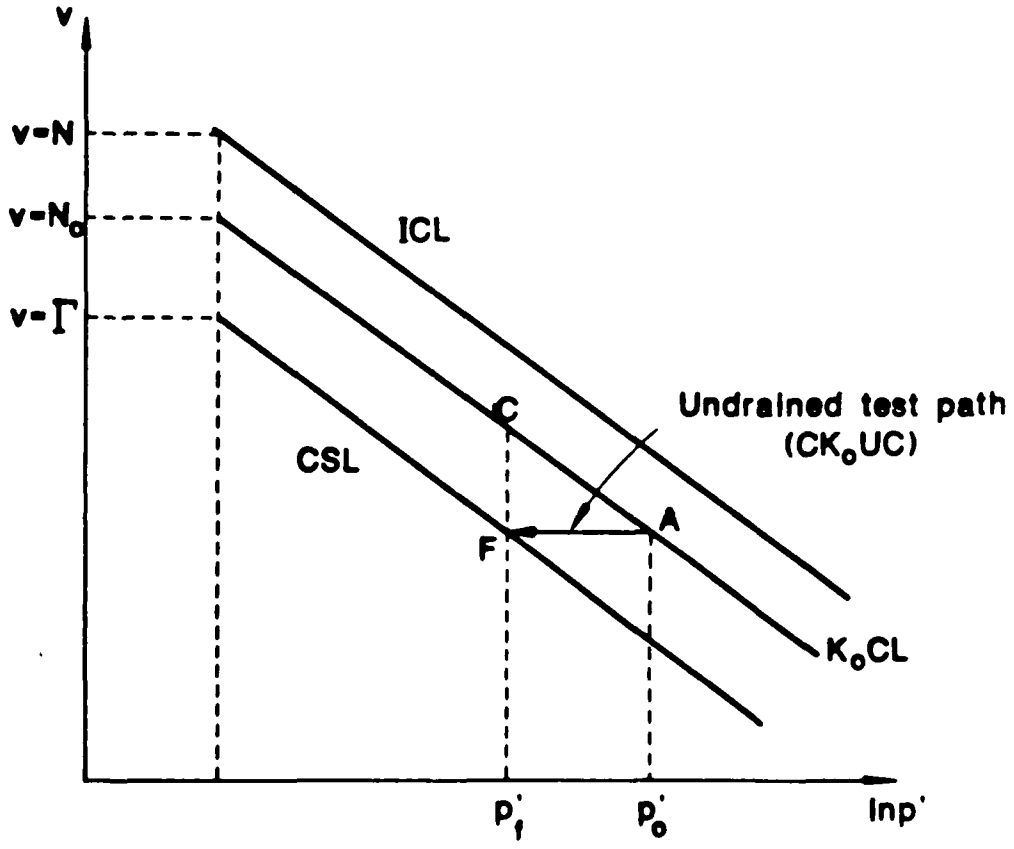

Figure 7.2 ICL, K_oCL, CSL, and CK_oUC Test Path on v - ln p' Plane

7.3.2 Extension of the Cam Clay Model

The test paths of a one dimensionally consolidated specimen (Point A) sheared undrained to failure (Point F) is shown in Fig. 7.3. The state boundary surface of the Cam Clay model is given by

$$q = \frac{M\, p'}{(\lambda - \kappa)} (N - v - \lambda \ln p') \tag{7.3}$$

This equation is valid immediately after consolidation (point A) and at failure (Point F); introducing the values of p', q, and v for these two limits in Eq. 7.3 and solving for the ratio p_o'/p_f' leads to:

$$\ln \left[\frac{p_o'}{p_f'} \right] = \Lambda \left[1 - \frac{\eta_o}{M} \right] \tag{7.4}$$

where

$$\Lambda = 1 - \frac{\kappa}{\lambda} \tag{7.5}$$

$$\eta_o = \frac{3\,(1 - K_o)}{(1 + 2K_o)} \tag{7.6}$$

Λ is known as the critical state pore pressure parameter or the irreversibility ratio.

Spacing Ratio

From the geometry in Fig. 7.2 and Eq. 7.4, λ can be expressed as

$$\lambda = \frac{N_o - 1}{\Lambda \left[1 - \frac{\eta_o}{M} \right]} \tag{7.7}$$

The spacing ratio r proposed in this study is defined as:

$$r = \frac{N_o - 1}{N - 1} \qquad (0<r<1) \tag{7.8}$$

For the Cam Clay model it can be shown that (Atkinson and Bransby, 1978):

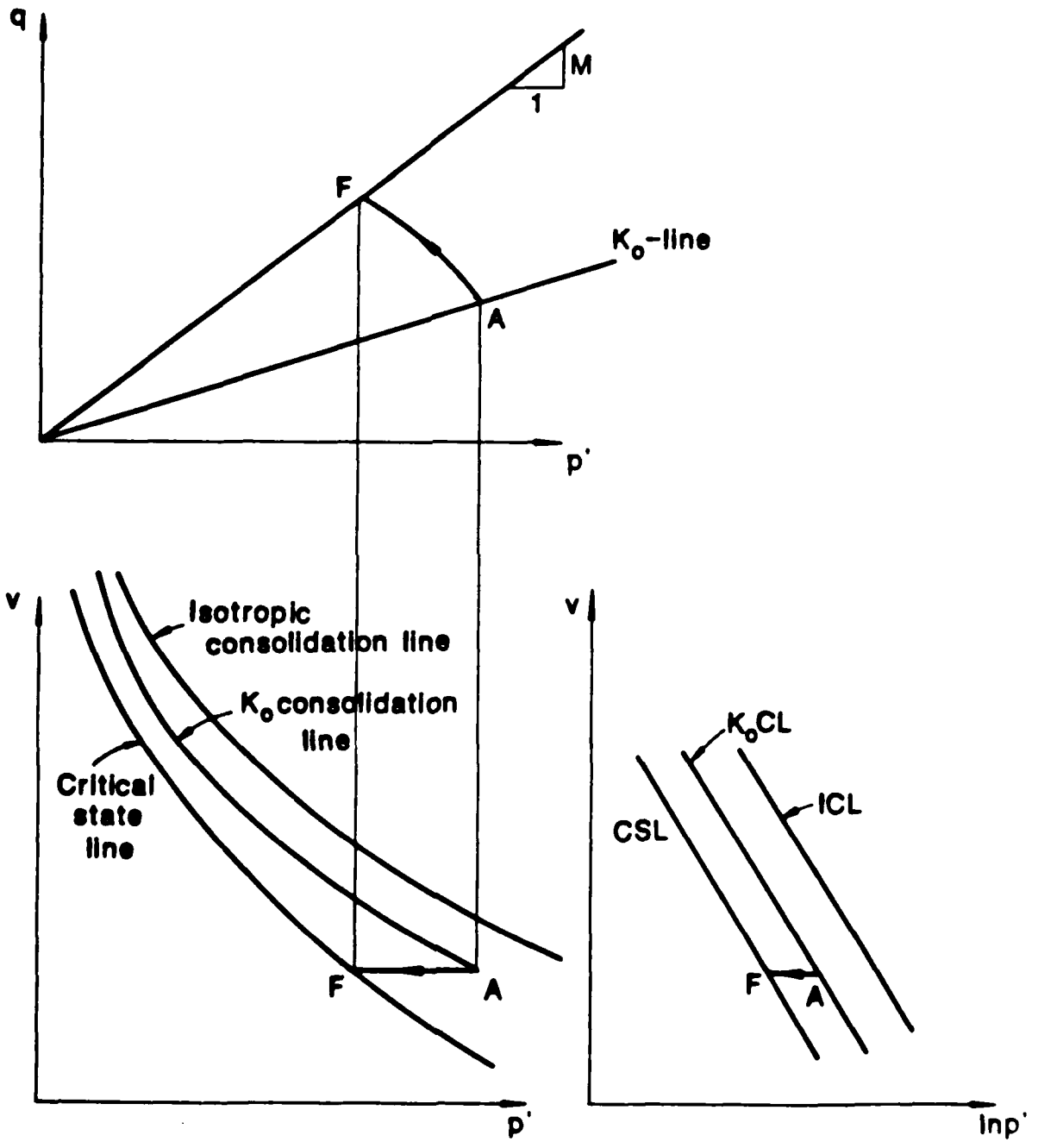

Figure 7.3 Stress Path (AF) of a CK_oUC Test

$$\lambda - \kappa = N - \Gamma \tag{7.9}$$

From Eqs. 7.7, 7.8, and 7.9:

$$r = 1 - \frac{\eta_o}{M} \tag{7.10}$$

This ratio is equal to 0 when $N_o = \Gamma$ (CSL) and equal to 1.0 when $N_o = N$ (ICL).

Pore Pressure Parameter

The total and effective stress paths for a CK_oUC test are shown in Fig. 7.4. The excess pore pressure at failure (Δu_f) and the change in deviatoric stress (Δq) are given by:

$$\Delta u_f = p_o' + \frac{1}{3}(q_f - q_o) - p_f' \tag{7.11}$$

$$\Delta q = q_f - q_o \tag{7.12}$$

Thus Skempton's A_f ($=\Delta u_f/\Delta q$) is:

$$A_f = \frac{1}{3} + \frac{(p_o' - p_f')}{(q_f - q_o)} \tag{7.13}$$

At failure:

$$q_f = M\, p_f' \tag{7.14}$$

From Eqs. 7.4, 7.10, 7.13, and 7.14, A_f can be written as:

$$A_f = \frac{1}{3} + \frac{\exp(r\Lambda) - 1}{M - \eta_o \exp(r\Lambda)} \tag{7.15}$$

Undrained Shear Strength

The undrained shear strength of of a CK_oUC test is given by:

$$\tau_f = \frac{1}{2} q_f$$

$$= \frac{1}{2} M\, p_f' \tag{7.16}$$

From Eqs. 7.4 and 7.16:

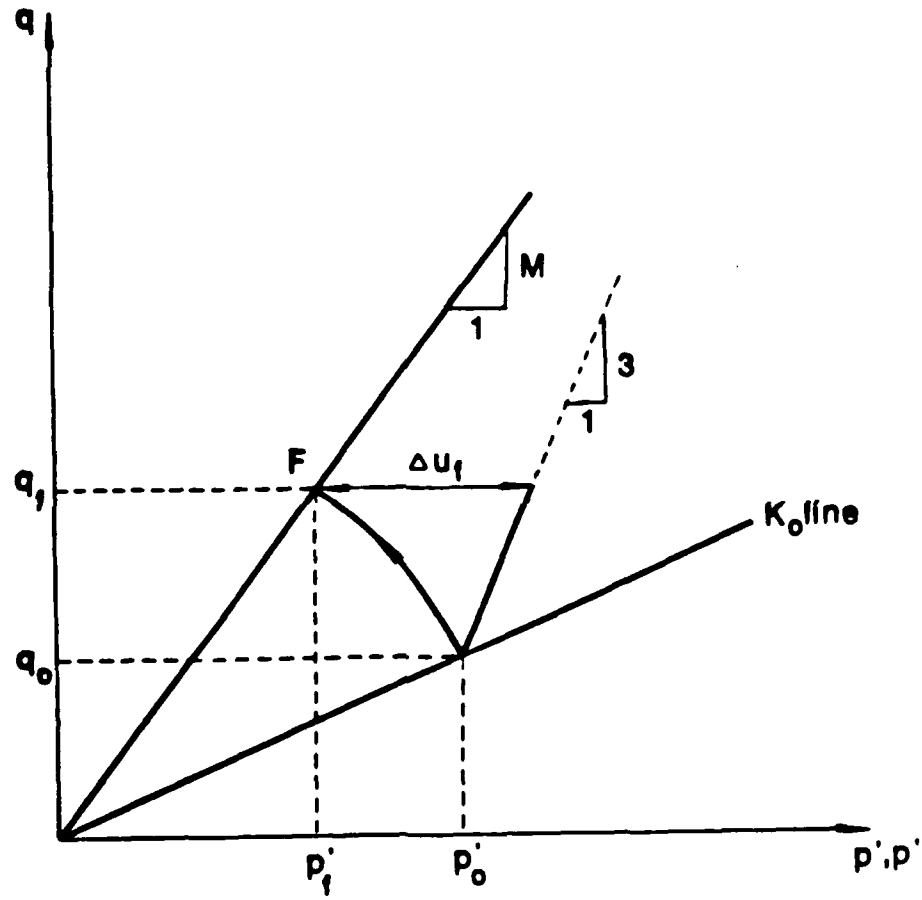

Figure 7.4 Effective and Total Stress Paths for CK_oUC Test

$$\tau_f = \frac{1}{2} M p_o' \left[\Lambda \left[\frac{\eta_o}{M} - 1 \right] \right]$$

In terms of the spacing ratio:

$$\frac{\tau_f}{\sigma_{vo}'} = \frac{M}{6} (1 + 2K_o) \exp(-r\Lambda) \tag{7.17}$$

In the Cam Clay model, the modified Cam Clay model, and the extensions proposed herein, the normally consolidated clay is idealized as an elasto-plastic medium exhibiting isotropic strain hardening. Ohta and Nishihara (1985) developed a similar expression as Eq. 7.17 for K_o consolidated clays, based on rheological and dilatancy characteristics of soils.

7.3.3 Extension of the Modified Cam Clay Model

The following derivations are similar to those in the extended Cam Clay model given above. The state boundary surface of the modified Cam Clay model is given by:

$$\ln \left[\frac{M^2 + \eta^2}{M^2} \right] = \frac{N - v - \lambda \ln p'}{\lambda - \kappa} \tag{7.18}$$

where $\eta = q/p'$. Substituting the values of p', q, and v at the end of consolidation and at failure, the following relationship is obtained:

$$\left[\frac{p_o'}{p_f'} \right] = \left[\frac{2 M^2}{M^2 + \eta_o^2} \right]^{\Lambda} \tag{7.19}$$

Spacing Ratio

From the geometry in Fig. 7.2 and Eq. 7.19, λ can be expressed as:

$$\lambda = \frac{N_o - 1'}{\Lambda \ln \left[\frac{2M^2}{M^2 + \eta_o^2} \right]} \tag{7.20}$$

For the modified Cam Clay model it can be shown that (Sivakugan, 1987):

$$N - \Gamma = (\lambda - \kappa) \ln 2 \tag{7.21}$$

From Eqs. 7.20, 7.21, and the definition of the spacing ratio r:

$$r = \frac{\ln \left[\frac{2M^2}{M^2 + \eta_o^2} \right]}{\ln 2} \tag{7.22}$$

Pore Pressure Parameter

From Eqs. 7.13, 7.14, 7.19, and 7.22, A_f can be written as:

$$A_f = \frac{1}{3} + \frac{\left[2^{r\Lambda} - 1 \right]}{\left[M - \eta_o \, 2^{r\Lambda} \right]} \tag{7.23}$$

Undrained Shear Strength

From Eqs. 7.16, 7.19, and 7.22

$$\frac{\tau_f}{\sigma'_{vo}} = \frac{M}{6} (1 + 2K_o) \, 2^{-r\Lambda} \tag{7.24}$$

7.3.4 Comparison of Extended Critical State Models

In the extended Cam Clay model as well as in the extended modified Cam Clay model, the derivations and the resulting equation are very similar. For both models A_f and τ_f/σ'_{vo} are given by the following equations:

$$A_f = \frac{1}{3} + \frac{F(r,\Lambda) - 1}{M - \eta_o \, F(r,\Lambda)} \tag{7.25}$$

$$\frac{\tau_f}{\sigma'_{vo}} = \frac{M}{6} (1 + 2K_o) \frac{1}{F(r,\Lambda)} \tag{7.26}$$

For the extended Cam Clay model:

$$F(r,\Lambda) = \exp (r\Lambda) \tag{7.27}$$

and for the extended modified Cam Clay model:

$$F(r,\Lambda) = 2^{r\Lambda} \tag{7.28}$$

Variations of $A_{f,ko}$ with ϕ'_{CIUC}, and τ_f/σ'_{vo} with ϕ'_{CIUC} for $K_o = 0.5$, are shown in Figs. 7.5 and 7.6, respectively. ϕ'_{CIUC} is the value of ϕ' obtained from a CIUC test. For low values of Λ, both models predict about the same $A_{f,ko}$. For higher Λ, the extended modified Cam Clay model gives lower values than the extended Cam Clay model. $A_{f,ko}$ decreases with increasing ϕ', decreasing Λ, and increasing K_o. For typical values of ϕ', Λ, and K_o, $A_{f,ko}$ varies between 0.9 and 4.0. Both models predict about the same shear strength. The normalized undrained shear strength varies approximately linearly with ϕ'_{CIUC}. For typical values of K_o, Λ, and ϕ', it varies between 0.25 and 0.45.

The undrained shear strength and pore pressure parameter in the critical state models and the extended critical state models are shown to be functions of friction angle and consolidation characteristics. The friction angle and the consolidation characteristics are represented by ϕ' and Λ, respectively. Few empirical correlations have been cited in the literature relating M with Λ. Schofield and Wroth (1968) proposed that $M/\Lambda = 1.5$. Karube (1975) suggested that it is 1.75. However, based on experimental data from the literature, Sivakugan and Holtz (1986) showed that there appears to be no correlation between M and Λ.

7.4 Intermediate Principal Stress in Plane Strain Compression of Normally Consolidated Clays

The main drawback with the critical state models is that they were developed essentially for conventional triaxial loading conditions, such as those existing under a uniformly loaded large area, or along the vertical center line of a circular footing. However, plane strain conditions are more common in the field; long strip footings, embankments, or retaining walls are

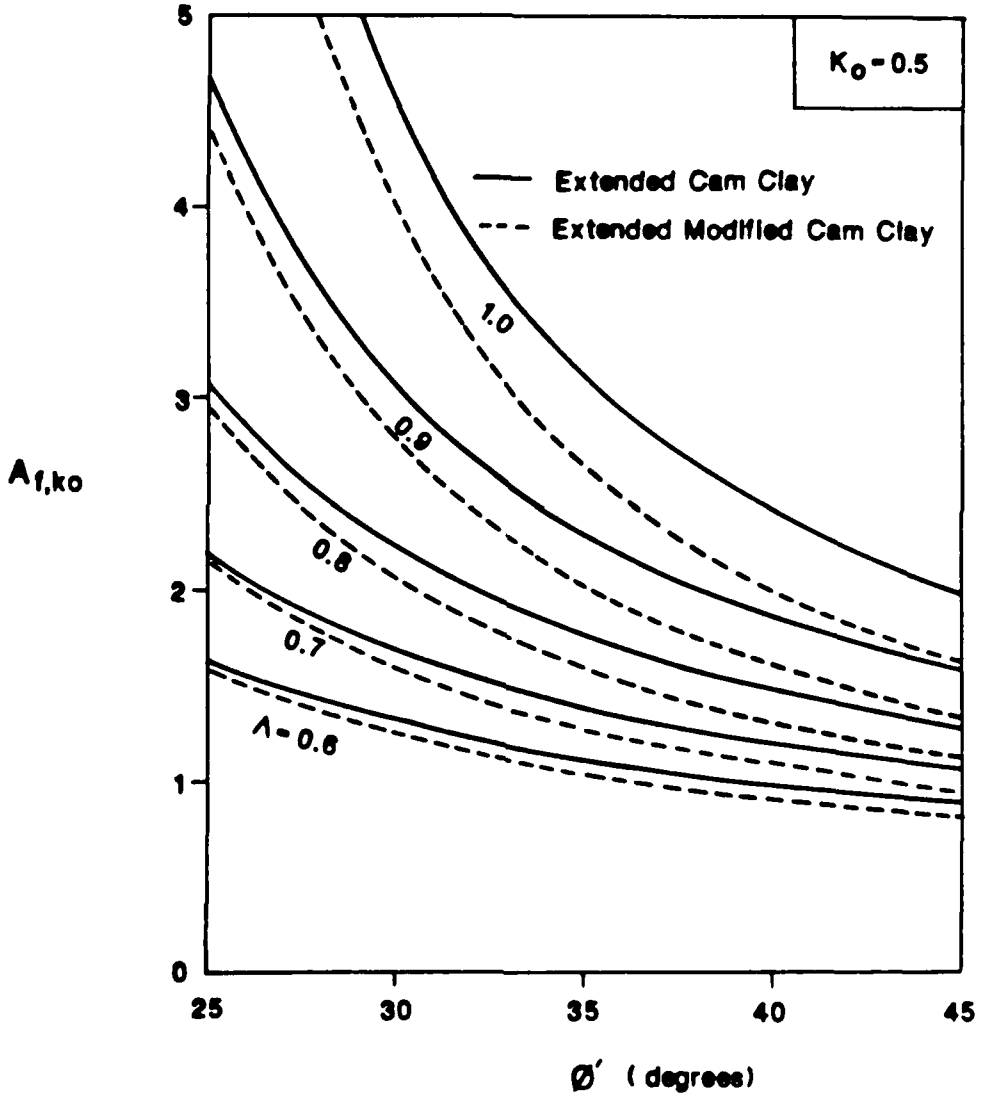

Figure 7.5 Variation of $A_{f,ko}$ with ø' for K_o = 0.5

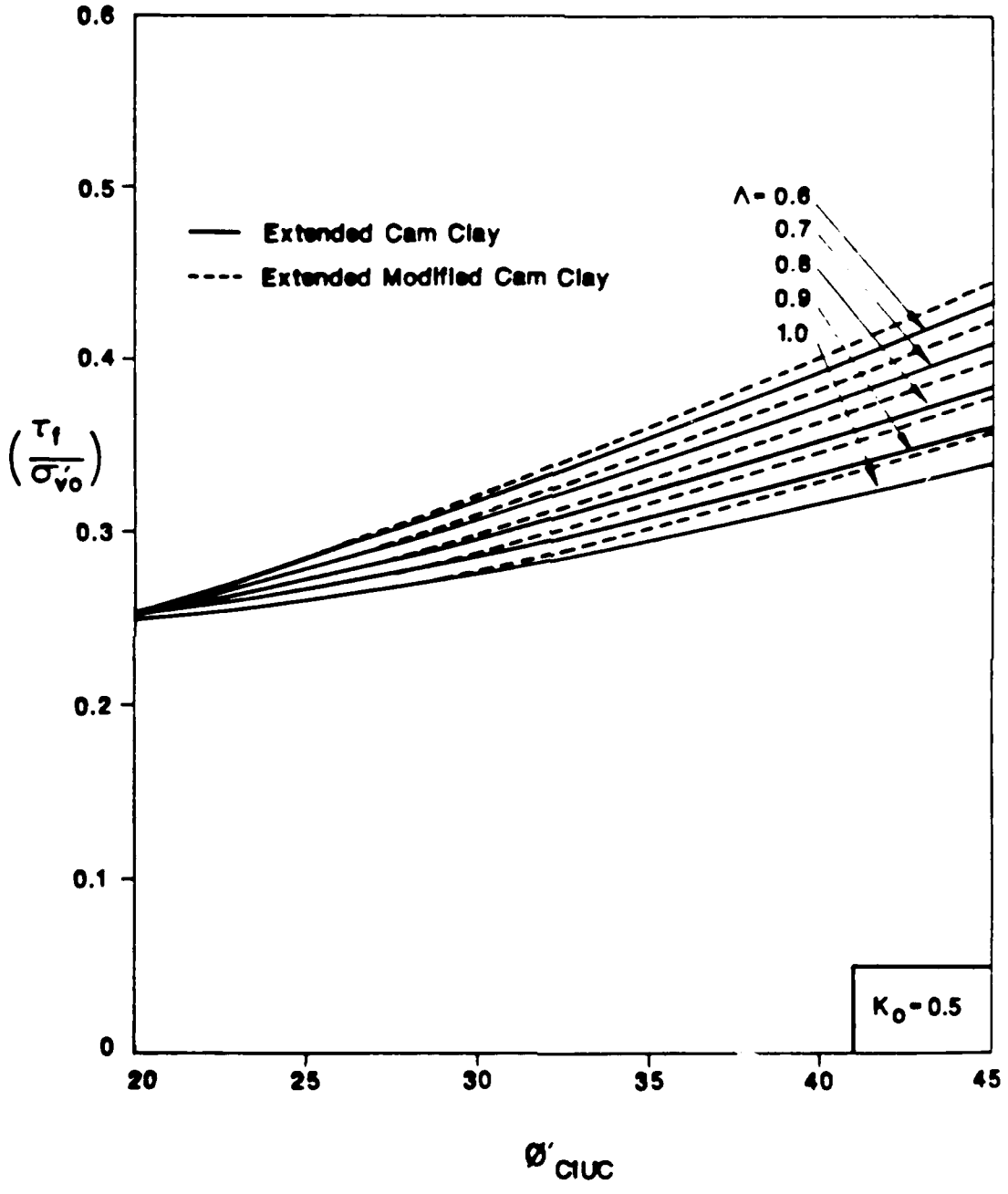

Figure 7.6 Variation of τ_f/σ'_{vo} with ϕ' for K_o = 0.5

good examples of plane strain problems. Pressuremeter loading can also be approximated by a plane strain problem if end effects are neglected.

Many geotechnical engineering problems can be better simulated or approximated by plane strain loading conditions than axisymmetric triaxial loading conditions. However, due to the ease of operation and simplicity of the apparatus, triaxial tests are often preferred to plane strain ones, even for obviously plane strain problems. Conversely, there are relatively few well documented data in the geotechnical literature for plane strain tests on soils (Cornforth, 1964; Henkel and Wade, 1969; Hambly and Roscoe, 1969; Ladd, et al., 1971; Campanella and Vaid, 1973; Mitachi and Kiago, 1980).

In plane strain tests, the intermediate principal stress is not known unless the sides of the specimen corresponding to the plane of zero deformation are instrumented. For analysis of plane strain situations, it is often necessary to know the magnitude of σ_2', the effective intermediate principal stress in the direction of zero deformation. σ_2' is often assumed to be $(\sigma_1' + \sigma_3')/2$ or given from elastic analysis by $\nu(\sigma_1' + \sigma_3')$, where ν is the Poisson's ratio.

Sivakugan (1987) studied the variation of principal stresses during plane strain compression of normally consolidated clays. The elastic model proposed by Cornforth (1964) and the semi-empirical equation given by Bishop (1966) were reviewed. An elasto-plastic model, based on the modified Cam Clay model was proposed to study the principal stress variation during plane strain compression. This research is summarized below.

7.4.1 Relationship between b, ϕ'_{mob}, and $\sigma_2'/(\sigma_1' + \sigma_3')$

The relative magnitude of σ_2' is often expressed as $\sigma_2'/(\sigma_1' + \sigma_3')$ or by the

b-parameter (Bishop, 1966) defined as:

$$b = \frac{\sigma_2' - \sigma_3'}{\sigma_1' - \sigma_3'} \tag{7.29}$$

Strictly speaking, to specify the relative magnitude of the intermediate principal stress, either b or $\sigma_2'/(\sigma_1' + \sigma_3')$ is not sufficient: both are required. It is only at failure one can be computed from the other. This is illustrated by a numerical example in Sivakugan (1987). Defining ϕ'_{mob} as:

$$\sin \phi'_{mob} = \frac{\sigma_1' - \sigma_3'}{\sigma_1' + \sigma_3'} \tag{7.30}$$

it can be shown that:

$$\frac{\sigma_2'}{\sigma_1' + \sigma_3'} = \frac{(2b - 1)}{2} \sin \phi'_{mob} + \frac{1}{2} \tag{7.31}$$

7.4.2 Cornforth's Model

Cornforth (1964) showed from elastic analysis that for soils loaded under plane strain conditions, the following relationship holds throughout the entire test:

$$\frac{\sigma_3'}{\sigma_1' + \sigma_3'} = \frac{K_o}{1 + K_o} = \nu \tag{7.32}$$

where ν is the Poisson's ratio. From incremental elasticity, it is shown later (Section 7.4.5) that this relationship holds only for K$_o$ consolidated soils.

7.4.3 Bishop's Model

Based on plane strain tests on compacted moraine, Bishop (1966) showed that for normally consolidated clays sheared under plane strain conditions $\sigma_2'/(\sigma_1' + \sigma_3')$ at failure is given by

$$\left[\frac{\sigma_2'}{\sigma_1' + \sigma_3'}\right]_f = \frac{1}{2}\cos^2\phi \qquad (7.33)$$

Available data on five different soils (Table 7.1) one dimensionally consolidated and sheared undrained under plane strain compression indicate that $\sigma_2'/(\sigma_1' + \sigma_3')$ increases, but only slightly, during plane strain compression. Therefore, it is a good approximation to assume that $\sigma_2'/(\sigma_1' + \sigma_3')$ is a constant during plane strain compression of a one dimensionally consolidated soil. Thus, for the entire plane strain compression test, Eq. 7.33 may be simply stated as:

$$\frac{\sigma_2'}{\sigma_1' + \sigma_3'} = \frac{1}{2}\cos^2\phi \qquad (7.34)$$

7.4.4 A Note on the Models Proposed by Cornforth and Bishop

Immediately after one dimensional consolidation σ_2' and σ_3' both are equal to $K_o\sigma_1'$. Therefore:

$$\left[\frac{\sigma_2'}{\sigma_1' + \sigma_3'}\right]_{initial} = \frac{K_o}{1 + K_o}$$

Therefore, predictions based on Cornforth's model can be expected to be closer to the initial value of $\sigma_2'/(\sigma_1' + \sigma_3')$ in the plane strain compression test. Bishop's semi-empirical equation was proposed for failure conditions. Hence, the predictions from Eq. 7.34 would be closer to the values of $\sigma_2'/(\sigma_1' + \sigma_3')$ at failure. Nevertheless, the difference between these two values is small, the latter being greater than the former. Experimental data (Table 7.1) and the elasto-plastic analysis described below show that $\sigma_2'/(\sigma_1' + \sigma_3')$ does increase, but only slightly, during the plane strain compression.

Table 7.1 Experimental and Predicted Results

Soil	K_o	ϕ'		$\frac{\sigma_2'}{\sigma_1' + \sigma_3'}$				Reference
		CIUC	K_oPSC	Cornforth	Bishop	Proposed*	Expt'l*	
Haney Clay	0.55	21.4	25.2	0.35	0.41	0.44-0.47	0.36-0.39	Campanella & Vaid, 1973
Spestone Kaolin	0.64	23.0	23.0	0.39	0.42	0.43-0.46	0.39-0.40	Hambly & Roscoe, 1969
Remolded Sapporo Clay	0.52	30.6	33.4	0.34	0.35	0.39-0.44	0.32-0.40	Mitachi & Kitago, 1980
Weald Clay	0.58	25.9	27.1	0.37	0.40	0.42-0.46	0.36-0.43	Henkel & Wade, 1966
Boston Blue Clay	0.50	27.5	29.0	0.33	0.39	0.39-0.44	0.33-0.37	Ladd, et al., 1971

* Initial and final values are given

7.4.5 Elastic Analysis

From the theory of elasticity

$$\epsilon_1 = \frac{1}{E}\left[\sigma_1' - \nu(\sigma_2' + \sigma_3')\right]$$

$$\epsilon_2 = \frac{1}{E}\left[\sigma_2' - \nu(\sigma_1' + \sigma_3')\right] \tag{7.35}$$

$$\epsilon_3 = \frac{1}{E}\left[\sigma_3' - \nu(\sigma_1' + \sigma_2')\right]$$

Here σ_1', σ_2', σ_3', ϵ_1, ϵ_2, and ϵ_3 are principal stresses and strains in the directions referred to by the subscripts. E is the Young's modulus. For plane strain conditions, ϵ_2 is null, and therefore:

$$\frac{\sigma_2'}{\sigma_1' + \sigma_3'} = \nu \tag{7.36}$$

Eqs. 7.35 and 7.36 are valid only if the element under consideration does not have initial stresses or strains. In the presence of initial stresses, it is appropriate to use incremental elasticity theory. Then Eqs. 7.35 and 7.36 become:

$$\Delta\epsilon_1 = \frac{1}{E}\left[\Delta\sigma_1' - \nu(\Delta\sigma_2' + \Delta\sigma_3')\right]$$

$$\Delta\epsilon_2 = \frac{1}{E}\left[\Delta\sigma_2' - \nu(\Delta\sigma_1' + \Delta\sigma_3')\right] \tag{7.37}$$

$$\Delta\epsilon_3 = \frac{1}{E}\left[\Delta\sigma_3' - \nu(\Delta\sigma_1' + \Delta\sigma_2')\right]$$

$$\frac{\Delta\sigma_2'}{\Delta\sigma_1' + \Delta\sigma_3'} = \nu \tag{7.38}$$

Without any reference to the initial state, Cornforth (1964) simply stated that $\sigma_2'/(\sigma_1' + \sigma_3')$ was a constant ($=\nu$) for the entire plane strain test. It is shown

below that Cornforth's expression is valid only for one dimensionally consolidated soils.

One Dimensional Consolidation

For one dimensionally consolidated soils, the initial effective stresses (i.e., immediately after the consolidation) are $\sigma'_{1o} = \sigma'_{vo}$ and $\sigma'_{2o} = \sigma'_{3o} = K_o \sigma'_{vo}$. Therefore:

$$\left[\frac{\sigma'_2}{\sigma'_1 + \sigma'_3}\right]_{\text{initial}} = \frac{\sigma'_{2o}}{\sigma'_{1o} + \sigma'_{3o}} = \frac{K_o}{1 + K_o} \tag{7.39}$$

For one dimensional consolidation $\Delta\sigma'_2 = \Delta\sigma'_3 = 0$, and $\Delta\sigma'_2 = \Delta\sigma'_3$. Substituting these values in Eq. 7.37 leads to:

$$= \frac{K_o}{1 + K_o} \tag{7.40}$$

At any stage of plane strain loading, let the stress increments from the initial state be $\Delta\sigma'_1$, $\Delta\sigma'_2$, and $\Delta\sigma'_3$. From Eqs. 7.38, 7.39, and 7.40:

$$\frac{\sigma'_{2o}}{\sigma'_{1o} + \sigma'_{3o}} = \frac{\Delta\sigma'_2}{\Delta\sigma'_1 + \Delta\sigma'_3} =$$

Therefore:

$$\frac{\sigma'_{2o} + \Delta\sigma'_2}{(\sigma'_{1o} + \Delta\sigma'_1) + (\sigma'_{3o} + \Delta\sigma'_3)} = \tag{7.41}$$

or:

$$\frac{\sigma'_2}{\sigma'_1 + \sigma'_3} =$$

Thus, $\sigma'_2/(\sigma'_1 + \sigma'_3)$ remains a constant throughout the entire loading for plane strain compression of a one dimensionally consolidated soil element. It is assumed that the Poisson's ratio is a constant for the entire loading.

Isotropic Consolidation

For $K_o = 0.5$, the variations of $\sigma_2'/(\sigma_1' + \sigma_3')$ with $(\sigma_1' + \sigma_3')/\sigma_{vc}'$ for several consolidation stress ratios are shown in Fig. 7.7. The consolidation stress ratio K is defined as:

$$K = \frac{\sigma_{3c}'}{\sigma_{1c}'}$$

For consolidation stress ratios below K_o, $\sigma_2'/(\sigma_1' + \sigma_3')$ increases during loading and becomes asymptotic to the value ν, whereas for consolidation stress ratios greater than K_o, $\sigma_2'/(\sigma_1' + \sigma_3')$ decreases and becomes asymptotic to ν.

For hydrostatically consolidated soils, immediately after consolidation σ_1' = σ_{2c}' = σ_{3c}'. Therefore:

$$\frac{\sigma_{2c}'}{\sigma_{1c}' + \sigma_{3c}'} = 0.5 \qquad (7.42$$

Since the incremental ratio (Eq. 7.38) is different from the initial ratio (Eq. 7.42), $\sigma_2'/(\sigma_1' + \sigma_3')$ does not remain constant as in the case of one dimensionally consolidated soils. It decreases from its initial value of 0.5 and becomes asymptotic to the value of ν (Fig. 7.7).

It is clearly seen from Fig. 7.7 that $\sigma_2'/(\sigma_1' + \sigma_3')$ remains a constant throughout the plane strain compression loading only when K = K_o. The error in assuming that $\sigma_2'/(\sigma_1' + \sigma_3')$ is a constant, that is equal to ν, for hydrostatically consolidated soils (K = 1) is evident from these figures. For example, in the case of K_o = 0.5, $\sigma_2/(\sigma_1' + \sigma_3')$ during the initial stages of loading is overestimated by as much as 50% with this assumption. This error decreases with increasing values of K_o. However, for typical values of K_o (0.4 - 0.6) the error is quite significant.

Previous experimental data on one dimensionally consolidated soils (Cornforth, 1964; Campanella and Vaid, 1973; Henkel and Wade, 1966; Mir-

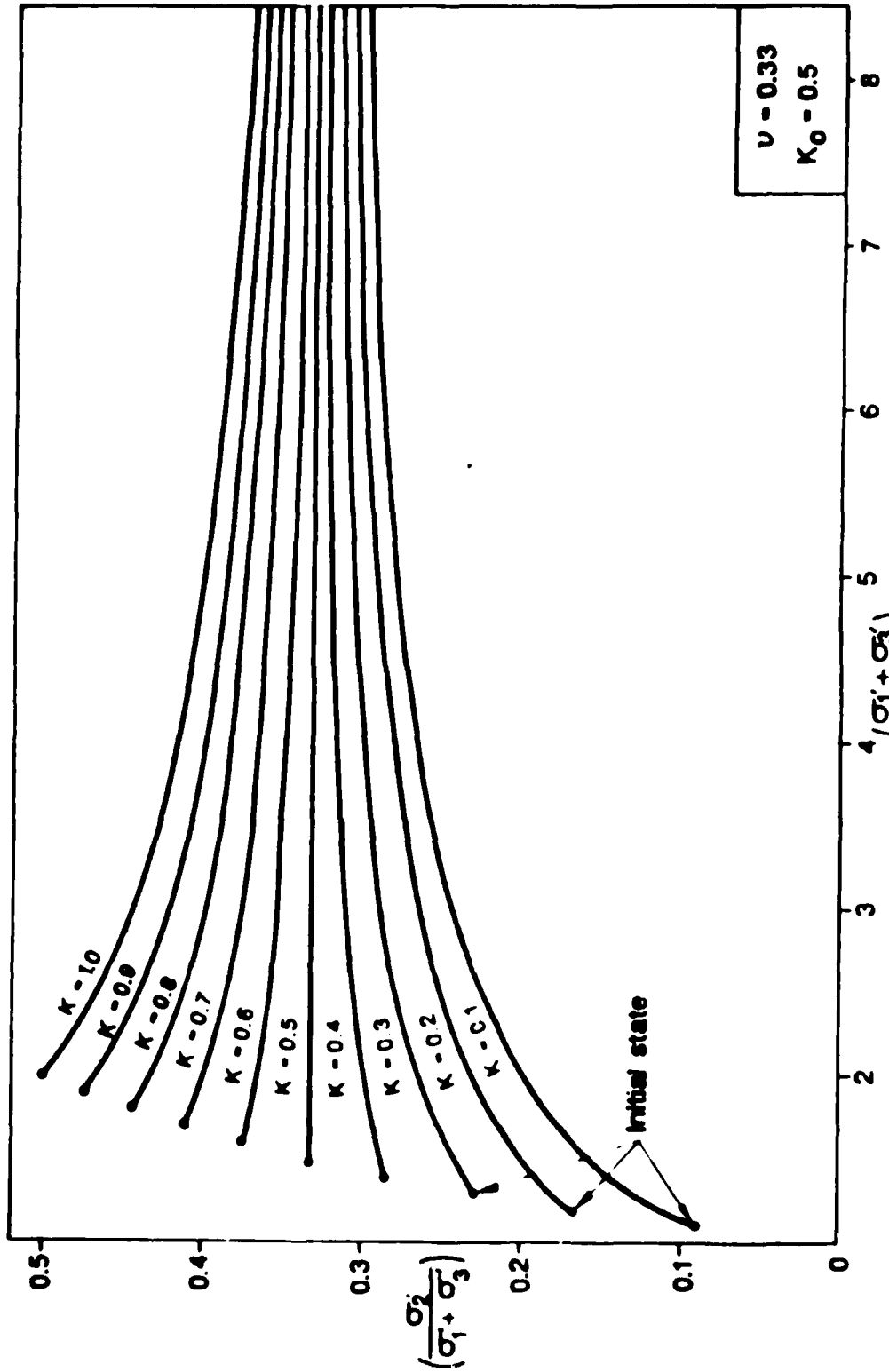

Figure 7.7 Variation of $\sigma_2'/(\sigma_1' + \sigma_3')$ with $(\sigma_1' + \sigma_3')/\sigma_{20}'$ for different consolidation stress ratios ($K_o = 0.5$)

chi and Kitago, 1980) show that the ratio $\sigma_2'/(\sigma_1' + \sigma_3')$ during plane strain compression remains constant or increases slightly with loading. This is in general agreement with elastic analysis because one dimensionally consolidated soils usually fail at low strains behaving "elastically" until a significant fraction of the failure stress is reached.

7.4.6 Elasto-Plastic Analysis

$\sigma_1'-\sigma_2'-\sigma_3'$ Space

The modified Cam Clay model proposed by Roscoe and Burland (1968) for a generalized three dimensional stress state is extended here to study the variation of the principal stresses during plane strain compression of a normally consolidated clay.

In $\sigma_1' - \sigma_2' - \sigma_3'$ space, the volumetric yield surface is given by (Roscoe and Burland, 1968) :

$$(M_*^2 + 6)(\sigma_1'^2 + \sigma_2'^2 + \sigma_3'^2) + 2(M_*^2 - 3)(\sigma_1'\sigma_2' + \sigma_2'\sigma_3' + \sigma_3'\sigma_1')$$

$$-3M_*^2 p_o' (\sigma_1' + \sigma_2' + \sigma_3') = o \qquad (7.43)$$

where,

$$M_* = \sqrt{\frac{2}{3}}\, M \qquad (7.44)$$

p_o' is the value of p' at the end of hydrostatic consolidation.

For deformation under plane strain conditions:

$$\delta\epsilon_2 = \delta\epsilon_2^p + \delta\epsilon_2^e = o \qquad (7.45)$$

or:

$$\delta\epsilon_2^p = -\delta\epsilon_2^e$$

The subscript 2 refers to the direction in which there is no deformation. The fact that $\delta\epsilon_2^e$ depends on the stress path makes it impossible to obtain a

closed form solution to plane strain problems. In conventional triaxial tests, the volumetric yield locus is uniquely defined under any state of stress. This is not the case under plane strain conditions where the imposed stress path has significant influence (Roscoe and Burland, 1968). This situation is simplified by assuming that all the components of elastic strains are negligible. In other words, the slope of swelling, κ, is assumed to be very small compared to the slope of the virgin consolidation line, λ. Therefore, for plane strain conditions:

$$\delta\epsilon_2 = \delta\epsilon_2^p = 0$$

The volumetric yield surface in $\sigma_1' - \sigma_2' - \sigma_3'$ space is shown in Fig. 7.8. The plane strain volumetric yield curve C'B'A'B'C' lies on this yield surface. Projection of the plane strain volumetric yield curve on the $\sigma_1' - \sigma_3'$ plane is given by CBABC. For plane strain conditions, the total strain vector $\overline{\delta\epsilon_1^p} + \overline{\delta\epsilon_3^p}$ must lie on a plane parallel to $\sigma_1'O\sigma_3'$. Assuming normality conditions, Roscoe and Burland (1968) showed that at any point on the plane strain volumetric yield curve:

$$\frac{\delta\sigma_1'}{\delta\sigma_2'} = \frac{\delta\sigma_3'}{\delta\sigma_2'} = 0 \tag{7.46}$$

Thus, from Eqs. 7.43, 7.44, and 7.46:

$$(2M^2 + 18)\sigma_2' + (2M^2 - 9)(\sigma_1' + \sigma_3') - 3M^2 p_o' = 0 \tag{7.47}$$

This is the equation of a plane which intersects the volumetric yield surface along the plane strain volumetric yield curve C'B'A'B'C'. Therefore, at any stage of volumetric yielding, σ_2' is given by:

$$\sigma_2' = \frac{3M^2 p_o' - (2M^2 - 9)(\sigma_1' + \sigma_3')}{(2M^2 + 18)} \tag{7.48}$$

Substituting this expression for σ_2' in Eq. 7.47, the plane strain volumetric yield locus in the $\sigma_1' - \sigma_3'$ plane is given by (curve CBABC in Fig. 7.8):

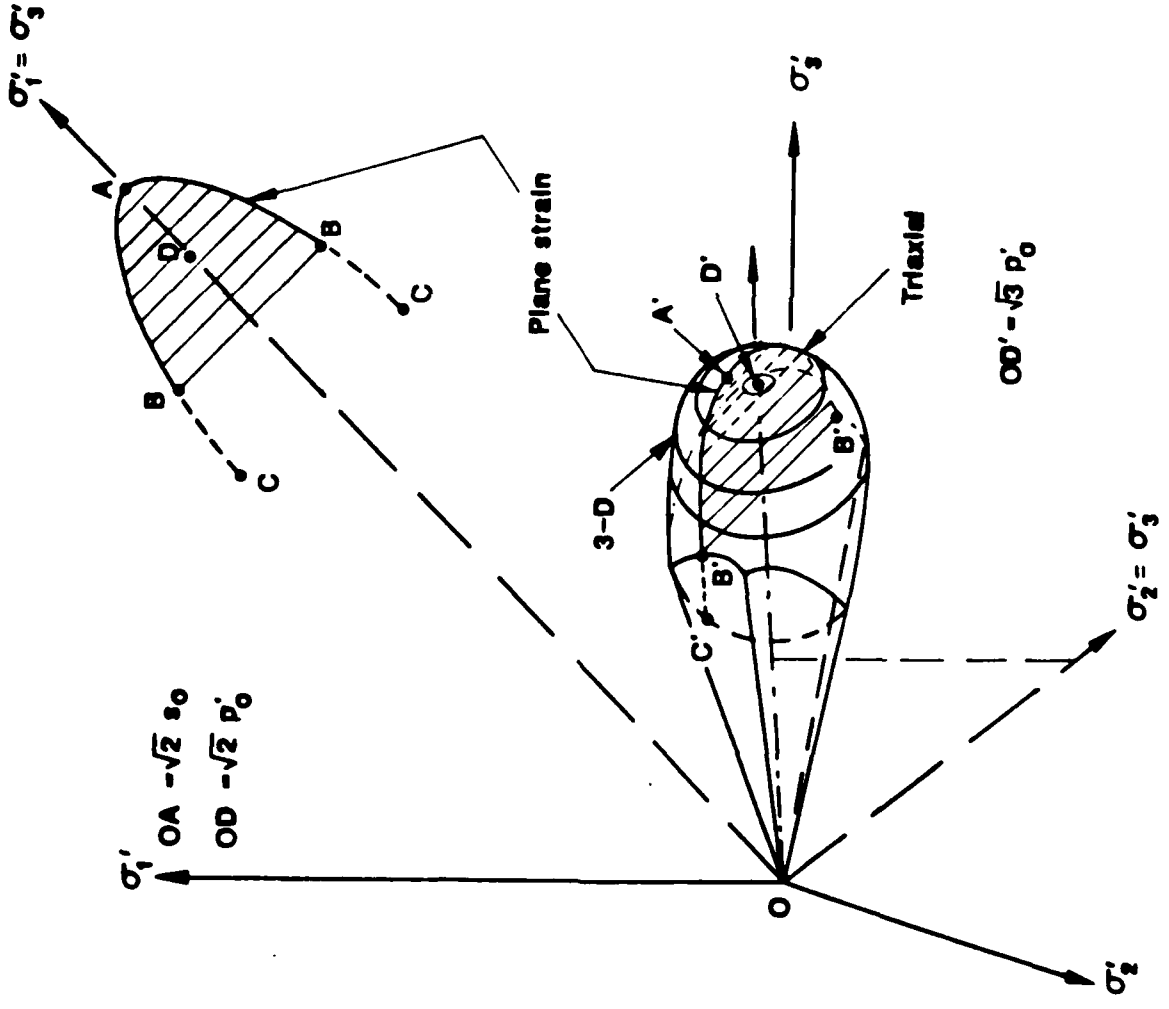

Figure 7.8 Volumetric Yield Curve for Plane Strain Compression

$$(4M^2 + 9)(\sigma_1'^2 + \sigma_3'^2) - 6M^2 p_o'(\sigma_1' + \sigma_3') + (4M^2 - 18)\sigma_1'\sigma_3'$$

$$- \frac{M^4}{3} p_o'^2 = 0 \qquad (7.49)$$

s-t Space

To simplify the analysis three variables s, t, and η' are introduced, defined as:

$$s = \frac{\sigma_1' + \sigma_3'}{2}$$

$$t = \frac{\sigma_1' - \sigma_3'}{2}$$

$$\eta' = \frac{t}{s} = \frac{\sigma_1' - \sigma_3'}{\sigma_1' + \sigma_3'} = \sin \phi_{mob}'$$

Substituting these in Eq. 7.49, the plane strain volumetric yield curve in the s-t plane becomes:

$$6M^2 s^2 + 2(M^2 + 9)t^2 - 6M^2 p_o' s - \frac{M^4}{4} p_o'^2 = 0 \qquad (7.50)$$

Since the isotropic state of stress corresponding to point D (p_o', p_o', p_o') can not be attained under plane strain conditions, a more convenient parameter s_o is used instead of p_o' in the following, where s_o is the value of s when t=0. Substituting t=0 in Eq. 7.50:

$$s_o = \frac{A_1}{2} p_o' \qquad (7.51)$$

where:

$$A_1 = 1 + \left[1 + \frac{M^2}{9}\right]^{1/2} \qquad (7.52)$$

The entire volumetric yield surface expands or contracts depending on the change in water content. With decreasing water content, the volumetric yield surface expands and vice versa. However, normalization of Eq. 7.49 with

respect to s_o, a parameter reflecting the consolidation stress level, leads to a unique plane strain volumetric yield curve independent of the water content. This is similar to normalizing the stress-strain curves with respect to the effective vertical consolidation pressure. The normalized plane strain volumetric yield curve is given by:

$$3M^2(s/s_o)^2 + (M^2 + 9)(t/s_o)^2 - \frac{6M^2}{A_1}(s/s_o)$$

$$- \frac{1}{3}\frac{M^4}{A_1^2} = 0 \qquad (7.53)$$

From Eqs. 7.48 and 7.53, and the definitions of s, t, and η', the normalized values of all three principal stresses can be obtained at any stage of plane strain yielding. Variations of normalized principal stresses with η' for M = 1.0 are shown in Fig. 7.9. During loading, σ_2' and σ_3' decrease steadily whereas, σ_1' increases during the initial stages and then decreases. For conventional triaxial compression test (CIUC) it can be shown that:

$$\sin \phi' = \frac{3M}{6 + M} = \eta_f' \qquad (7.54)$$

where η_f' is the value of η' at failure. Eq. 7.54 is used in addition to Eqs. 7.48 and 7.53 to obtain the stress state at failure.

7.4.7 Comparison of Models

From the values of normalized principal stress $\sigma_2'/(\sigma_1' + \sigma_3')$ throughout the plane strain loading is also derived. A parametric study shows that, for all values of M, $\sigma_2'/(\sigma_1' + \sigma_3')$ increases slightly during the loading. Also shown in Fig. 7.9 are the variations of $\sigma_2'/(\sigma_1' + \sigma_3')$ according to Cornforth's and Bishop's models. According to these two models, $\sigma_2'/(\sigma_1' + \sigma_3')$ is a constant for the entire loading.

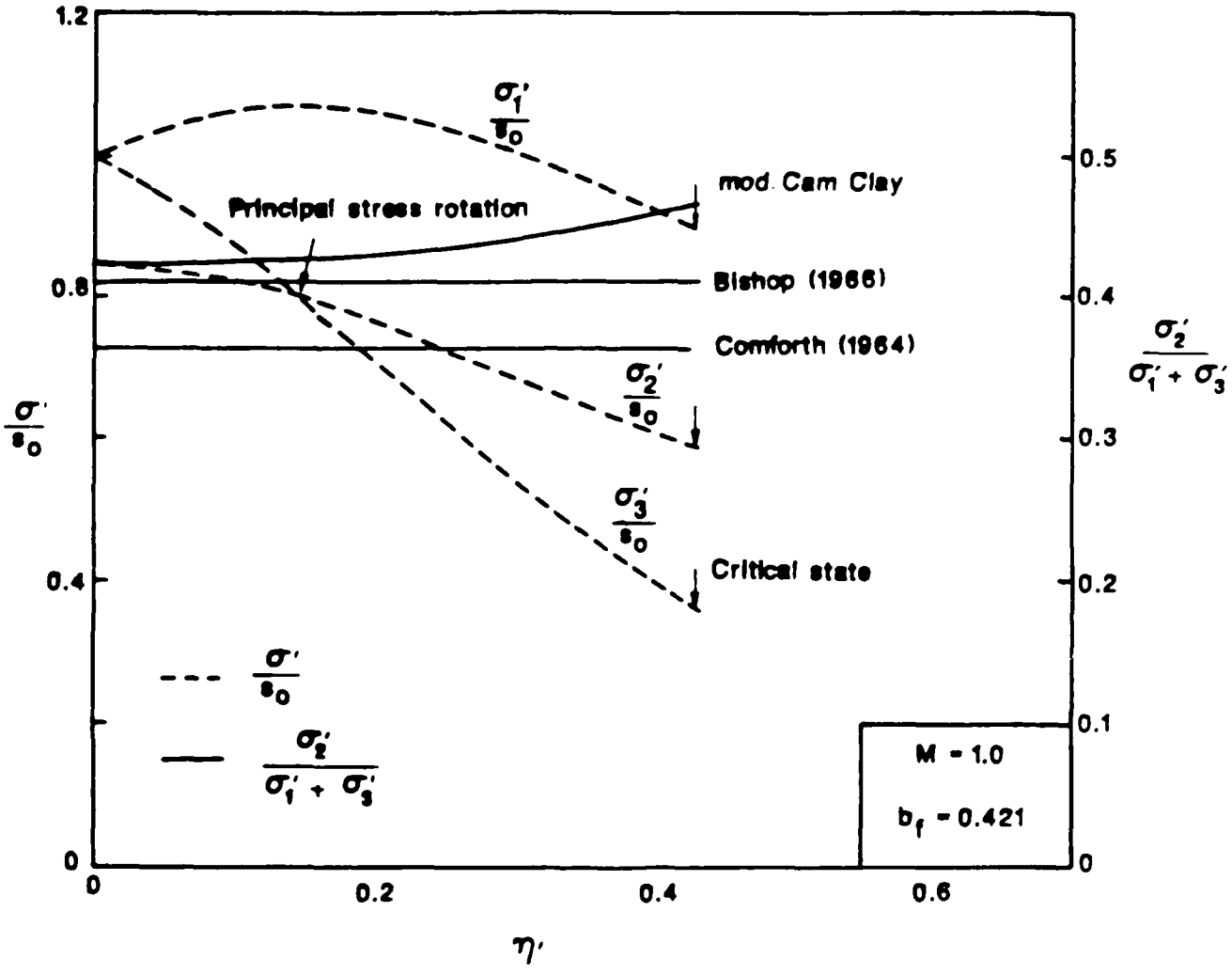

Figure 7.9 Variation of Normalized Principal stresses and $\sigma_2'/(\sigma_1' + \sigma_3')$ with η' for M = 1.0

Predicted and experimental values of $\sigma_2'/(\sigma_1' + \sigma_3')$ for five different remolded and undisturbed clays are shown in Table 7.1. Interestingly, Cornforth's elastic model and Bishop's semi-empirical model give a good estimate of this ratio, assuming it to be a constant. The modified Cam Clay model slightly overestimates $\sigma_2'/(\sigma_1' + \sigma_3')$, but clearly shows the trend of this ratio increasing during shear. Similar trends have been observed by Henkel and Wade (1966), and Mitachi and Kitago (1980). Campanella and Vaid (1973) reported that this ratio is a constant, but a slight increase with strain is evident from their data (Fig. 7 of Campanella and Vaid, 1973). The proposed model, because it is based on modified Cam Clay, is essentially for isotropically consolidated clays. All the available data is for one dimensionally consolidated clays. Therefore, the slight overestimation could be partly due to the anisotropy in consolidation stresses (i.e., stress induced anisotropy).

7.5 Summary

The effects of anisotropic consolidation on undrained shear strength was studied by comparing CIUC and CK_oUC tests. A simple procedure with a sound theoretical basis was developed to predict the in situ or K_o consolidated undrained shear strength from ordinary CIUC test results. The procedure was validated with experimental data from the literature (Sivakugan, et al., 1987).

The Cam Clay and the modified Cam Clay models were extended to consider a K_o consolidated initial state. A new state parameter, the spacing ratio, is introduced to simplify the analysis. Expressions were developed for the undrained shear strength and Skempton's A-parameter at failure, $A_{f,ko}$ for K_o consolidated soils.

The variation of principal stresses during plane strain compression was studied using the modified Cam Clay model. It was shown that $\sigma_2'/(\sigma_1' + \sigma_3')$

steadily increases, but only slightly, during plane strain compression. During the initial stages of shearing $\sigma_2'/(\sigma_1' + \sigma_3')$ is approximately equal to [illegible]. At failure, $\sigma_2'/(\sigma_1' + \sigma_3')$ takes the value of 0.5 cos^2 [illegible]. In between, there is a gradual increase in this ratio. Nevertheless, for practical purposes, it is a good approximation to assume that $\sigma_2'/(\sigma_1' + \sigma_3')$ is a constant throughout the plane strain compression loading. The magnitude of the constant is a function of soil [illegible] of

It is also shown from incremental elasticity theory that $\sigma_2'/(\sigma_1' + \sigma_3')$ is a constant, equal to [illegible], only for one of the [illegible] considered. For normally consolidated soils, $\sigma_2'/(\sigma_1' + \sigma_3')$ decreases from 0.5 and reaches a minimum at very high stresses which may never be attained in reality.

CHAPTER 8

CONCLUSIONS

This chapter summarizes the main conclusions drawn from this research during both our experimental and theoretical investigations. The reader can refer to the different discussions of results and conclusions presented in the [illegible] chapters for more detail. The conclusions which have direct impact on the [illegible] of pressuremeter test results are presented first, followed by [illegible] which are of a more general nature and can have an impact on [illegible] areas than pressuremeter testing.

1. The undrained shear strengths derived from model pressuremeter tests with strain rates between 0.1 and 0.73%/minute agree well with the plane strain shear strengths predicted using the Prevost (1979) procedures and the corresponding triaxial test results. A higher pressuremeter expansion rate [illegible] a greater initial pressure increase in the early part of the test, however the limit pressures were found to be relatively insensitive to strain rate. [illegible] derived [illegible] shear moduli increase with strain rate.

2. The maximum principal stress difference [illegible] increase with strain [illegible]

3. Regardless of [illegible]

and strength response to be predicted from pressuremeter expansion curves than if these effects are included. If conventional laboratory results are the reference (lower strain rates), then the usual pressuremeter test creates an overestimate of the undrained strength. In parametric studies, the strength was overestimated by about 13% for strain softening soils.

4. Stress disturbance, applied in laboratory experiments either by overstressing or understressing the soil around the probe, primarily affected the early part of the pressuremeter curve. This does, however, result in a significant variation of the lateral earth pressure and initial shear modulus. These variations in turn affect the interpretation of the undrained shear strength.

5. The presence of a remolded annulus can result in an overestimation of the undrained strength and underestimation of the modulus, and the error increases with the thickness of the remolded annulus. If the thickness of the remolded annulus is half the radius of the cavity, then the errors in the undrained strength and the modulus can be as high as 15% and 40%, respectively.

6. The unloading of the borehole during the drilling overwhelms the effect of the presence of a remolded annulus when the initial unloading is large. For small amounts of initial unloading (i.e. initial strain less than 0.1 to 0.2%), the remolded annulus has the strongest influence on strength estimates; however the error in the undrained strength will be less than 20%. For a large amount of initial unloading, initial strain overwhelms the effect of remolded annulus, and the undrained strength can be overestimated by as much as 100% for an initial strain of 1%. The modulus, however, is affected by the size of the disturbed annulus as well as the amount of initial unload-

ing, and can be underestimated by as much as 40%.

7. A close examination of the reported results of self-boring pressuremeter tests in various soils revealed that the error in the undrained strength is very large for highly anisotropic and strain softening soils, compared to relatively insensitive soils. It is hypothesized that this large error is caused by the initial unloading of the borehole during drilling, and a significant amount of initial unloading is more likely to occur in strain softening soils.

8. Partial drainage significantly affects the pore pressure generated in the soil mass during the pressuremeter test. However, our theoretical results indicate that the pressuremeter expansion curves obtained from commercially available probes with a standard strain rate of 1%/minute should not be significantly affected by partial drainage. As a result, the interpretation procedures developed to derive the stress-strain curve from the undrained pressuremeter expansion curve can still be used, even if the expansion is not perfectly undrained.

9. The initial shear moduli are very sensitive to strain rate, stress disturbance, and the method of interpretation. Therefore, it is suggested that for practical applications, the determination of this soil property from pressuremeter tests be accorded careful scrutiny and perhaps abandoned, at least for soils of the type studied in this research.

10. Laboratory experiments indicated that both the pore pressure distribution at the end of probe expansion and the shear modulus as determined from unload-reload loops are not sensitive to stress disturbance occurring prior to the test.

11. Comparison of the experimental and the predicted pressuremeter curves showed that the anisotropic model proposed by Prevost (1979) can be

used to predict the pressuremeter expansion curve. However, the model does not describe the strain softening behavior very well. The proposed curve fitting equations describe the theoretical and the experimental pressuremeter curves adequately. It has also been shown that the Simplex method is an efficient algorithm to interpret pressuremeter data.

12. The pressuremeter testing program shows that a small scale calibration chamber system can be used to perform tests on cohesive soils. Uniform and reproducible samples of soils can be prepared and tested. The system appears to be particularly suited for the evaluation of other in situ testing devices.

13. Pore size distribution analysis can provide the means to estimate the thickness of the remolded annulus around the pressuremeter probe; this concept could be extended to other devices.

14. The coefficient of horizontal consolidation c_h determined from stress controlled holding tests with probe pressure exceeding the lateral preconsolidation pressure agrees well with those obtained from virgin loading in oedometer tests. However, strain controlled holding tests tend to overestimate c_h by three to four times.

15. It was shown theoretically that the undrained shear strength s_u is governed by the effective vertical consolidation pressure and not by the mean effective consolidation pressure. Thus stress anisotropy during consolidation does not have significant influence on the undrained shear strength. Comparing isotropically and one dimensionally consolidated specimens, the difference in s_u is generally within $\pm 15\%$. Therefore, the consistent overestimation of c_h from pressuremeter testing can not be attributed to different stress ratios during consolidation in laboratory experiment.

Depending on the consolidation ratio, pore pressure development and A_f can vary considerably. $A_{f_{K_o}}$ can differ from A_{f_i} by as much as 100%.

16. Cam Clay and modified Cam Clay models were developed for isotropically consolidated clays. Soil deposits encountered in practice are typically one dimensionally consolidated. Therefore, the extension of these critical state models to consider K_o consolidated initial states provides a basis for further analytical studies of in situ behavior of clays.

17. Isotropic or anisotropic virgin consolidation lines and the critical state line are parallel in v - ln p' space. For anisotropically consolidated specimens, the relative position of the consolidation line, between the CSL and the ICL, depends primarily on the consolidation stress ratio. A new state parameter r was introduced to quantify the relative position of the K_o CL. For one dimensionally consolidated clays, γ_f and A_f were shown to be functions of r and N.

Based on Cam Clay and modified Cam Clay models, the pore pressure development during a CIUC test was quantified. Skempton's A-parameter increases during shear and reaches the maximum, A_f, at failure. For the modified Cam Clay model, the initial value of A is 1/3 for all clays irrespective of

18. Expressions were developed for A_{f_i} and $A_{f_{K_o}}$. Both are functions of and N. Thus, for isotropically or anisotropically consolidated clays, A_f is governed by shear strength and compressibility characteristics. Shear strength was also shown to be governed by γ' and N.

19. The ratio $\sigma'_2/(\sigma'_1 + \sigma'_3)$ during plane strain compression is often assumed to be a constant. Based on the modified Cam Clay model, it was shown that γ_2 increases slightly during shear. This is in agreement with

experimental observations. Nevertheless, this slight increase may be ignored for practical purposes and $\sigma_2'/(\sigma_1' + \sigma_3')$ may be assumed a constant.

20. A significant increase in ϕ' was observed for horizontal loading of one dimensionally consolidated specimens in the cuboidal shear device. Thus, it is necessary to use the appropriate value of ϕ' depending on the loading situation. For horizontal loading, as in the case of the pressuremeter testing in clays, such high values of ϕ' may contribute significantly to the overestimation of undrained shear strength when compared to laboratory experiments.

REFERENCES

[1] Aas, G. (1965). "A Study of the Effect of of Vane Shape and Rate of Strain on the Measured Values of In Situ Shear Strength of Clays", *Proceedings of the 6th International Conference on Soil Mechanics and Foundation Engineering*, Montreal, Vol. 1, pp. 141-145.

[2] Altschaeffl, A. G. and Lovell, C. W. (1983), "Improving Embankment Design and Performance," *Report No. FHWA/IN/JHRP-83/14*, Purdue University, West Lafayette, Indiana, 168 pp.

[3] Arnold, M. (1981). "An Empirical Evaluation of Pressuremeter Test Data," *Canadian Geotechnical Journal*, Vol. 18, No. 3, pp. 455-459.

[4] Atkinson, J. (1983). "Is Soil Mechanics in a Critical State?", *Ground Engineering*, Vol. 16, No. 1, pp. 2-6.

[5] Atkinson, J. H. and Bransby, P. L. (1978). *The Mechanics of Soils: An Introduction to Critical State Soil Mechanics*, McGraw-Hill, London, 375 pp.

[6] Baguelin, F., Jezequel, J. F., Le Mee, E., and Le Mehaute, A. (1972). "Expansion of Cylindrical Probes in Cohesive Soils", *Journal of the Soil Mechanics and Foundations Division*, ASCE, Vol. 98, SM11, pp. 1129-1142.

[7] Baguelin, F., Jezequel, J. F., and Shields, D. H. (1978). *The Pressuremeter and Foundation Engineering*, Trans Tech Publication, 618 pp.

[8] Baligh, M. M. (1985), "Strain Path Method," *Journal of Geotechnical Engineering*, ASCE, Vol. 111, No. 9, pp. 1108-1136.

[9] Battaglio, M., Ghionna, V., Jamiolkowski, M., and Lancellotta, R. (1981). "Interpretation of Self-Boring Pressuremeter Tests in Clays," *Proceedings of the 10th International Conference on Soil Mechanics and Foundation Engineering*, Vol. 2, Stockholm, pp. 433-438.

[10] Benoit, J. and Clough, G. W. (1986). "Self Boring Pressuremeter Tests in Soft Clay", *Journal of Geotechnical Engineering*, ASCE, Vol. 112, No. 1, pp. 60-78.

[11] Berre, T. and Bjerrum, L. (1973). "Shear Strength of Normally Consolidated Clays", *Proceedings of the 8th International Conference on Soil Mechanics and Foundation Engineering*, Moscow, Vol. 1, Part 1, pp. 39-49.

[12] Biot, M. A. (1941), "General Theory of Three Dimensional Consolidation," *Journal of Applied Physics*, Vol. 12, pp. 155-164.

[13] Bishop, A. W. (1966). "The Strength of Soils as Engineering Materials", Sixth Rankine Lecture, *Geotechnique*, Vol. 16, No. 2, pp. 91-130.

[14] Bjerrum, L. (1972). "Embankments on Soft Ground", *Proceedings of the ASCE Specialty Conference on Performance of Earth and Earth Supported Structures*, Vol. 2, Purdue University, West Lafayette, Indiana, pp. 1-54.

[15] Cacci, M. S. and Cacheris, W. P. (1984). "Fitting Curves to Data, the Simplex Algorithm is the Answer," *Byte, The Small Systems Journal*, Vol. 9, No. 5, McGraw Hill Inc., May 1984, pp. 339-360.

[16] Campanella, R. G. and Vaid, Y. P. (1973). "Influence of Stress Path on the Plane Strain Behavior of a Sensitive Clay", *Proceedings of the 8th International Conference on Soil Mechanics and Foundation Engineering*, Moscow, Vol. 1, pp. 85-92.

[17] Carter, J. P., Randolph, M. F., and Wroth, C. P. (1979). "Stress and Pore Pressure Changes in Clay during and after the Expansion of a Cylindrical Cavity," *International Journal for Numerical and Analytical Methods in Geomechanics*, Vol. 3, pp. 305-322.

[18] Cornforth, D. H. (1984). "Some Experiments on the Influence of Strain Conditions on the Strength of the Sand", *Geotechnique*, Vol. 14, pp. 143-167.

[19] Clarke, B. G., Carter, J. P., and Wroth, C. P. (1979). "In Situ Determination of the Consolidation Characteristics of Saturated Clays", *Proceedings of the 7th European Conference on Soil Mechanics*, Vol. 2, pp. 207-213.

[20] Denby, G. M. (1978). "Self-Boring Pressuremeter Study of the San Francisco Bay Mud," *Ph.D. Thesis*, Stanford University.

[21] Desai, C. S. and Christian, J. T. (1977). *Numerical Methods in Geotechnical Engineering*, McGraw Hill Inc., pp. 88-89.

[22] Duncan, J. M. and Seed, H. B. (1966). "Anisotropy and Stress Reorientation in Clay", *Journal of the Soil Mechanics and Foundations Division*, ASCE, Vol. 92, SM5, pp. 21-50.

[23] Egan, J. A. (1977). "A Critical State Model for Cyclic Loading Pore Pressure Response for Soils", *M.Sc. Theses*, Cornell University, Ithaca.

[24] Gibson, R. E. and Anderson, W. F. (1961). "In Situ Measurement of Soil Properties with the Pressuremeter", *Civil Engineering and Public Works Review*, Vol. 56, No. 658, pp. 615-618.

[25] Henkel, D. J. and Wade, N. H. (1966). "Plane Strain Tests on a Saturated Remolded Clay", *Journal of the Soil Mechanics and Foundations Division*, ASCE, Vol. 88, SM6, pp. 67-80

[26] Huang, A. B. (1986). "Laboratory Pressuremeter Experiments in Clay Soils", *PhD Thesis*, Purdue University.

[27] Huang, A. B., Chameau, J. L., and Holtz, R. D. (1986). "Interpretation of Pressuremeter Data in Cohesive Soils by Simplex Algorithm", *Geotechnique*, Vol. 36, No. 4, pp. 599-603.

[28] Huang, A. B., Holtz, R. D., and Chameau, J. L. (1985). "Calibration Tests of Pressuremeters in Clay", *Proceedings of the second Symposium on the Interaction of Non Nuclear Munitions with structures*, Panama City, Florida, pp. 313-318.

[29] Huang, A. B., Holtz, R. D., and Chameau, J. L. (1987). "A Calibration Chamber for Cohesive Soils", *Geotechnical testing Journal*, ASTM, (Submitted for Publication).

[30] Karube, D. (1975). "Nonstandardized Triaxial Testing Method and its Problems", *20th Symposium in Soil Engineering*, Japanese Society of Soil Mechanics and Foundation Engineering, pp. 45-60 (in Japanese).

[31] Kjellman, W. (1936). "Report on an Apparatus for Consummate Investigation of the Mechanical Properties of Soils", *Proceedings of the 1st International Conference on Soil Mechanics and Foundation Engineering*, Cambridge, Vol. 2, pp. 16-20.

[32] Kreko, B. (1968). *Linear Programming*, American Elsevier Publishing Company, Inc., New York.

[33] Krishnamurthy, M., Nagaraj, T. S., and Sridharan, A. (1980). "Strength Anisotropy of Layered Soil System", *Journal of the Geotechnical Engineering Division*, ASCE, Vol. 106, GT10, pp. 1143-1147.

[34] Ladanyi, B. (1972). "In Situ Determination of Undrained Stress-Strain Behavior of Sensitive Clays with the Pressuremeter", *Canadian geotechnical Journal*, Vol. 9, No. 3, pp. 313-319.

[35] Ladd, C. C., Bovee, R. B., Edgers, L., and Rixner, J. J. (1971). Consolidated Undrained Plane Strain Shear Tests on Boston Blue Clay, *Research report R71-18*, U. S. Army Engineer Waterways Experiment Station, Corps of Engineers, Vicksburg, Mississippi, 244pp.

[36] Ladd, C. C., Germaine, J. T., Baligh, M. M., and Lacasse, S. M. (1980). "Evaluation of Self-Boring Pressuremeter Tests in Boston Blue Clays", Report No. FHWA/RD - 80/052, Dept. of Civil Engineering, M.I.T., Cambridge, Mass.

[37] Lo, K. Y. and Morin, J. P. (1972). "Strength Anisotropy and Time Effects of Two Sensitive Clays", *Canadian Geotechnical Journal*, Vol. 9, pp. 261-277.

[38] Mitachi, T. and Kitago, S. (1980). "Undrained Triaxial and Plane Strain Behavior of Saturated Remolded Clay", *Soils and Foundations*, Vol. 20, No. 1, pp. 13-28.

[39] Nakase, A. and Kamei, T. (1983). "Undrained Shear Strength Anisotropy of Normally Consolidated Cohesive Soils", *Soils and Foundations*, Vol. 23, No. 1, pp. 91-101.

[40] Nakase, A. and Kamei, T. (1986). "Influence of Strain Rate on Undrained Shear Characteristics of K_0 consolidated Cohesive Soils", *Soils and Foundations*, Vol. 26, No. 1, pp. 85-95.

[41] Palmer, A. C. (1972). "Undrained Plane Strain Expansion of a Cylindrical Cavity in Clay: A Simple Interpretation of the Pressuremeter Test", *Geotechnique*, Vol. 22, No. 3, pp. 451-457.

[42] Pender, M. J. (1978). "A Model for the Behavior of the Overconsolidated Soil", *Geotechnique*, Vol. 28, No. 1, pp. 1-25.

[43] Prapaharan, S. (1982). "Prediction of Soil Equilibrium Water Content and Mineralogy Effect on Permeability Using Pore Size Distribution", *MSCE Thesis*, Purdue University, West Lafayette, Indiana, 171 pp.

[44] Prapaharan, S. (1987). "Effects of Disturbance, Strain Rate, and Partial Drainage on Pressuremeter Test results in Clay", *PhD Thesis*, Purdue University.

[45] Prevost, J. H. (1978). "Anisotropic Undrained Stress-Strain Behavior of Clays," *Journal of Geotechnical Engineering*, ASCE, GT8, pp. 1075-1090.

[46] Prevost, J. H. (1979). "Undrained Shear Tests on Clay", *Journal of the Geotechnical Engineering Division*, ASCE, Vol. 105, GT1, pp. 49-64.

[47] Prevost, J. H. and Hoeg, K. (1975). "Analysis of Pressuremeter in Strain Softening Soils," *Journal of the Geotechnical Engineering Division*, ASCE, Vol. 101, GT8, pp. 717-732.

[48] Randolph, M. F. and Wroth, C. P. (1979). "An Analytical solution for the Consolidation Around a Driven Pile", *International Journal for Numerical and Analytical Methods in Geomechanics*, Vol. 3, pp. 217-229.

[49] Roscoe, K. H. and Burland, J. B. (1968). "On the Generalized Stress-Strain Behaviour of Wet Clay", *Engineering Plasticity*, Eds. Heyman, J. and Leckie, F. A., Cambridge University Press, U. K., pp. 535-609.

[50] Roscoe, K. H. and Poorooshasb, H. B. (1963). "A Theoretical and Experimental Study of Strains in Triaxial Compression Tests on Normally Consolidated Clays", *Geotechnique*, Vol. 13, No. 1, pp. 12-38.

[51] Roscoe, K. H., Schofield, A. N., and Thurairajah, A. (1963). "Yielding of Clays in State Wetter than Critical", *Geotechnique*, Vol. 13, No. 3, pp. 211-240.

[52] Saada, A. S. and Bianchini, G. F. (1975). "Strength of One Dimensionally Consolidated Clays", *Journal of the Geotechnical Engineering Division*, ASCE, Vol. 101, GT11, pp. 1151-1164.

[53] Schofield, A. N. and Wroth, C. P. (1968). *Critical State Soil Mechanics*, McGraw-Hill, London, 310pp.

[54] Sills, G. C. (1975). "Some Conditions under which Biot's Equations of Consolidation Reduces to Terzaghi's Equation", *Geotechnique*, Vol. 2[illegible], No. 1, pp. 129-132.

[55] [illegible]

[56] [illegible] ... H. Ohta and A. N. [illegible] *Soils and Foundations* [illegible] No. 1, pp. 132-13[illegible].

[57] [illegible] (1986). [illegible] *Proceedings of the Asian regional Symposium on Geotechnical Problems and Practices in Foundation Engineering*, Sri Lanka, pp. 118-1[illegible].

[58] [illegible]

59 Vaid, Y. P. and Campanella, R. G. (1977). "Time Dependent Behavior of Undisturbed Clay." *Journal of the Geotechnical Engineering Division*, ASCE, Vol. 103, GT7, pp. 693-709.

60 van Eekelen, H. and Potts, D. M. (1978). "The Behavior of Drammen Clay under Cyclic Loading". *Geotechnique*, Vol. 28, No. 2, pp. 173-196.

61 Wood, D. M. (1980). "The Fabric of a Medium Plastic Clay Compacted in the Laboratory and in the Field." *MSCE Thesis*, Purdue University.

62 Wood, D. M. and Wroth, C. P. (1977). "Some Laboratory Experiments Related to the Results of Pressuremeter Tests". *Geotechnique*, Vol. 27, No. 2, pp. 181-201.

63 Wroth, C. P. (1984). "The Interpretation of In Situ Soil Tests". *Geotechnique*, Vol. 34, No. 4, pp. 449-489.

APPENDIX I

WRITTEN PUBLICATIONS

Three Ph.D. students were partly supported by the research project. Two dissertations have been completed:

1. Huang, A. B., "Laboratory Pressuremeter Experiments in Clay Soils", Ph.D. Thesis, December 1986.

2. Prapaharan, S., "Effects of Disturbance, Strain Rate, and Partial Drainage on Pressuremeter Test Results in Clays", Ph.D. Thesis, May 1987.

A third thesis is under preparation:

Sivakugan, N., "Effects of Anisotropy and Stress Path on Interpretation of Pressuremeter Results in Clays", Ph.D. Thesis, in preparation, 1987.

Six technical papers have already been published or accepted for publication:

1. Huang, A. B., Holtz, R. D. and Chameau, J. L., "Calibration Tests of Pressuremeter in Clay", 2nd Symposium on the Interaction of Non-Nuclear Munition and Structures, Panama City Beach, FL, 1985.

2. Sivakugan, N., Prapaharan, S., Altschaeffl, A. G., Holtz, R. D. and Chameau, J. L., "Review of Pressuremeter Testing in Clays", Proceedings, Asian Regional Symposium on Geotechnical Problems and

Practice in Foundation Engineering, Colombo, Sri Lanka, 1986.

[3] Sivakugan, N. and Holtz, R. D., "Discussion of Anisotropy of Undrained Shear Strength of Clays Under Axi-Symmetric Loading Conditions" by Ohta, H. and Nishihara, A., *Soils and Foundations*, Vol. 26, No. 1, Jan. 1986, pp. 132-133.

[4] Huang, A. B., Chameau, J. L. and Holtz, R. D., "Interpretation of Pressuremeter Data in Cohesive Soils by Simplex Algorithm", *Geotechnique*, Vol. XXXVI, No. 4, Dec. 1986, pp. 599-603.

[5] Sivakugan, N., Holtz, R. D. and Chameau, J. L., "In-Situ CK_oUC Shear Strength of Normally Consolidated Clays from CIUC Tests", accepted for publication by the Journal of Geotechnical Engineering Division, ASCE, 1987.

[6] Huang, A. B., Holtz, R. D. and Chameau, J. L., "A Calibration Chamber for Cohesive Soils", submitted to the Journal of Geotechnical Testing, ASTM, Jan. 1987.

Two of these papers (#1 and #6) present the laboratory equipment (e.g., ... for clays) specifically developed for this research, as well ... paper by Sivakugan et al. (#2) is a review of all the ... testing. The three other papers (#3, 4 and 5) ... and techniques developed during the ... paper in preparation, which will provide ... work described in this report and ... we are planning to submit the ... for publication.

"Analysis of Calibration Chamber Pressuremeter Tests in Cohesive Soils", (Chameau, Holtz, Huang).

"A Procedure for Preparing Undisturbed Clay Samples", (Chameau, Holtz, Huang).

"Pressuremeter Holding Tests -- A Reconsideration", (Chameau, Holtz, Huang).

"Spacing Ratio - A New State Parameter for Anisotroically Consolidated Clays", (Chameau, Holtz, Sivakugan).

"Servo-Controlled Cuboidal Shear Device", (Altschaeffl, Chameau, Holtz, Sivakugan).

"Intermediate Principal Stress in Plane Strain", (Chameau, Holtz, Sivakugan).

"Solenoid Valves in Laboratory Automation", Technical Note, (Chameau, Holtz, Sivakugan).

"Preparation of Silicone Rubber Membranes", Technical Note, (Chameau, Holtz, Sivakugan).

"Application of Pore Size Distribution to the Evaluation of Disturbance", Technical Note, (Altschaeffl, Chameau, Holtz, Prapaharan).

"Effect of Strain Rate on Pressuremeter Tests in Clays", (Altschaeffl, Chameau, Holtz, Prapaharan).

"Disturbed Annulus and Initial Unloading in Pressuremeter Tests in Clays", (Chameau, Holtz, Prapaharan).

"Analytical and Experimental Investigations of Partial Drainage in Pressuremeter Testing", (Chameau, Holtz, Prapaharan).

"Prediction of Pressuremeter Expansion Curves Using a Multi-Yield Surface Model", (Altschaeffl, Chameau, Holtz, Prapaharan).

Depending upon their topics, these papers will be submitted to either one of the following journals: ASTM Geotechnical Testing Journal, ASCE Geotechnical Journal, Geotechnique, Canadian Geotechnical Journal, International Journal for Numerical and Analytical Methods in Geomechanics. We also expect to diffuse the research results through presentations at technical meetings, and interaction with our colleagues in the geotechnical community.

APPENDIX II

ACOUSTIC EMISSION TECHNIQUES FOR DETECTION OF POSSIBLE CRACKING DURING CHAMBER PRESSUREMETER TESTS

Introduction

Acoustic emission (AE) are internally generated sound waves in a material produced when it is stressed. Sometimes these sounds are audible to the human ear but because of their low amplitude or high frequency they usually are not. However, a piezoelectric transducer can be used to detect these waves. The signals can be detected, amplified and quantified. Because AE events are produced as a result of stress or some other variable

According to Koerner et al (1976) the application of acoustic emission began in the mining industry to detect instability in mine roofs, faces or pillar rooms. Beginning in the 1950's the technique was also used in the testing of metals. AE in soils testing was initiated by Koerner and his coworkers (Koerner et al. 1976) about a decade ago. Since then, AE has been used in soils testing (Koerner and Mitchell 1981, Lord and Koerner 1984) to monitor the progress of earth dams or retaining walls (Koerner et al. 1978 and 1981), to evaluate the quality of compacted fills (Koerner et al. 1979) and determine the stress history (Koerner et al. 1981 and 1984)

AE Monitoring in Chamber Pressuremeter Tests

According to Koerner and Lord (1986) the accumulation of AE events is monitored during pressuremeter expansion. The rate of the accumulation

increases sharply as the probe pressure exceeds the creep pressure. Some researchers (e.g., Mori and Tajima, 1964; Lukas and LeClerc De Bussy, 1976) state that the creep pressure is equivalent to the horizontal preconsolidation pressure. On the other hand, this has not been the experience in France (Baguelin, et al., 1978). In order to study the relationships among AE, pressuremeter expansion and soil stress conditions, AE monitoring during the chamber pressuremeter tests was attempted.

Acoustic Emission Instrumentation

A schematic diagram of the AE system is shown in Fig. II.1. It was manufactured by Acoustic Emission Technology Corp. The sensor (Model No. AC30L) has a resonant frequency of 30 kHz. The output from the AE console (Model 201G) contains both the counts of AE signals exceeding a pre-set threshold and the RMS reading which represents the signal level (amplitude in volts) of the amplified AE signal. All output goes directly to the computer data logging system.

Because soil attenuates AE signals, it was necessary to use waveguides to "pick up" the signals in the soil (Lord et al., 1982). The needle piezometers placed in the soil sample were ideal waveguides since they are made of stainless steel. The piezometers are soldered to the pore pressure transducer ports which are in turn fastened to the chamber top plate. The AE sensor was then glued to the chamber top plate.

Results of AE Readings During Chamber Pressuremeter Tests

Figure II.2 shows the AE data from test CP3. The counts increase linearly with the radial strain in the pressuremeter. Since the pressuremeter test was controlled strain controlled, the AE counts also increase linearly with

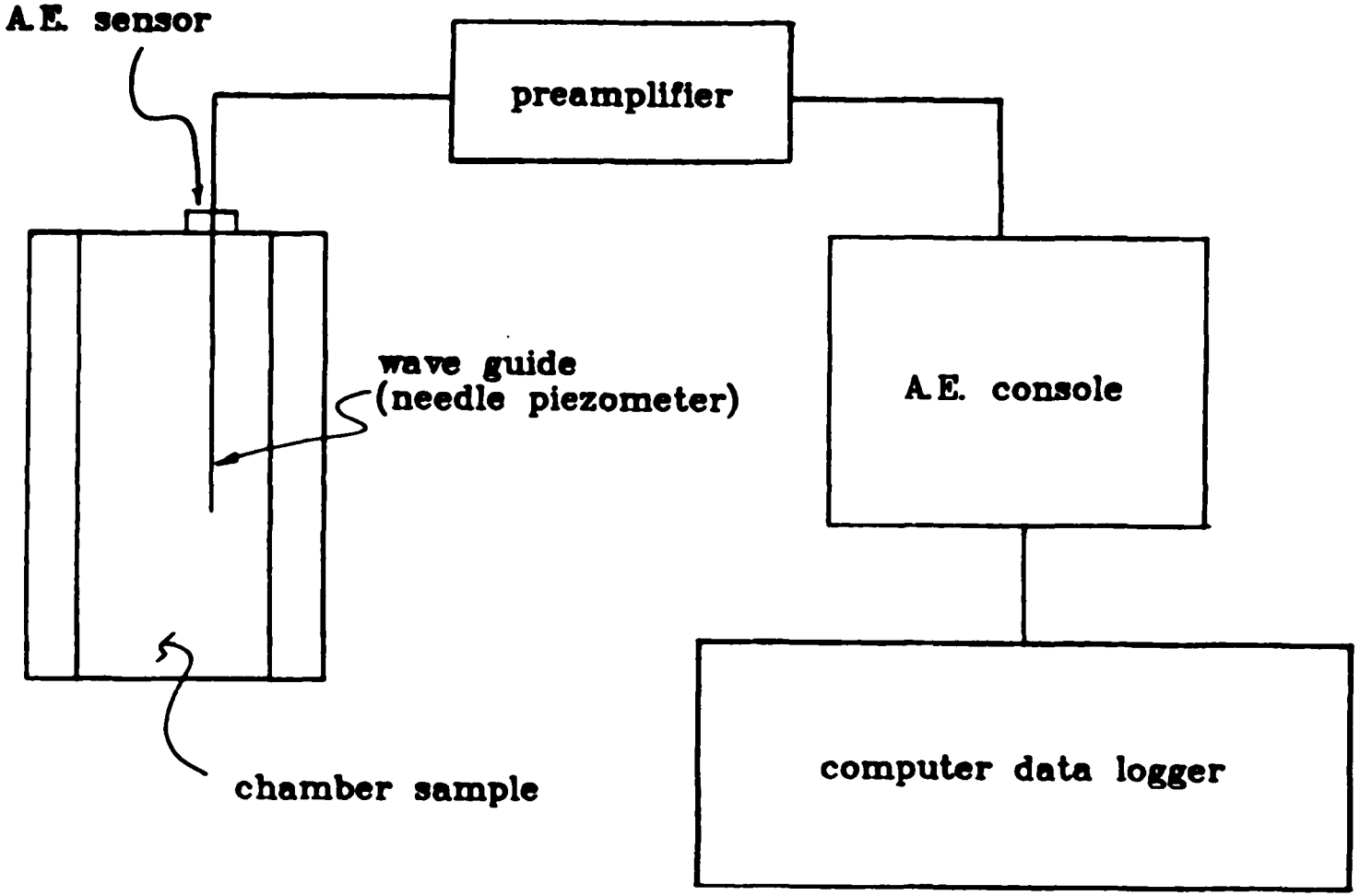

Figure II.1 Schematic diagram of the A.E. monitoring system.

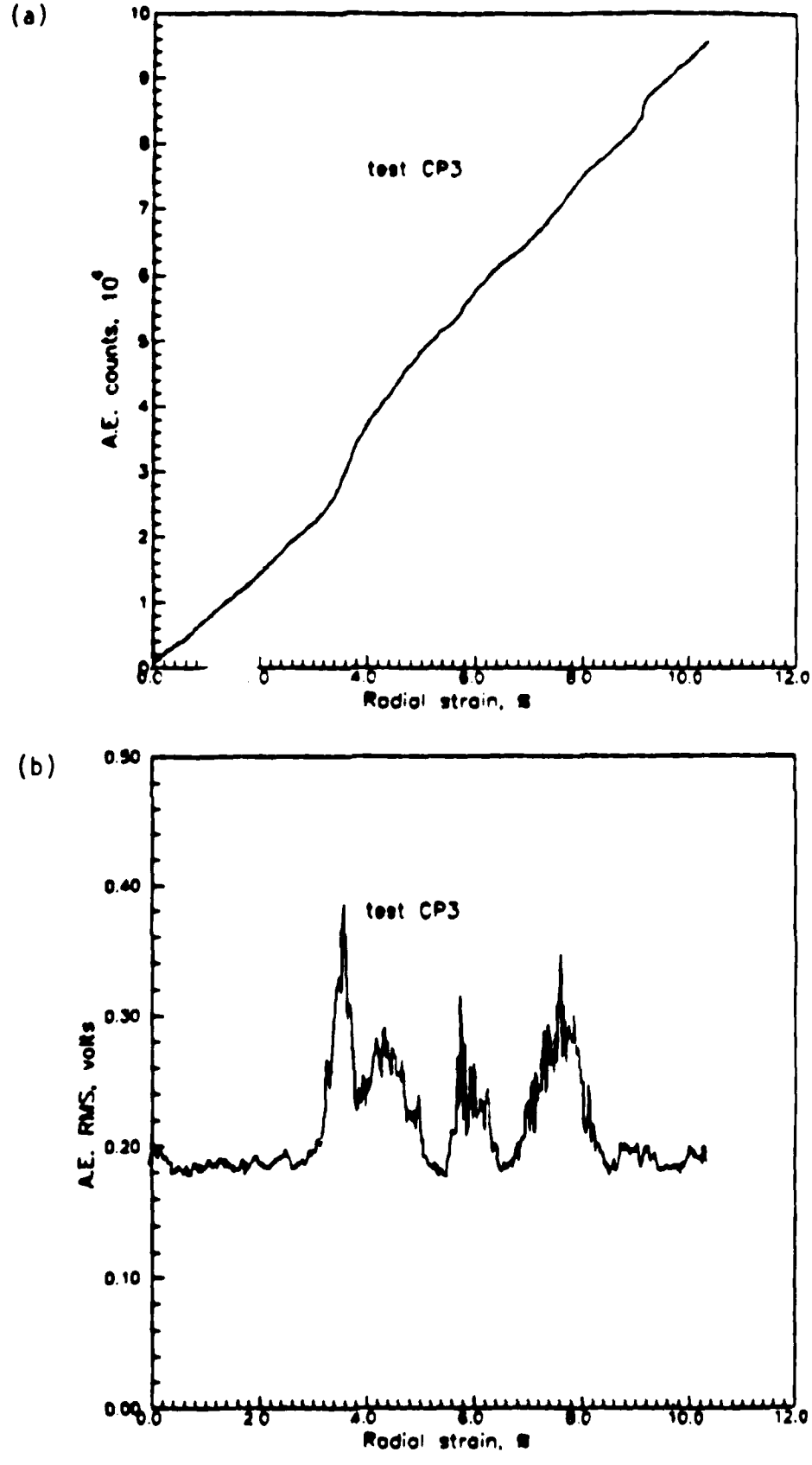

Figure 11.2 AE data for chamber pressuremeter test No. CP3.

time. The RMS readings remain relatively low and stable throughout the test. Both the AE count and RMS readings represent combined effects of the AE signals actually generated due to the stress increase in the soil and noise during the test which was not filtered out. In order to isolate the effects of noise, a dummy test was performed. The pressuremeter was installed in the empty chamber under the same cell pressure as in the real test. The AE signals monitored during the pressuremeter expansion are shown in Fig. II.3. Since there was no soil to be stressed, the AE signals in the dummy test are generated by noise only.

Theoretically, the deduction of the values shown in Fig. II.3 from those in Fig. II.2 represents the net AE signals resulting from the stressing of soil during pressuremeter tests. However, Figs. II.2 and II.3 indicate that the magnitudes of RMS and AE counts are similar in both tests. This means that the recorded AE signals are essentially all due to the noise in the environment. Similar results were also obtained in other tests. A possible explanation for this phenomenon is that the clay sample was completely saturated and water does not transmit AE signals.

Further evaluation of the AE records was therefore not performed, and no additional experiments using AE counts to detect radial cracking were carried out.

References

Baguelin, F., Jezequel, J. F. and Shields, D. H., (1978), The Pressuremeter and Foundation Engineering, Trans Tech Publications, 617 pp.

Beatie, A. G., (1983) "Acoustic Emission, Principles and Instrumentation", *Journal* of Acoustic Emission, Vol. 2, No. 1/2, pp. 95-127.

Koerner, R. M., Lord, A. E., McCabe, M. W., and Curran, J. W., (1976) "Acoustic Emission Behavior of Granular Soils", Journal of the Geotechnical Engineering Division, ASCE, Vol. 102, No. GT7, pp. 761-773.

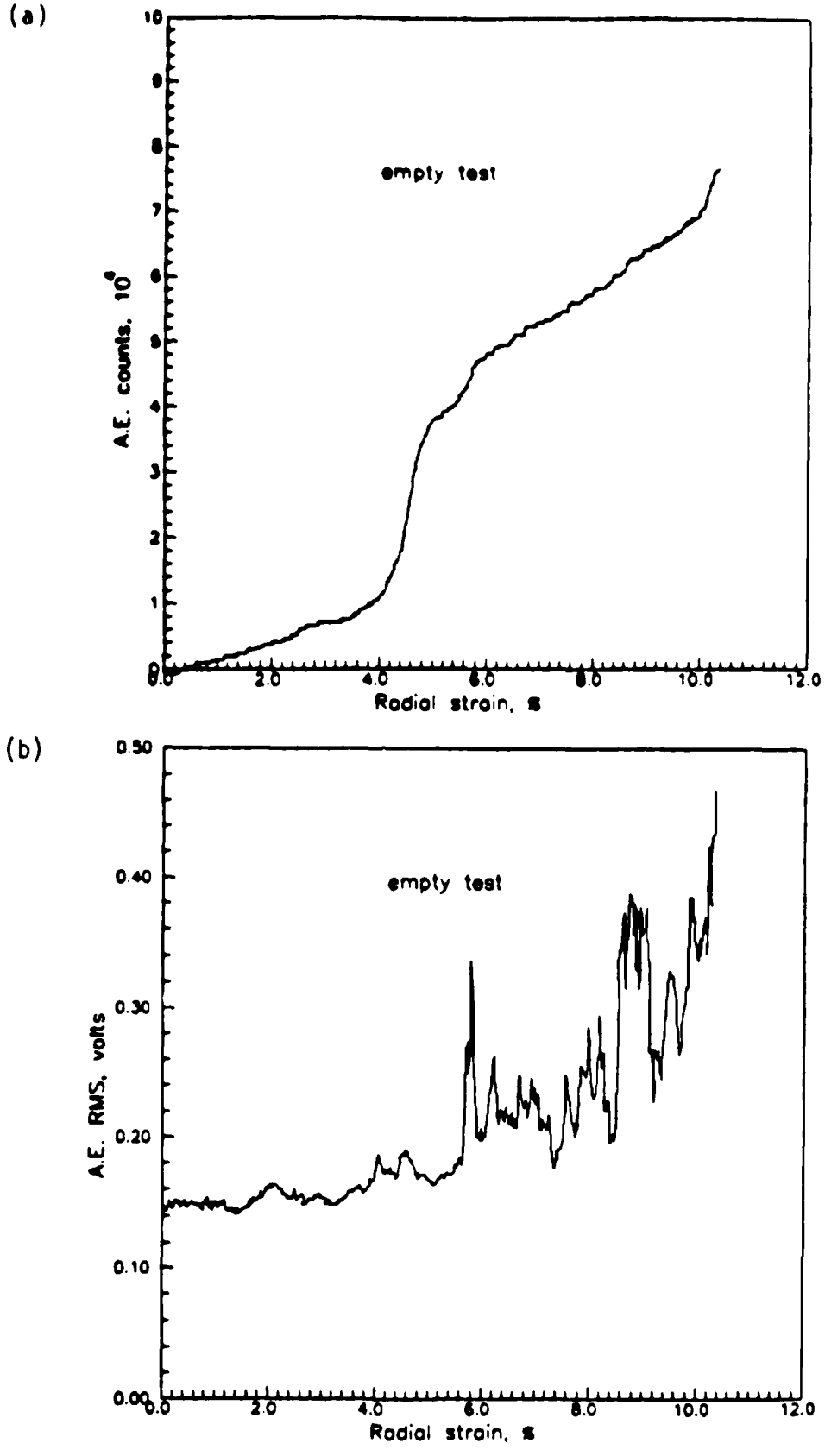

Figure II.3 AE data on an "empty" test.

Koerner, R. M., Lord, A. E., and McCabe, W. M., (1978) "Acoustic Emission Monitoring of Soil Stability", Journal of the Geotechnical Engineering Division, ASCE, Vol. 104, No. GT5, pp. 571-582.

Koerner, R. M., McCabe, W. M. and Baldiviesco, L. F. (1981) "Acoustic Emission Monitoring of Seepage", Journal of the Geotechnical Engineering Division, ASCE, Vol. 107, No. GT4, pp. 521-526.

Koerner, R. M., Leaird, J. D. and Welsh, J. P., (1983) "Use of Acoustic Emission as Nondestructive Testing Method to Monitor Cement Grouting", Proceedings, ACI Symposium on Cement Grouting.

Koerner, R. M., Lord, A. E., and Deutsch, W. L., (1984a) "Determination of Prestress in Granular Soils Using AE", Journal of the Geotechnical Engineering Division, ASCE, Vol. 110, No. GT3, pp. 346-358.

Koerner, R. M., Lord, A. E., and Deutsch, W. L., (1984b) "Determination of Prestress in Cohesive Soils Using AE", Journal of the Geotechnical Engineering Division, ASCE, Vol. 110, No. GT11, pp. 1537-1548.

Koerner, R. M. and Lord, A. E., (1986) "Subsurface Soil Monitoring via Acoustic Emission", Proc. of In Situ '86, ASCE Specialty Conference, Blacksburg, Virginia, pp. 176-190.

Lord, A. E., Frisk, C. L., and Koerner, R. M., (1982) "Utilization of Steel Rods as AE Waveguides", Journal of the Geotechnical Engineering Division, ASCE, Vol. 108, No. GT2, pp. 300-304.

Lord, A. E. and Koerner, R. M., (1983) "An Acoustic Pressuremeter to Determine In-Situ Soil Properties", Journal of Acoustic Emission, Vol. 2, No. 3, pp. 187-190.

Lukas, R. G. and LeClerc De Bussy, B., (1976) "Pressuremeter and Laboratory Test Correlations for Clays", Journal of the Geotechnical Engineering Division, ASCE, Vol. 102, No. GT9, pp. 945-963.

Mori, H., and Tajima, S., (1964) "The Application of the Pressiometre Method to the Design of Deep Foundations", Soils and Foundations, Vol. 4, No. 2, pp. 34-44.

Villet, W.C.B. and Mitchell, J. K., (1981) "Cone Resistance, Relative Density and Friction Angle", Proceedings, ASCE St. Louis Convention, Session 35, Cone Penetration Testing and Experience, pp. 178-208.

END

7-87

DTIC